Modern Applied Science

www.ccsenet.org/journal.html

Vol. 3, No. 3

March 2009

Planning of Access Road Using Satellite Technology and Best Path Modeling

Mohd Hasmadi Ismail

Faculty of Forestry, Universiti Putra Malaysia, 43400 UPM, Serdang, Selangor, Malaysia

Tel: 60-3-8946-7220 E-mail: mhasmadi@putra.upm.edu.my

Hj. Kamaruzaman, Jusoff (Corresponding author)

Yale University, Yale's Centre for Earth Observation-Environment Science Centre

21 Sachem St, New Haven, CT 06511, USA

Tel: 203-676-7761 E-mail: jusoff.kamaruzaman@yale.edu

The research is financed by Universiti Putra Malaysia and Public Service Department, Government of Malaysia (Sponsoring information)

Abstract

Forest road construction for harvest operation are always been subjected to certain constrictions and limitations. Engineering practices on forest road alignment are hindered by costly environmental and operational assessment. GIS tools and related data such as remote sensing allows in allocating suitable access road by taking consideration of environmental and cost implication. The aim of this study is to present the method of integration of remote sensing data and GIS in allocating access road for forest harvesting using best path modeling. Therefore, the specific objectives of this study are to allocate the optimal forest roads network in forest operation, and to determine the density of forest road network. Allocating the best paths for forest road access for timber harvesting is a problem that can be solved by computer based approaches using spatial modeling. Spatial modeling is used to compute the indicative factors that suit road allocation. The model developed and designed using GIS to propose feasibility forest road allocation in the hill area. The method was designed to produce road layouts taking topographical features and forest environmental constraints into special consideration. In this study, four grid themes influencing the road construction were identified; elevation, slope, barrier of lake and distance to existing roads. The total of access road aligned and proposed in the respective area was 28,745.35m. Meanwhile the overall density calculated in selected compartments was about 9.93m/ha (0.80%). The densities of road paths presented here were achieved below as outlined by the forestry department. Thus, there is potential to reduce damage to the residual stand and to the ground area disturbance by the harvesting operation. The forest road alignment and information in this study provides an initial foundation on which GIS can be used for this kind of analysis in forest road planning. The result is not only associated with forest transportation, but at the same time is useful to identify a risk of road construction to the environment. This revealed that the minimum density of forest road construction can help mitigate the loss of ecological services of tropical forest subject to logging pressure and lead to greater financial benefit in future operations.

Keywords: Forest road allocation, Hill tropical forest, Remote sensing, GIS, Best path modeling

1. Introduction

Currently, most of the forest roads in Peninsular Malaysia are located in the hilly region, characterized by steep terrain and dense river of networks. The construction of a forest road has the most potential of any forest harvesting operation to cause damage to the environment. In most cases, the problem of transporting timber in tropical forests is very different from that in temperate forests, as tropical forests have seldom been subjected to rational management. Most tropical countries have not had the necessary means or tools to provide their forests with a system of roads or railways where they are required. However, one of the major problems is that extreme slopes often occur when constructing forest roads especially in hilly areas.

Harvesting operations have always been subject to certain constrictions. Restrictions and regulations on slope limitations, buffer zones, minimum cutting limits, prohibited species and road density which pose little problem to loggers in the past have now become major problems as operations are shifting from the gentler and richer flat land to the steeper and unevenly stocked terrain of tropical hill forests. This constraint represents a major impediment in use of specific areas,

which restrain the use of the area for road allocation. In Brazil, FOA (1977) reported that obstacles when using of mechanization in Brazil forest are mainly from slope, elevation and soil characteristics. Thus, constraints are imposed by those factors can effect the path allocation. Muhammad and Rahman (1995) noted that the most problematic feature in the harvesting operation is to establish the accessibility of forest network into a forest area. Because roads are long-term features, their location must be carefully chosen, to meet the loggers need for safe access, avoid long-term maintenance problems, reduce potential risk of water and soil degradation, and minimize costs over the short and long term. For instance it has been reported that an estimated 90 percent or more of soil erosion resulting from timber harvesting in the tropic is directly attribute to inadequate road design (FAO, 1977).

Nowadays, computerized methods are very useful in the solution of these problems. However, a clear application of this approach is probably limited to relative simple plain conditions with homogeneous tree species and technology composition. It is not possible to evaluate in detail ecological parameters. Liu and Session (1993) have illustrated and discussed the influence of terrain topography on the quality of the planning process and relative forest accessibility. It seems that approaches in technology and ecology evaluation for more alternatives, are more effective for mountains where conditions change frequently. In planning many alternatives there may be a need to investigate in a DEM and Geographical Information System (GIS) environment before roads construction. This approach is not new but still used since it was formulated (Epstein, 1994; Kitagawa, 1995). A philosophy to understand forest operation as a scientific discipline was presented by Heinimann (1995). He also analyzed the role and need for computer technology in connection with future needs.

Forest road alignment practices are hindered by costly environmental and operational assessment. GIS tools and related data such as remote sensing data allows harvest managers and planners to dynamically assign the timing of access and haul cost attributing to the existing inventory database for several road access alternatives. When combined with other standard features such as species composition and merchantable timber volume, it is possible to analyze the effect a road network design has on delivered wood costs. Planning of forest road networks have already been discussed extensively, for example, Kanzaki (1996), Sakai (1995), Samsul (2000), and Judibal (2000). However, there is no precedent for a routing system based on the road density and cost analysis which focuses on decision making. Other studies by Yoshimura and Kanzaki (1995) were focused on forest road planning using quantitative risk assessment approaches to estimate the degrees of slope failure potentially using topographic maps. In addition, the degrees of slope failure potential were calculated automatically using DEM (Yoshimura et al. 1996). It could be applied to GIS, which made it much simpler to plan forest roads in steep areas. However, FOA (1982) reported that despite some models, developed mainly using the method of cost effectiveness analysis, none of these trials were very compatible with practical performance.

The aim of this study is to present the method of integration of remote sensing data and GIS in allocating access road for forest harvesting using best path modeling. Therefore, the specific objectives of this study are two folds: (i) to allocate the optimal forest roads network in forest operation, and (ii) to determine the density of forest road network.

2. Methodology

2.1 Description of study area

The study area is in the Sungai Tekai forest reserve at Jerantut district in Pahang State, Peninsular Malaysia, about 240 km north-east of the capital Kuala Lumpur. It is situated within latitude 04°10´N - 04°30´N and longitude 103°03´E - 103°30´E, covering an area of approximately 10,000 hectares (Figure 1). Figure 2 illustrates the 3D view of the study area and demonstration site clipped from the entire study area, which consists of several compartments. The clipped off demonstration site of about 5758.32 ha, where from a total of 26 compartments, only 11 compartments in the area of non served forest were namely selected compartment 170, 171, 173, 174, 175, 176b, 196, 197, 199a, 199b and 200. These compartments covered an area of about 2509.13ha. The forest area is composed of mixed virgin hill forest, high in species diversity with predominance of Shorea species such as Meranti Seraya (*Shorea curtisii*) and Meranti Rambai Daun (*Shorea acuminate*). The elevation is mostly over 600 m above sea level. The slope gradient of the study area is undulating with steep rugged slopes ranging from 100 to 800. The annual precipitation is about 210cm with a high tropical climate with mean temperatures ranging from 20^0C -31^0C. The precipitation occurs mainly in two seasons: April to May and November to December. The relative humidity is high ranging from 62.3% to 97.0%, with a daily mean of 85.7%.

<Figure 1: Peninsular Malaysia showing the study area in Jerantut District in Pahang State>

2.2 Procedure for accessibility modeling

The model developed in this study was designed to propose feasibility forest road allocation in the presence of constraints. The suitability of forest road allocation must meet the topographical constraints and produce an acceptable level of forest road network, and meet the environmental requirements. In tropical dipterocarp forest, an area with a low timber stock to be harvested, very steep slopes, excessive high elevation and located in a sensitive area, forest operation would not be feasible from a financial and environmental point of view.

Allocating the best paths for forest road access for timber harvesting is a problem that can be solved by computer based approaches using spatial modeling. Spatial modeling is used to compute the indicative factors that suit road allocation. The method is designed to produce road layouts taking topographical features and forest environmental constraints into special consideration. The main process in designing forest road suitability allocation is to establish the weighted distance analysis by mapping the indicative factors and find the least accumulative cost from source to the destination cell or point. The shortest path function is used to route the optimal costly road through selected forest compartments.

<Figure 2: 3D view of study area (top), demonstration site clipped over Landsat TM imagery (bottom left) and selected non-served forest (bottom right)>

The accessibility factors (in grid theme) of road construction in the study area were assigned into uniform class range to show its effect on the cost of moving through an individual cell. Then, data were normalized where each of grid themes is classified on a scale of 1-4 according to the effect on the cost of constructing forest road. The grid themes of accessibility factors are then given a weighted value and added together to produce a single grid theme that identifies the appropriate path through each cell. Finally the most effective road corridor can be identified between two or each portions of forest compartment. In this study, four grid themes influencing the road construction through the study area were identified; elevation, slope, lake barrier and distance to existing roads. Classifications of factors for suitable road allocation in the study were based upon the Malaysian Forestry Department guideline, Muziol (1999) and Judibal (2000). From a forest harvesting aspect, the following factors were selected, namely (a) Slope (degree): Slope was expressed in degrees. The original slope classification was drawn up by the Department of Agriculture and modified for forestry application to the study area based on a study by Muziol (1999), (b) Elevation (m): Elevation limit/factor is different from the state legislation and new ruling by Forestry Department of P. Malaysia. In this case guideline prescribed by Forestry Department of P. Malaysia was applied, and (c) Distance from existing road (m): Transportation cost constitutes one of the largest capital expenditures in this harvesting area. The cost may vary widely depending on the terrain and distance to the processing area, which needs to be justified with the volume of timber and value of tree crop. The road constructed in the Sungai Tekai Forest Reserve concession has a simpler standard dictated by low travel speed and moderate to steep sloping.

Taking the above consideration into account, the classification of the distance of new access roads to existing roads is divided into four classes as given in Table 1. In general, there are six basic main stages required in order to generate the road location. They are: (1) Data input, (2) Data modification, (3) information derivation, (4) Computer based approach, (5) analysis and evaluation, and (6) Output. A simplified flow diagram summarizing the stages of operation is shown in Figure 3.

<Table 1: Classification factors for the harvest compartment (road allocation)>

From the entire grid theme, only the slope and distance from existing road imposed a major constraint in locating forest access. Therefore, the other constraints were expressed in terms of forest function class or class within some of the GIS layers. However the conditions of soil depth and soil type were not available as an indicative factor, since such investigation is time consuming and labour intensive to carry out. In this process, only slope on topographical map and distance from existing road theme were the salient factors to be evaluated, while the other factors were not so important but remain complementary to the optimum forest road alignment.

<Figure 3: A simplified flow diagram of suitable road allocation>

The cost path grid theme requires the entire friction theme to be merged together into one to create the total cost of road construction through each cell. The ideal surface for this application is one in which all cell values are equal since the layer takes care of the travel space and the later cost weighted function will take care of distance and direction. A weighted cost approach is taken to prepare the cost layer using cost datasets as input. Assigning weight to these cost layers was done based on personal experience and discussion with the forestry officers. Accessibility factor maps were assigned a weight by giving 80.00% to the slope, 20.00% to distance from existing road and 0.00% to the lake. A lake entry was deleted since it is impossible to move across the lake, so this lake is called absolute barrier. Each percentage then was divided by 100 to normalize the values. Using raster calculation in ArcGIS the following equation is derived which generates the required cost layer:

(0.80*[slope_cost] + 0.20*[distoexistroad_cost] + 0.00*[lake_barrier])

From the cost weighted function, the direction was created to give a raster direction of the least cost path from each cell to each source. With the cost distance and direction of raster were created, the shortest path to the destination were run automatically. A total of six destinations and 11 established target locations were created according to assumption as (i) a harvest compartment might be represented by the centroid point, unless when the centroids were located in an unsuitable point, this can be relocated at the a suitable point, and (ii) The only way to gain access to inaccessible compartments is to access one of its adjacent harvest compartments, but the road network system as a whole is designed for the entire harvest forest area. The raster of distance and direction gives the least forest path from destination to the target and back to the

destination. The selected destination and target in each compartment is presented in Figure 4. Planning of new forest road path carried out from available data and at the standard scale of 1:50000 used by forestry department in planning a road at compartment level. In this study the cost of planning is considered rather than expenses cost of the road construction. In order to realize that, shortening the total cost can be made by reducing the distance and earth moved in the forest.

<Figure 4: A selected target and destination created for this study>

2.3 Road density derivation

The road system is the basis of economic timber extraction and it is the task of the engineer to plan a forest road system, which minimizes the total cost of road construction and environmental impact. Excessive length of road construction leads to high cost for cross country movement, means higher road cost are incurred and leads to a larger size of open area. The road density network represents relationship between the length of the road and the total harvest area that gravitates towards them (Session, 1992), and is expressed in meters per hectare. The density of road construction determined in this study is based on the average total length of road network in meters per total harvest area in ha. The following formulae were used to derive the density of road.

$$Y = \frac{RL}{f}$$

where,

Y = Density of forest roads network

RL = Road length (m)

f = Total harvest area (ha)

While percentage of opening of surface area was expressed as:

$$Y = \frac{RL \times RW \times 100\%}{f}$$

where,

Y = Percentage surface area

RL = Road length (m)

RW = Road width (m)

f = Total harvest area (m2)

2.4 Development of class of intensity scale

It is desirable to construct forest road density by also considering environmental conditions. The road density scale should be applied on a regional and a forest-wide basis. The development of road intensity scale should clearly define based on ecological parameters. The main objective of the design of road density scale of a forest transportation system is to find the most workable and economic road network with the lowest cost in the long term (FAO, 1982). Also, this scale should include establishment of track and road density limits for non-monetary value of multiple-use management and environmental protection. In this study the scales used are based on the per area basis.

Forestry Department of Peninsular Malaysia has produced guidelines for the standard of Malaysia classification for forest road density in the Specification for Forest Road in Peninsular Malaysia (Anonymous, 1988). Under this classification, the overall road density has been determined based on slope conditions of the harvest area [i.e. very steep ($>31^0$), steep (16^0-31^0) and moderate ($<16^0$)], and overall road density in m/ha is 140, 160 and 200, respectively. However, the classification is not practically used in practice where the forest operation management is being executed in different compartments and by different loggers. Consequently, the road density in this study is determined on compartment-by-compartment basis but still considers the general guideline by the Forestry Department of P. Malaysia. The main factor is the volume of timber to be harvested per unit area. This can determine the road layout that would in turn affect the road density. The volume of timber harvested within a particular logging area will affect the optimum density within a logging compartment. Area with timber volume that is in clusters would have lower road density as compared with the areas where the timber stands are sparsely distributed. In general, because of the low volume of harvestable log per hectares in selected study areas, the optimum road density can be set lower where selective management system is practiced. The following scale of road density followed the guideline on a compartment by compartment basis as given by the State Forestry Department and the following classes are identified as given in Table 2.

<Table 2: The scale of road density class used in the study>

Based on this classification, the study area was considered as moderate to very steep slope conditions, thus the overall proposed road density in this study area must not exceed 40m/ha.

3. Results and discussion

3.1 Proposed access road location and analysis

This section discusses the use of shortest path technique in locating access road locations. Based on the data provided by the forestry department and evaluation factors on selected compartments, the access road location was executed to determine the road net pattern. The developed access road location procedure was designed in the non-served forest compartment by constructing access roads along existing secondary forest road. In this case, in the non-served forest compartment new access roads were located to serve the harvesting process at a minimum construction cost. All cost data sets (slope, distance from existing road and lake barrier) were merged together to create one grid theme as shown in Figure 5. This output grid theme shows the total cost of constructing road paths through each cell or how suitable each location is for locating the new access road. The final cost layer was classified into four classes as Low-Moderate, Moderate-High, High-Very High and Very High. Locations with low values indicates the cell in which it will be the least costly to build a forest road path. The lake barrier in white was assigned as 'no data' and considered as an absolute barrier since it is impossible to build an access road through the lake.

Evaluation of cell area revealed that Very High cost class represents only a tiny portion with 19804 counted cells (about 0.85 %). This shows that allocation of access roads to very costly area can be easily avoided. Among them, a High-Very High class indicates the major portion with 950523 cells counted (40.82 %). This followed by other classes such as Low-Moderate and Moderate-High with counted cells of 694412 (29.82%) and 663494 (28.50%), respectively. With the human expertise to plan and analyses areas of interest, overlay and intersect various types of information such as slope, elevation, river network and timber volume is carried out. The locations of road design in the stable areas shall as far possible be kept away from natural streams in order to minimise stream sedimentation, exception was allowed to cross the stream with minimal construction. Therefore, the road location was designed to fit to the topography features so that only minimum alterations of the natural conditions are necessary. On the other hand, the proposed road should be located on a gentle slope on wider hill ridges and reach hill tops by as short a route as possible.

<Figure 5: Cost layer for road construction depicts the cost of road path through an individual cell>

The access road locations were determined after all cost distance and directions were performed to each created target and destination point. The cost distance calculates the least cumulative cost starting from one or several targets or destinations and travel through a cost surface. The optimal lay out of all the forest road accesses are depicted in Figure 6, which is showing exactly where the access road location has been constructed by applying 50% transparency on hill shade of DEM. The 3D views of the access road path are shown in Figure 7. In this view, it gives a clear path and direction and shows how the road locality is laid out on the elevation range and slope according to the three accessibility factors.

<Figure 6: Proposed access road location in demonstrated area>

<Figure 7: Access road from 3D views of elevation and slope range>

A profile analysis was performed in terms of elevation and slope of the terrain for road alignment. Profiles show the change in elevation and slope of the road surface along a path. Profile graphs from selected 3D lines are used for evaluating the difficulty of hilly terrain or assessing a corridor for road alignment. From the profile graph it easy to see and measure elevation and slope along the alignment road. The example series of profile graph presentation for selected road paths is illustrated in Figures 69a and 69b. In general, it is emphasized that the access road is aligned to avoid the most cost anomalies; where as noted the higher slope indicates possibly a higher construction cost. It is estimated that most of the slopes involved in the alignment are more than 10 degrees but do not exceed 40 degrees. It is concluded that the location of access path were established in the area will reduce the cost and environmental impact when building the road.

The important point to understand from this result is that it is important to spend time considering how to weigh the cost datasets to layout forest roads. The potential path to build a new forest road depends on how the weight is allocated to the cost dataset. The road line represented here is created using cost raster where each raster (slope, distance from existing road and barrier of lake) had a different influence, and where the slope input had a weight 80%. By giving the slope input a higher weight that means more attention was given to avoid steeper slopes in the forest road path. On the other hand, the structure developed in this accessibility model permitted some relative modification that could improve its capability. Inclusion of more specific indicators with more accurate description and use of different techniques in creating targets and destination points could be helpful, since this basic indicator presented here was based only on three indicators. This can be conducted by performing the cost weight and shortest path analyses on the new raster to compare the results with the previous work.

<Figure 8: Elevation and slope profile graph for path 1a>

<Figure 9: Elevation and slope profile graph for path 2a>

3.2 Density analysis of forest road

The problem of choosing the optimum forest road density is important in theory but in practice it is difficult to solve. The variables of spatial analysis such as topography (slope and elevation), and area per ha were considered. The main issue in selecting the route for a forest road is cost. To minimize the cost of forest road construction, the lower percentage of surface opening to align the forest road is required. Determining the optimal route by which transportation can get from one point to another point is a crucial element to any logging company. The initial cost of construction of a forest road is reflected in the future cost in maintenance. The improper alignment of forest road will result in high construction costs. A low quality road will also result in high road maintenance and high transportation costs.

In order to calculate the density of a proposed road in a demonstrated area, data were first summarised at the compartment levels. The summary describes the access road information considered on selected harvest compartments, the effect of topography and difficulty of terrain. Then, for each compartment, the total km of road in each of the road classes was calculated. Lastly, the lengths in km of road were totalled for the entire demonstrated area and divided by the represented study site to produce the density information. The summaries of road construction information for all harvest compartments are shown in Table 3.

<Table 3: Information of access road in selected harvest compartments>

From the analyses it can be seen that the access roads, which have been delineated in 11, selected compartments showed an overall of 9.93m/ ha. In term of length, it represents about 0.80% of the open forest floor area. Across the analysed compartments, the density of access road was highest in compartment 171, followed by compartment 200 and compartment 176b. Their densities were 23.82m/ha, 13.45m/ha and 11.95m/ha. The lowest density was in the compartment 199a with about 2.98m/ha. Apparently, the entire proposed forest road are laid out in low category density table outlined by the forestry department. However, bear in mind this evaluation does not include feeder road assessment where the information for this road type was not available to this study. The determination of access road density and network allowed on the site is based on the presumption that all other applicable standards shall be met. The maximum density established for a compartment area is not a guarantee that such densities may be obtained, nor a valid justification for varying other dimensional or constructional standards. A total of 19 road segments were merged into 11 paths, with a total length of 287,45.35 m costing RM718,750.00, which was required to construct an access road to all selected compartments. This estimation is based on RM25, 000.00 costs to construct an access road (secondary road type) per ha. in the demonstrated area supplied by the forestry department. It can be seen that more than 80% access road location are located in the class of Low-moderate and Moderate-High cost layer. The proposed access road planned by GIS capability dramatically allow forest managers to easily review the cost and modify or update forest road patterns if change is need. However in this estimation, it is important to note that this cost will be different and change if different material is used and intensity of earthwork is taken into account.

Although the approach had many advantages for access road planning, two major problems were encountered. First, as in case of the forest path model, solutions proposed by the shortest path modeling system were limited to the type and quality of data used to derived information. Ideally, access roads to new harvest compartments should consider financial criteria. However, since no financial information on timber harvest cost was contained in the modeling system, the approach of access road had to be performed from a purely an environmental point of view. Secondly, in the development of access road locations the size of the harvest compartment contained varying gradient and ground conditions that requires the development of criteria based on respective area. Despite that, the different contractors hired for each harvest compartment created a "planning conflict" for constructing new forest road access. This happened when road planning by different contractors are not connected between compartment. Determining the road alignment in the field took longer to be accomplished, therefore this aspect is important since the success of the reduced impact logging philosophy ultimately depends on the commitment of field workers.

4. Conclusion

The use of remote sensing data and best path modeling in GIS with the additional supportive information was able to facilitate design of a proposed forest road more easily. This study however has developed a key approach, which integrated the computer system into forestry application that could assist planners and foresters in the planning and design stages for establishing an optimum forest road for forest harvest operations. Specifically, in the future, development of forest roads by means of GIS can be dynamically accessed by all user agencies in managing forest road systems. The overall total of access road aligned and proposed in the respective study area is 28,745.35m. Meanwhile the overall density calculated in selected compartments is about 9.93m/ha (0.80%). The densities of road paths presented here are achieved below as outlined by the forestry department. Thus, there is potential to reduce damage to the residual stand and to the ground area disturbance by the harvesting operation. The forest road alignment and information in this study provides an initial foundation on which GIS can be used for this kind of analysis in forest road planning. The result of the study is not only associated with forest transportation, but at the same time is useful to identify a risk of road construction to the environment. Proper planning of forest road by forest managers could significantly decrease sediment production to

rivers. As a result, drainage from roads planning and location can cause severe erosion. This implies that the minimum density of forest road construction can help mitigate the loss of ecological services of tropical forest subject to logging pressure and lead to greater financial benefit in future operations. Further, the result of the access road costing about RM 718,750.00 from this study should be used with constraint and local perception. The local perception on road cost planning may differ significantly with those found in other research work. Nevertheless, the procedure developed here should be helpful to further endeavor in considering the use of GIS spatial modeling for harvest road planning.

References

Anonymous. (1988). Specification for forest road in P. Malaysia. Forestry Department Peninsular Malaysia Press. 47p.

Epstein, R. 1994. Planex - Software for operational planning. Proceedings of Int. NEFU/IUFRO/FAO/FEI Seminar. Harbin.

FAO. (1977). A framework for land evaluation. Food and Agriculture Organisation. International Institute for land Reclamation and Improvement, Publication No. 22, Wangeningen, The Netherland.

FAO. (1982). Logging of mountain forest. Report of the 3rd FAO Training Course on Mountain Forest Roads and Harvesting. Food and Agriculture Organization of The United Nation, Rome, Italy. 285p.

Heinimann, H.R. (1994). Conceptual design of a spatial decision support system for harvest planning, Proceedings of Int. NEFU/IUFRO/FAO/FEI Seminar. Harbin.

Judibal,C.C. (2000). GIS-based support system for tactical timber Harvesting planning:Design and development. Ph.D (Thesis), Universiti Putra Malaysia, Serdang, Selangor, Malaysia.174p.

Kanzaki, K. (1996). A planning of the forest road network by the theory of graphs. Journal Japan Forestry Society, 48: 365-371.

Kitagawa,K. (1995). Basic concept of a method for systematically laying out forest road network of the endless type. Paper presented at IUFRO XX World Congress, 6-12 August 1995,Tampere, Finland: 13p.

LIU, K. and J. SESSION. (1993). Preliminary planning of road system using digital terrain model. Journal of Forest Engineering, 4(2):27-32

Muhammad,F.A.R. and Rahman,D. (1995). Design of forest road for hill forest management: A case study at Ulu Muda Forest Reserve, Baling,Kedah. Paper presented at Seminar Kajian Pembalakan Terhadap Waduk Di Hutan Simpan Ulu Muda, 23 January 1995, UTM, Skudai, Johor, Malaysia. 15p.

Muziol,C. (1999). The zoning of production forest as a management tool. Paper presented at the Conference on Forestry and Forest Product Research, 20-24 November 1999,Kuala Terengganu, Malaysia. 23p.

Sakai, T. (1995). Two algorithms for forest road planning using digital terrain map (DTM). Journal Japan. For. Eng. Assoc. 10(3): 225-231.

Samsul, S. (1999). Geographical information system for forest road planning: A case study of Balah Forest Reserve, Ulu Kelantan. Bac. Sc. (Thesis), Faculty of Forestry, Universiti Putra Malaysia, Serdang, Selangor,Malaysia.71p.

Session,J.(1992). Using network analysis for road and harvest planning. Proceeding IUFRO Workshop on Computer Supported Planning of Road and Harvesting, Feldafing, Germany.pp:36-41.

Yoshimura, T. and Kanzaki, K. (1995). Method of planning a forest road network using the degrees of slope failure potentials: Estimation of the degrees of slope failure potentials with topographic maps. Journal Japan Forestry Society, 77:1-8.

Table 1. Classification factors for the harvest compartment (road allocation)

Factor	Class range	Class factor	Verbal class
Slope (degree)	0-10	1	Gentle
	10-20	2	Moderate
	20-40	3	Steep
	>40	4	Very steep
Elevation (m)	0-1000	1	Productive
	>1000	2	Protected
Distance from existing road (m)	0-750	1	Low
	750-1500	2	Moderate
	1500-3000	3	High
	>3000	4	Very high

Table 2. The scale of road density class used in the study

Road density description class	Road density (m/ha)
Very high	> 40
High	30-40
Moderate	20-30
Low	< 30

Table 3. Information of access road in selected harvest compartments

Path no.	Length (m)	Merged path.	Length after merged(m)
1a	894.17	1a	2503.51
1b	1609.34		
1c	2213.91	1b	2213.91
2a	1098.32	2a	3258.29
2b	2159.97		
2c	1539.24		
2d	1868.49	2b	5195.42
2e	1787.69		
3a	573.46	3a	1525.71
3b	952.25		
3c	1415.27	3b	1415.27
4a	1038.29		
4b	1657.92	4a	4999.16
4c	2302.95		
4d	1419.73	4b	1419.73
5a	1477.53	5a	1477.53
6a	1725.22	6a	3312.10
6b	1586.88		
6c	1424.72	6b	1424.72
Total	**28745.35**	**11 paths**	**28745.35**
Overall road density for 11 paths: 11.46 m/ha ; 0.92% surface area			

Compartment no.	Road length (m)	Density (m/ha)
170	2147.19	10.67
171	2613.87	23.82
173	2249.46	8.00
174	2498.30	7.35
175	2924.56	9.65
176b	1970.32	11.95
196	3454.97	10.72
197	1522.07	9.39
199a	656.76	2.98
199b	1753.74	10.22
200	3132.89	13.45
Total	**24924.13**	**118.20**
Overall road density in 11 compartment: 9.93m/ha ; 0.80% surface area		

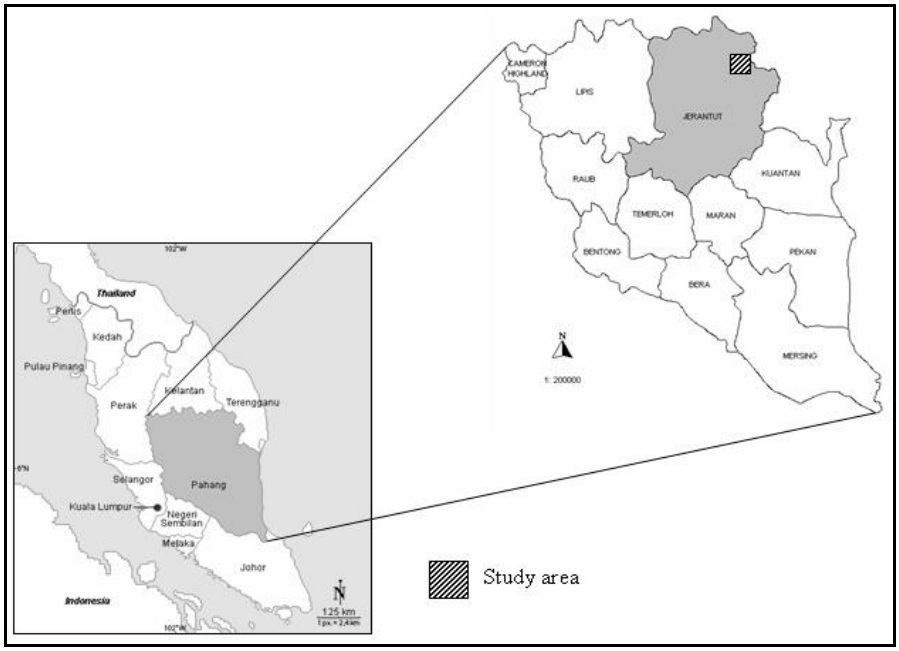

Figure 1.

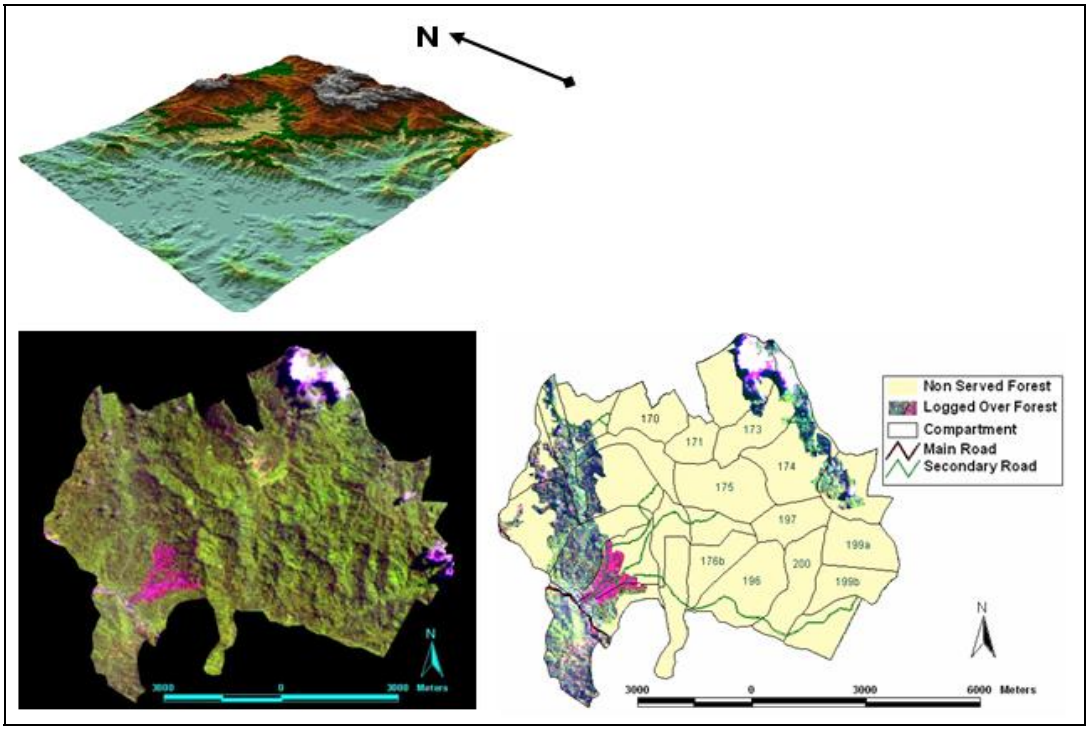

Figure 2.

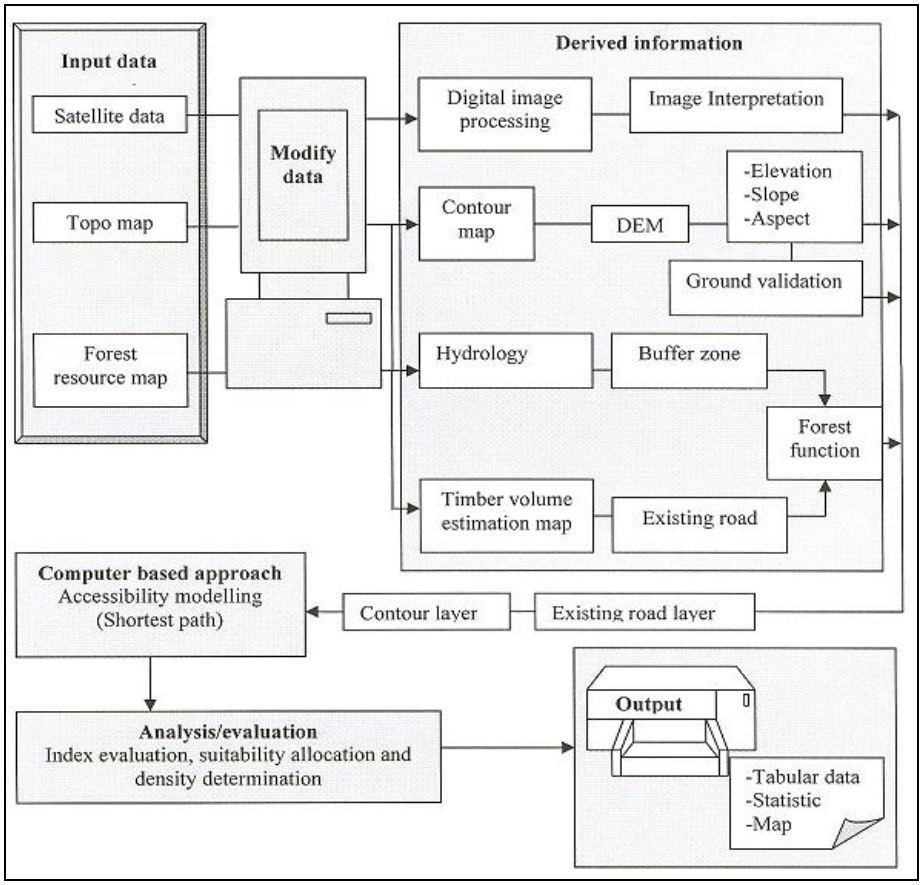

Figure 3.

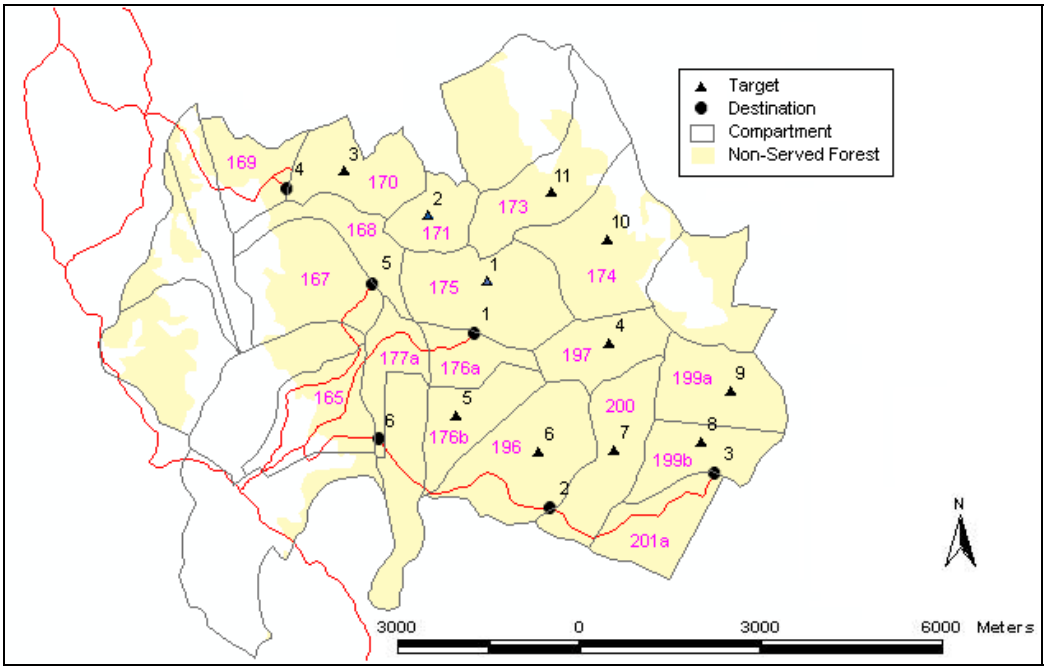

Figure 4.

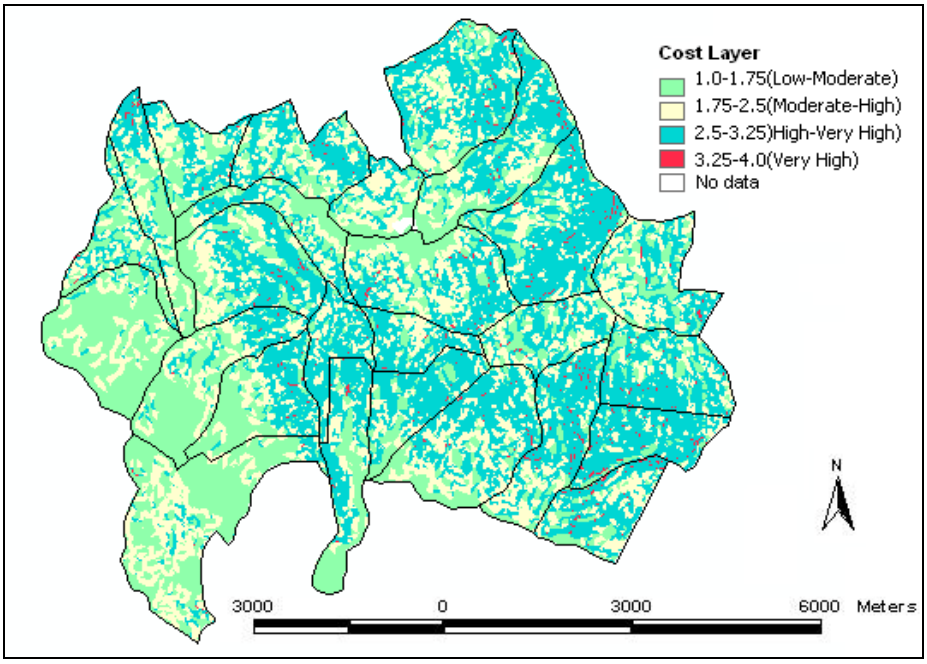

Figure 5.

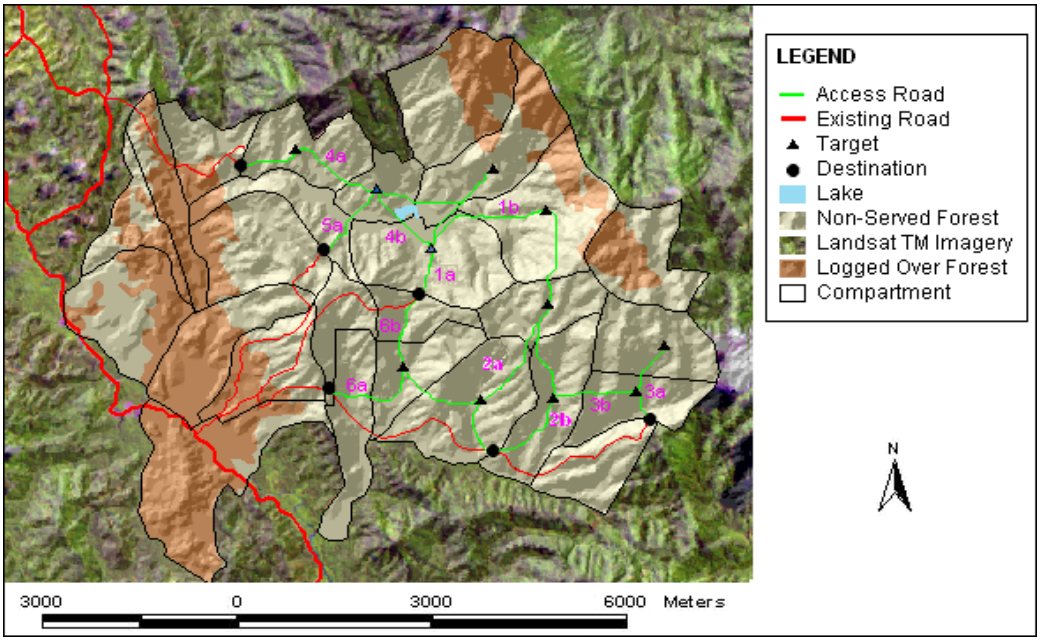

Figure 6.

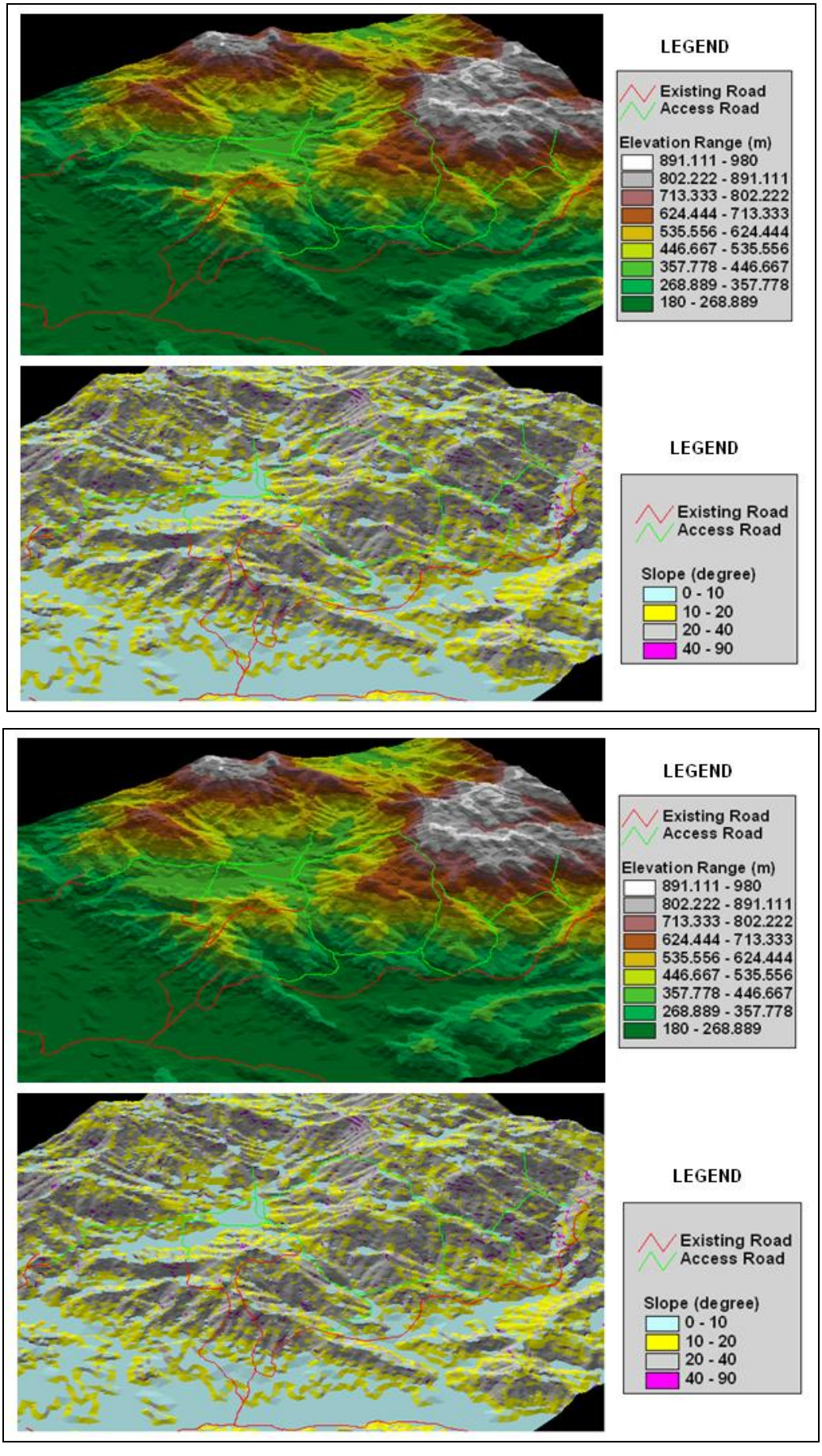
LEGEND
Existing Road
Access Road
Elevation Range (m)
891.111 - 980
802.222 - 891.111
713.333 - 802.222
624.444 - 713.333
535.556 - 624.444
446.667 - 535.556
357.778 - 446.667
268.889 - 357.778
180 - 268.889
LEGEND
Existing Road
Access Road
Slope (degree)
0 - 10
10 - 20
20 - 40
40 - 90
LEGEND
Existing Road
Access Road
Elevation Range (m)
891.111 - 980
802.222 - 891.111
713.333 - 802.222
624.444 - 713.333
535.556 - 624.444
446.667 - 535.556
357.778 - 446.667
268.889 - 357.778
180 - 268.889
LEGEND
Existing Road
Access Road
Slope (degree)
0 - 10
10 - 20
20 - 40
40 - 90

Figure 7.

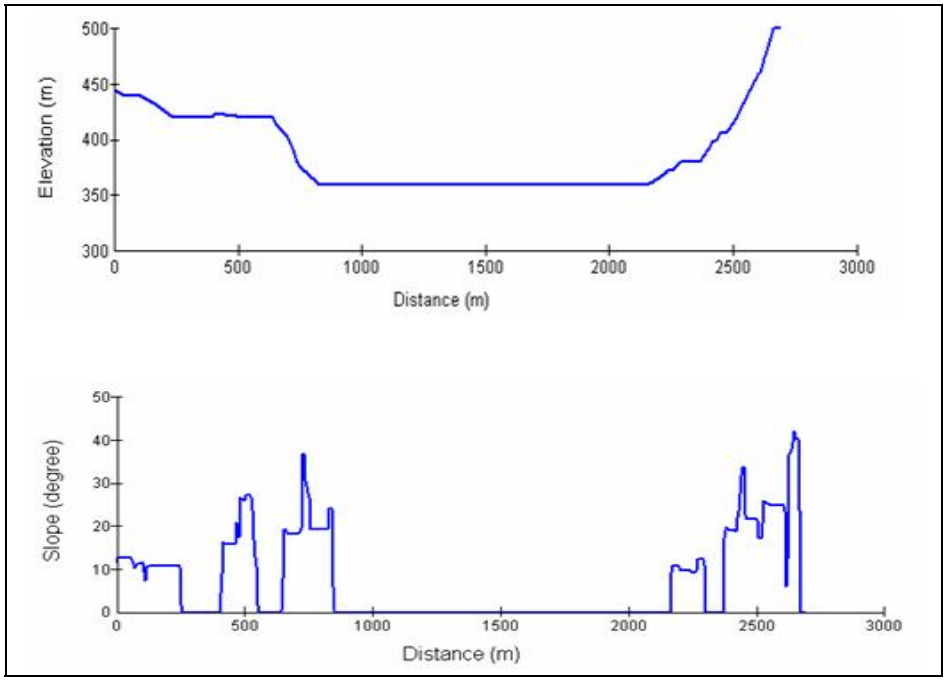

Figure 8.

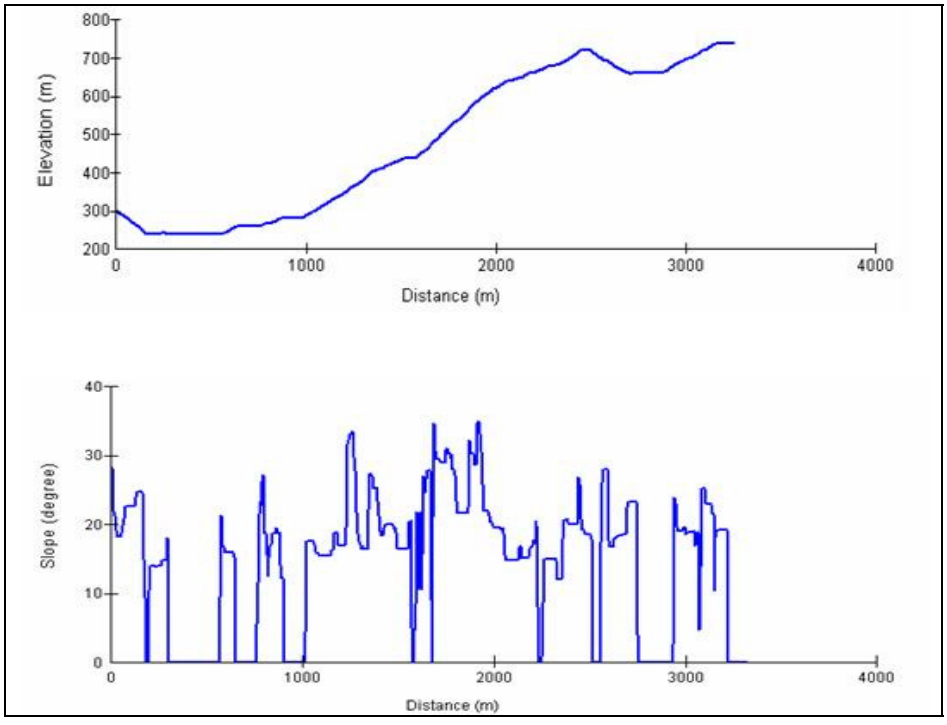

Figure 9.

Modern Applied Science

www.ccsenet.org/journal.html

Vol. 3, No. 3

March 2009

The Regional Resource Supply and Environmental Capacity Analysis Based on the Ecological Footprint--a Case Study in Shijiazhuang of Hebei Province

Juanmin Cui (Corresponding author)

Chengde National Teachers College

Chengde 067000, China

E-mail: cuijuanmin@163.com

Baolin Yu

Hebei Institute of Land-Resources Using and Planning

Shijiazhuang 050051, China

Abstract

Based on the theory of ecological footprint this paper analyzed the ecological economic system in Shijiazhuang city in the view of demands of economic system to natural resource and supply of ecosystem for natural resources. Quantitative analysis of the ecosystem of Shijiazhuang city was attempted to estimate the status of sustainable development and give some insight into protection of the ecological environment of it and its province, Hebei province.

Keywords: Ecological footprint, Resource supply, Environmental capacity

1. Introduction

The term ecological footprint was first proposed by Rees and later refined by Wackernagel, a Canadian economist (1996) to describe quantitatively the use of natural resources by humans and their supply via nature to indicate regional sustainable development ability. Ecological footprint analysis compares human demand on nature with the biosphere's ability to regenerate resources and provide services. It does this by assessing the biologically productive land and marine area required to produce the resources a population consumes and absorb the corresponding waste, using prevailing technology. Footprint values at the end of a survey are categorized for biomass (food, fiber), build-up lands, water and energy and as well as the total footprint number of Earths needed to sustain the world's population at that level of consumption. This resource accounting is similar to life cycle analysis wherein the consumption of cropland, forestry, build-up land, water area, pastureland and ocean are converted into a normalized measure of land area called 'global hectares' (gha).Per capita ecological footprint (EF) is a means of comparing consumption and lifestyles, and checking this against nature's ability to provide for this consumption. The tool can inform policy by examining to what extent a nation uses more (or less) than is available within its territory, or to what extent the nation's lifestyle would be replicable worldwide. The higher the footprint is the more human demand.

Due to no conspicuous distinguish between "ecological capacity" and "environmental capacity " by our government and researchers all over the world, in view of the particularity and availability of the land resource, the ecological capacity in the present paper is environmental capacity.

2. Background introduction

Located in the vicinity of the North China Plain, Shijiazhuang, the capital of Hebei Province, neighbors Beijing and Tianjin in the north, Henshui city in the east, and lies against the continuous Taihang Mountain in the west and Xingtai city in the south. Covering an area of 15.8 thousand square kilometers (6100.4 square miles), it has 6 districts, 12 counties, 5 county-level cities and 1 national-level new and high-tech development zone under its prefecture. Shijiazhuang has a population of 9.395 million, 2.313 million of whom live in the urban area. Sitting in the central south of vast North China Plain, Shijiazhuang City is located at the longitude of 113°31′~115°29′, and the latitude of 37°26′~38°46′. Shijiazhuang City enjoys convenient transportation conditions, called as "a gate from south to north and

the throat from Hebei to Shanxi" and "One of the cardinal foundation of pharmacy industry". Enveloped in the temperature continental monsoon climate, it's clearly distinguished between seasons with yearly average temperature of 13.3 centigrade, the coldest month of the year (January) at–2.9 centigrade, compared with the warmest (July) at 26.5 centigrade. The average precipitation is 534.6mm, sunshine hours more than 2513.9 hours. The city gross product increased from 78.1 billion yuan in 1997 to 178.6 billion yuan in 2005, and thus the city is during a mew period to adjust economic structure at present.

3. Analysis of resource supply and environmental capacity in 2005

3.1 Analysis of resource consumption

3.1.1 Biomass consumption

Biomass resource is categorized for farm, animals, water and forestry products, and each category has its small sort. Calculation of biomass productive area was adopted the average yield from the data of World and Agricultural Organization (FAO) of United Nations in 2003, which facilitate to the comparison with countries and regions. Biomass consumption of Shijiazhuang city in 2005 was converted into ecological arable land area which this consumption demands, and the data in detail was list in Table 1.

3.1.2 Energy consumption and built-up land

Energy balance accounts dealt with several kinds of energy as follows: raw coal, coke, gasoline, diesel and power according to the energy consumption data of Shijiazhuang city. Fuel consumption was converted into fossil energy yield land area, based on the the criterion of average calorific value per fossil energy yield land area in the world, and heat resulted from local energy consumption was converted into fossil land area. According to the land area derived from Shijiazhuang land census data in 2005, built-up land data and its area converted by power consumption was processed with results listed in Table 2 in detail.

3.2 Trade adjustment of Ecological footprint calculation

Calculation of ecological footprint indices demands for net consumption, and thus trade adjustment should be taken into account in the expenditure of biomass and energy, namely calculating the ecological footprint of biomass consumption, energy consumption, net expenditure of the population in regions. Due to no access to detail external trade information from regions, trade adjustment of import and export was not considered in the present paper.

3.3 Per capita ecological footprint demand

The results of ecological footprint of Shijiazhuang city in 2005 were list in Table 3.

3.4 Environmental capacity calculation

Equivalence factors were selected from the reports of ecological footprint all over the world. When yield land area of Shijiazhuang city was converted into comparable biology yield land area, equivalence factors of arable land, grassland, forestry land, water area and built-up land were limited by data. Then we multiplied the corresponding equivalence factor by present physical spatial areas—arable land, grassland, forestry land, water area and built-up land. 'Yield factor' selected in the paper was once used to calculate Chinese ecological footprint by Wackernagel (1996) and the average yield factor applied was 1.66, 0.19, 0.91, 1 and 1.66 respectively. At the same time, based on the proposal by World Commission on Environment and Development (WCED), 12% of the biologically productive land area should be taken away from ecological footprint to protect biodiversity (Wackernagel, 2000, PP. 21-42, Lenzen, 2001, PP. 229-255, Xu, 2007, PP. 56-57). Available environmental capacity of Shijiazhuang city was listed in Talbe 4.

3.5 Analysis of resource carrying capacity and environmental capacity

Consequence of ecological footprint was composed of its demand and available ecological yield land area, namely environmental capacity.

4. Conclusions and proposals

According to the analysis above, per capita ecological footprint demand, environmental capacity and ecological deficit of Shijiazhuang city in 2005 were 2.7159 hm^2, 0.3899 hm^2 and 2.326 hm^2, respectively. Those numbers were far higher than ecological deficit in China.(According to "Report on sustainable development of domestic land resource in China (2004) " compiled by Land Resource Information Centre in China, per capita ecological footprint increased during the period of 1978~2003, and amounted to 0.890 hm^2 in 2003). The ecological deficit indicated that Shijiazhuang city was in a situation of unsustainable development.

According to per capita ecological footprint demand structure, there was conspicuous discrepancy between the structures of productive land supply and social economy development demand in ecological economy system of Shijiazhuang city, which was mainly ascribed to no preservation of CO_2 absorption land and failure service for fossil fuel demand. Per capita ecological footprint of built-up land was 0.0022 hm^2, while that of ecological supply was

0.0899 hm^2 which was 0.0877 hm^2 higher than demand with surplus supply. Meanwhile, there was great discrepancy between the demand and supply of arable land and forestry land. Demand of arable and forestry land was 0.8061 hm^2 and 0.5761 hm^2 while supply was 0.2947 hm^2 and 0.0583 hm^2, respectively. Per capita supply of built-up land exceeded ecological demand. Moreover, according to planning revision of land utilization, more and more cropland was occupied, especially for arable land. Demand of grassland and water area was 1.0008 hm^2 and 0.0217 hm^2 while supply was 0 hm^2 and 0.0002 hm^2, respectively. This acute discrepancy was attributed to the calculation and analysis based on the conversion of average level of the world, however, it was not necessarily the case in fact. Local stockbreeding industries rely on not only the natural grassland, but mainly feedstuff which resulted from development of feedstuff through internal structure adjustment of agriculture and establishing of professional livestock farm. Annual pork products from farmers rank the top in the region, not totally provided by grassland. Based on less invalidity of the serious imbalance of local demand and supply proportion, aquatic product doesn't rely on large amount of water area but intensive artificial propagation, and thus improving the resource utilization could solve the supply deficiency problem of water area.

According to the supply structure of the resource carrying area, per capita footprint of arable land was attained to 0.2947 hm^2 accounting for 5.58%. In addition, in order to protecting biodiversity 12% of the biologically productive land area was not retained. Taken together, natural ecological system degraded, configuration of land utilization was unreasonable and configuration of ecological spatial category for local population consumption was somehow single in Shijiazhuang city.

Without reducing the standard of living, the ecological deficit mainly ascribed to excess utilization of natural resource could be ameliorated by the following measures:

1) Alter consumption manners of produce and life, establish resource-economizing consumption system of social production.

2) Based on the development of science and technology, adopt new technology and improve per capita yield of natural resource.

3) Utilize the present resource efficiently.

4) Import inadequate resource from other regions to balance ecological footprint.

References

Lenzen, M., Murray, S.A. (2001). A modified ecological footprint method and its application to Australia. *Ecological economics*, 37(2):229-255.

Wackernagel, M., David, Y. (2000). Footprints for sustainability: The next steps. *Environment, development and sustainability*, (2):21-42.

Wackernagel, M., Rees, W. (1996). *Our Ecological Footprint: Reducing human impact on the earth*. Gabriola Island: New Society publishers.

Xu, Y. (2007). Dynamic analysis of sustainable development in Sichuan province based on the ecological footprint. *Journal of China west normal University(Natural science)*, (2):56-57.

Table 1. Biomass accounts of Shijiazhuang city

Category	Total average product (kg/hm^2)	Biomass(t)	Ecological footprint (hm^2)	Per capita ecological footprint (hm^2/cap)	Land category	Total population (million)
Farm product				0.2879		
cereal	2744	4824262	1758112.9738	0.1897	Arable land	92.7
Oil	1856	238671	128594.2888	0.0139	Arable land	92.7
Cotton	429	17529	40860.1399	0.0044	Arable land	92.7
Vegetable and melon	18000	13338048	741002.6667	0.0799	Arable land	92.7
Animal product				2.0015		
Meat	74	1072719	14496202.7027	1.5638	Grassland	92.7
Milk	502	740108	1474318.7251	0.1590	Grassland	92.7
Poultry egg	400	1033251	2583127.5000	0.2787	Grassland	92.7
Aquatic product	29	29232	1008000.0000	0.1087	Water area	92.7
Forestry product				0.5237		
Fruit	3500	1725579	493022.5714	0.0532	Forest land	92.7
Dry fruit	3000	22239	7413.0000	0.0008	Forest land	92.7
Pricky-ash	1600	3098	1936.2500	0.0002	Forest land	92.7
Other forestry product	1.99	8662	4352763.8191	0.4696	Forest land	92.7

Table 2. Energy account of Shijiazhuang city

Category	Global average energy footprint (GJ/ hm^2)	Conversion coefficient (GJ/t)	Consumption (t)	Consumption (GJ)	Ecological footprint (hm^2)	Per capita footprint (hm^2/cap)	Yield land category
Energy						0.2809	
Raw coal	55	20.934	5856765	122605518.5100	2229191.2456	0.2405	Fossil energy land
Cork	55	28.470	392259	11167613.7300	203047.5224	0.0219	Fossil energy land
Gassoline	93	43.124	215579	9296628.7960	99963.7505	0.0108	Fossil energy land
Diesel	93	42.705	155611	6645367.7550	71455.5673	0.0077	Fossil energy land
Power	1000	11.840	628170 (10^4kw.h)	7437532.8000	7437.5328	0.0008	Built-up land

Table 3. Per capita ecological footprint of Shijiazhuang city

Land category	Primary per capita ecological footprint (hm^2/cap)	Equivalence factor	Per capita ecological footprint after balance (hm^2/cap)
Arable land	0.2879	2.8	0.8061
Grassland	2.0015	0.5	1.0008
Forest land	0.5237	1.1	0.5761
Fossil energy land	0.2809	1.1	0.3090
Built-up land	0.0008	2.8	0.0022
Water area	0.1087	0.2	0.0217
Per capita ecological footprint demand			2.7159

Table 4. Environmental capacity of Shijiazhuang city

Land category	Total area (hm^2)	Per capita area (hm^2/cap)	Yield factor	Equivalence factor	Per capita area after balance (hm^2/cap)
Arable land	587688.97	0.0634	1.66	2.8	0.2947
Grassland	0	0.0000	0.19	0.5	0.0000
Forestry land	539671	0.0582	0.91	1.1	0.0583
CO_2 absorption	0	0.0000	0	1.1	0.0000
Built-up land	179205.95	0.0193	1.66	2.8	0.0899
Water area	11567	0.0012	1.00	0.2	0.0002
Total supply area					0.4430
Biodiversity protection12%					0.0532
Per capita environmental capacity					0.3899

Table 5. Ecological footprint and environmental capacity of Shijiazhuang city

Ecological footprint demand		Ecological footprint supply		Discrepancy between supply and demand (hm^2/cap)
Land category	Per capita ecological footprint (hm^2/cap)	Land category	Per capita environmental capacity (hm^2/cap)	
Arable land	0.8061	Arable land	0.2947	0.5114
Grassland	1.0008	Grassland	0.0000	1.0008
Forestry land	0.5761	Forestry land	0.0583	0.5178
Fossil energy land	0.3090	CO_2 absorption	0.0000	0.3090
Built-up land	0.0022	Built-up land	0.0899	-0.0877
Water area	0.0217	Water area	0.0002	0.0215
Per capita ecological footprint demand	2.7159	Total supply area	0.4430	
		Biodiversity protection12%	0.0532	
		Per capita environmental capacity	0.3899	
		Per capita ecological deficit		2.3260

Modern Applied Science

www.ccsenet.org/journal.html

Vol. 3, No. 3

March 2009

Effect of Hydrotropes on Solubility and Mass Transfer Coefficient of Methyl Benzoate

Senthil Nathan, M., Jayakumar, C. & Nagendra Gandhi, N

Department of Chemical Engineering, A.C. College of Technology

Anna University, Chennai 600025, India

Tel: 91-44-2220-3515 E-mail: n_nagendra2002@yahoo.com

Abstract

A comprehensive investigation on the solubility and mass transfer coefficient enhancement of methyl benzoate through hydrotropy has been undertaken. The solubility and mass transfer coefficient studies were carried out using hydrotropes such as citric acid, urea and nicotinamide under a wide range of hydrotrope concentrations (0 to 3.0 mol/L) and different system temperatures (303 to 333 K). The effectiveness of hydrotropes was measured in terms of Setschnew constant K_s and reported for all hydrotropes used in this study.

Keywords: Hydrotropy, Solubilization, Mass transfer co-efficient, Separation

1. Introduction

Hydrotropy is a unique and unprecedented solubilization technique in which certain chemical compounds termed as hydrotropes can be used to effect a several fold increase in the solubility of sparingly soluble solutes under normal conditions. This increase in solubility in water is probably due to the formation of organized assemblies of hydrotrope molecules at critical concentrations.

Hydrotropes in general are water-soluble and surface-active compounds which can significantly enhance the solubility of organic solutes such as esters, acids, alcohols, aldehydes, ketones, hydrocarbons, and fats.

The solubility enhancement in the organic compounds could be due to the formation of molecular structures in the form of complexes. Previous experimental findings have concluded that hydrotropy is a process which goes beyond conventional solubilization methods such as miscibility, co-solvency, salting-in effect since the solubilization effected by hydrotropy was higher and more selective compared to other solubilization techniques. The effect of hydrotropes on the solubility and mass transfer coefficient for a series of organic esters such as butyl acetate, ethyl benzoate, amyl acetate, methyl salicylate and benzyl acetate was studied in our earlier publications.

It has been observed that, in many two-phase reaction systems involving a sparingly soluble organic compound like methyl benzoate, the mass-transfer coefficient was found to be very low solely due to the poor solubility of methyl salicylate in the aqueous phase. Since methyl benzoate serves as raw material/intermediate for a wide variety of chemicals and allied products and the separation of methyl benzoate from any liquid mixture seems to be difficult, this hydrotropic technique can be adapted to increase the solubility as well as to separate such mixtures effectively. Data on various aspects of hydrotropic study on the solubility and mass-transfer coefficient for methyl benzoate-water system are reported for the first time.

2. Experimental

All the chemicals used in this work were procured from S.D.Fine Chemicals Pvt. Ltd.,Mumbai with a manufacturer's stated purity of 99%.

The experimental setup for the determination of solubility values consisted of a thermostatic bath and a separating funnel. For each solubility test, about 100 ml of methyl benzoate previously saturated with distilled water was taken in a separating funnel and 100 ml of a solution of the hydrotrope of known concentration was added. The separating funnel was immersed in a constant-temperature bath fitted with a temperature controller which could control the temperature within $\pm$0.1 °C. The setup was kept overnight for equilibration. After equilibrium was attained, the aqueous layer was carefully separated from the ester layer and transferred into a beaker. The ester concentration was estimated by the addition of excess NaOH using a standardized Hcl solution with phenolphthalein as an indicator. All the solubility experiments were conducted in duplicate to check the reproducibility. The observed error in the reproducibility was <2%.

The experimental setup for the determination of the mass-transfer coefficient consisted of a vessel provided with baffles and a turbine impeller run by a motor to agitate the mixture. The vessel used for mass transfer studies is of height 40 cm and of inner diameter 15 cm. The turbine impeller diameter is 5 cm, the width is 1 cm and the length is 1.2 cm. It has four blades. The baffle is 40 cm high with a diameter of 1.5 cm. There are about four baffles that rotate at a speed of 600 rpm.

For each run to measure the mass-transfer coefficient, about 250 ml of the ester previously saturated with distilled water was added to the hydrotrope solution of known concentration. The sample was then agitated for a known time of 600, 1200, 1800, and 2400 seconds. After the end of fixed time t, the entire mixture was transferred to a separating funnel. After allowing to stand for some time, the aqueous layer was carefully separated from the ester layer. The concentration of the solubilized organic ester in aqueous hydrotrope solutions at time t was analyzed as done for solubility determinations. A plot of $-\log [1 - C_b/C^*]$ versus t is drawn where C_b is the concentration of methyl benzoate at time t and C^* is the equilibrium solubility of methyl benzoate at the same hydrotrope concentration. The slope of the graph gives $k_La/2.303$, from which k_La, the mass-transfer coefficient was determined. Duplicate runs were made to check the reproducibility. The observed error was <2%.

3. Results and Discussion

3.1 Solubility

The solubility of methyl benzoate standard in water is 1.43×10^{-3} mol/L at 303 K, compared to 1.41×10^{-3} mol/L as reported by Dean (1987). Thus, the solubility values in water are in excellent agreement with the earlier reported values.

Experimental data representing the average of duplicate determinations on the effect of hydrotropes, i.e., citric acid, urea and nicotinamide on the solubility of methyl benzoate are presented in Tables 1-4 and are plotted in Figures 1-4. Citric acid is one of the hydrotropes used in this study. The solubility of methyl benzoate in water at 303 K in the absence of any hydrotrope is 1.43×10^{-3} mol/L (Table 1). It has been observed that the solubility of methyl benzoate in water increases significantly only after the addition of 0.40 mol/L of citric acid in the aqueous phase. This concentration in referred to as the Minimum Hydrotrope Concentration (MHC).

Therefore, it is evident that hydrotropic solubilization is displayed only above the MHC, irrespective of system temperature. This MHC value assumes greater significance in the context of recovery of hydrotrope solutions. Since hydrotropy appears to operate only at significant concentrations of hydrotrope in water, most hydrotropic solutions release the dissolved methyl benzoate on dilution with water below MHC. The knowledge of MHC values is necessary especially at industrial levels, as it ensures ready recovery of the hydrotrope for reuse. The MHC values remained unaltered even at increased system temperatures.

The solubilization effect varies with concentration of hydrotropes (Table 1). In the present case, a clear increasing trend in the solubility of methyl benzoate was observed above the MHC of citric acid. This increasing trend is maintained only up to a certain concentration of citric acid in the aqueous phase, beyond which there is no appreciable increase in the solubility of methyl benzoate. This concentration of citric acid (hydrotrope) in the aqueous phase is referred to as the maximum hydrotrope concentration (C_{max}). From the analysis of the experimental data, it is observed that further increase in hydrotrope concentration beyond C_{max} does not bring any appreciable increase in the solubility of methyl benzoate even up to 3.00 mol/L of citric acid in the aqueous phase. Similar to the MHC values, C_{max} values of hydrotropes also remained unaltered at increased system temperatures.

The knowledge of MHC and C_{max} values of each hydrotrope with respect to a particular solute assumes greater significance in this study since it indicates the beginning and saturation of the solubilization effect of hydrotropes. The values of MHC and C_{max} of a hydrotrope with respect to methyl benzoate may be useful in determining the recovery of the dissolved methyl benzoate even to an extent of the calculated amount from hydrotrope solutions at any concentration between MHC and C_{max} by simple dilution with distilled water. This is the unique advantage of the hydrotropic solubilization technique.

From the experimental data plotted in Figure 1, it can further be observed that, in order to achieve the particular solubility of methyl benzoate, say 20×10^{-3} mol/ L, the citric acid concentration should be 2.00 mol/L at 303 K, 1.60 mol/L at 313 K, 1.40 mol/L at 323 K and 1.20 mol/L at 333K in the aqueous phase. Thus it can be seen that as the system temperature increases, the concentration of citric acid required in the aqueous phase to achieve a particular solubility of methyl benzoate decreases. A similar trend has been observed for other systems also.

It has also been observed that the solubilization effect of citric acid was not a linear function of the concentration of the citric acid. The solubilization effect of citric acid increases with increase in hydrotrope concentration and also with system temperature.

A similar trend has been observed in the solubilization effect of other hydrotropes namely urea and nicotinamide. It has also been observed that the MHC values of hydrotrope used in this work range between 0.40 and 0.60 mol/L (Table 5),

which seem to depend on the hydrophilicity of a hydrotrope. The C_{max} values of hydrotropes range between 2.20 and 2.40 mol/L (Table 5) in most cases. The highest value of solubilization enhancement factors φ_s, which is the ratio of solubility values in the presence and absence of a hydrotrope has been observed in the case of citric acid as 26.66 at a system temperature of 333 K (Table 6).

3.2 Mass-Transfer Coefficient

The mass-transfer coefficient of methyl benzoate + water system in the absence of any hydrotrope was determined to be 0.92×10^{-5} s^{-1} at 303K (Table 7). The effect of different hydrotropes on the mass-transfer coefficient of methyl benzoate at different hydrotrope concentrations is also given in the same table. It can be seen that a threshold value of 0.40 mol/L is required to effect significant enhancement in the mass transfer coefficient of the methyl benzoate + water system, as observed in the case of solubility determinations. The mass-transfer coefficient of methyl benzoate + water system increases with an increase in citric acid concentration. The maximum enhancement factor for mass-transfer coefficient of methyl benzoate + water system in the presence of citric acid was found to be 23.83(Table 7). A similar trend in the mass-transfer coefficient enhancement (φ_{mtc}) of methyl benzoate has been observed for other hydrotropes also namely urea and nicotinamide. The highest value of φ_{mtc} (23.83) has been observed in the presence of citric acid as hydrotrope at C_{max} of 2.40 mol/L.

3.3. Effectiveness of Hydrotropes

The effectiveness factor of each hydrotrope with respect to methyl benzoate at different system temperatures has been determined by analyzing the experimental solubility data for each case applying the model suggested by Setschenow (1951) and later modified by Pathak and Gaikar (1992), as given by the equation

$$\log[S/S_m]) = K_s[C_s - C_m] \quad (1)$$

where S and S_m are the solubility of methyl benzoate at any hydrotrope concentration C_s and the minimum hydrotrope concentration C_m (same as MHC) respectively. The Setschenow constant K_s can be considered as a measure of the effectiveness of a hydrotrope at any given conditions of hydrotrope concentration and system temperature. The Setschenow constant values of hydrotropes namely citric acid, urea and nicotinamide for methyl benzoate + water system at different system temperatures are listed in Table 8. The highest value has been observed as 0.565 in the case of citric acid as hydrotrope at 333K.

4. Conclusion

The solubility of methyl benzoate, which is practically insoluble in water has been increased to a maximum of 26.66 times in the presence of citric acid as hydrotrope with a corresponding increase in the mass transfer coefficient. This would be useful in increasing the rate of output of the desired product made from methyl benzoate. The MHC and C_{max} values of the hydrotrope with respect to methyl benzoate can be used for the recovery of the dissolved methyl benzoate and hydrotrope solutions at any hydrotrope concentration between the MHC and C_{max} by simple dilution with distilled water. This will eliminate the huge cost and energy normally involved in the separation of the solubilized methyl benzoate from its solution. The unprecedented increase in the solubilizing effect of hydrotropes is attributed to the formation of organized aggregates of hydrotrope molecules at a particular concentration.

References

Agarwal, M.; Gaikar, V. G. (1992). Extractive Separation Using Hydrotropes. *Sep. Technol. 2*, pp.79-84.

Agrawal et al., P. (2004).Hydrotropic Solubilization of nimesulide for parenteral administration. *Int. J. Pharm. 274*, pp. 149-155.

Badwan et al., (1982). The Solubility of Benzodiazepines in Sodium Salicylate Solutions and a Proposed Mechanism for Hydrotropic Solubilization. *Int. J. Pharm. 13*, pp.67-74.

Balasubramanian et al., M. (1989). Aggregation Behaviour of Hydrotropic Compounds in Aqueous Solutions. *J. Phys. Chem. 93*, pp.3865-3870.

Chen, X.; Micheu, J. C. (2002).Hydrotropes Induced Auto Catalysis in the Biphasic Alkaline Hydrolysis of Aromatic Esters. *J. Colloid Interface Sci. 249*, pp.172-179.

Colonia et al., (1998).Phase Relations of *o*and *p* Chlorobenzoic Acids in Hydrotrope Solutions. *J. Chem. Eng. Data .43*, pp.220-225.

Deepak V. Dandekar, G.K. Jayaprakasha, Bhimanagouda S. Patil. (2008). Hydrotropic extraction of bioactive limonin from sour orange (*Citrus aurantium* L.) seeds. *Food Chemistry*, *Volume 109, Issue 3*,pp. 515-520.

Friberg et al., (1996). Reversible Extraction Process of Phenyl Ethyl Alcohol, a Fragrance. *Ind. Eng. Chem. Res. 35*, pp.2856-2859.

Friberg, S. E.; Brancewicz, C. (1994). O/W Microemulsions and Hydrotropes: The Coupling Action of a Hydrotrope. *Langmuir. 10*, pp. 2945-2949.

Gaikar, V. G.; Phatak, P. V. (1999). Selective Solubilisation of Isomers in Hydrotrope Solution o-/p-Chlorobenzoic acids and o-/p-Nitro anilines. *Sep. Sci. Technol. 34*, pp.439-459.

Gaikar, V. G.; Sharma M. M. (1986). Extractive Separation with Hydrotropes. *Solvent Extr. Ion Exch. 4*,pp. 839-846.

John, A. D. (1987).*Lange's Handbook of Chemistry*; McGraw-Hill: New York.

Laura J. Rovetto, Timothy A. Strobel, Carolyn A. Koh, E. Dendy Sloan Jr. (2006*).* Is gas hydrate formation thermodynamically promoted by hydrotrope molecules? *Fluid Phase Equilibria*, Volume 247, Issues 1-2,pp. 84-89.

Laxman, M.; Sharma, M. M. (1990). Reduction of Isophorone with Borohydride: Change in Regio Selectivity with Hydrotropes. *Synth. Commun. 20*, pp.111-117.

Mahapatra et al., (1988). New Strategies in Extractive Distillation; Use of Aqueous Solution of Hydrotropes and Organic Bases as Solvent for Organic Acids. *Sep. Sci. Technol. 23*, pp.429-436.

Miguel G. Neumann, Carla C. Schmitt, Katia R. Prieto, Beatriz E. Goi. (2007*).* The photophysical determination of the minimum hydrotrope concentration of aromatic hydrotropes. *Journal of Colloid and Interface Science*, Volume 315, Issue 2,pp. 810-813.

Nagendra Gandhi et al. (1998). Solubility and Mass Transfer Coefficient Enhancement of Ethyl Benzoate through Hydrotropy. *Hungarian J. Ind. Chem. 26*, pp.63-68.

Nagendra Gandhi et al., (1998). Effect of Hydrotropes on Solubility and Mass-Transfer Coefficient of Butyl Acetate. *J. Chem. Eng. Data.* 43, pp.695-699.

Nagendra Gandhi, N.; Dharmendira Kumar, M. (2000).Effect of Hydrotropes on Solubility and Mass Transfer Coefficient of Amyl Acetate. *Bioprocess Eng*.pp. 449/0116.

Nagendra Gandhi, N.; Dharmendira Kumar, M. (2000). Effect of Hydrotropes on Solubility and Mass Transfer Coefficient of Methyl Salicylate. *J. Chem. Eng. Data 45*, pp.419-423.

Nagendra Gandhi, N.; Meyyappan, N. (2004). Solubility and Mass Transfer Coefficient Enhancement of Benzyl Acetate in Water through Hydrotropy. *J. Chem. Eng. Data. 49*, pp.1290-1294.

Nagendra Gandhi, N.; Meyyappan, N. (2005).Solubility and Mass Transfer Coefficient Enhancement of Benzyl Benzoate in Water through Hydrotropy. *J. Chem. Eng. Data. 50*, pp.796-800.

Neuberg, C. (1916). Hydrotropy. *Biochem. Z. 76*, pp.107-108.

Perry, R. H. (1997). *Perry's Chemical Engineer's Handboo*k, 7th ed.; McGraw-Hill: New York.

Raynaud-Lacroze, P. O.; Tavare, N. S. (1993). Separation of 2-naphthol: Hydrotropy and Precipitation. *Ind. Eng. Chem. Res. 32*, 685-691.

Sara Nicoli, Franca Zani, Stefania Bilzi, Ruggero Bettini, Patrizia Santi.. (2008). Association of nicotinamide with parabens: Effect on solubility, partition and transdermal permeation. *European Journal of Pharmaceutics and Bio pharmaceutics*, Volume 69, Issue 2, pp. 613-62.

Tooru Ooya, Kang Moo Huh, Masato Saitoh, Eiichi Tamiya, Kinam Park (2005*).* Self-assembly of cholesterol-hydrotropic dendrimer conjugates into micelle-like structure: Preparation and hydrotropic solubilization of paclitaxel. *Science and Technology of Advanced Materials*, Volume 6, Issue 5,pp. 452-456.

Table 1. Effect of citric acid concentration (C) on the solubility (S) of methyl benzoate in water

C, mol/L	10^3 S, mol/L			
	T=303 K	T = 313 K	T = 323 K	T = 333 K
0.00	1.43	1.49	1.62	1.81
0.10	1.44	1.54	1.67	1.85
0.20	1.47	1.61	1.72	1.96
0.30	1.48	1.68	1.85	2.01
0.40(MHC)	2.51	3.01	3.36	3.58
0.50	3.20	3.68	4.31	4.72
0.60	3.94	4.61	5.54	6.60
0.70	4.88	5.69	7.01	8.55
0.80	5.70	6.57	8.22	10.52
0.90	6.59	8.11	10.00	12.51
1.00	7.57	9.10	12.00	15.03
1.10	8.48	10.90	14.03	17.11
1.20	9.32	12.40	16.40	20.05
1.30	10.85	14.61	19.10	22.93
1.40	11.83	16.23	21.62	25.46
1.50	13.38	18.21	24.50	28.91
1.60	14.43	20.65	27.53	32.01
1.70	15.62	22.50	30.21	35.50
1.80	17.33	24.70	32.26	38.36
1.90	18.20	25.92	34.15	40.56
2.00	20.11	28.52	36.00	43.62
2.20	21.92	30.95	38.97	46.75
2.40(C_{max})	23.04	32.06	40.20	48.25
2.60	23.09	32.32	40.50	48.28
2.80	23.15	32.35	40.54	48.31
3.00	23.15	32.35	40.65	48.31

Table 2. Effect of urea concentration (C) on the solubility (S) of methyl benzoate in water

C, mol/L	10^3 S, mol/L			
	T=303 K	T = 313 K	T = 323 K	T = 333 K
0.00	1.43	1.49	1.62	1.81
0.10	1.43	1.52	1.71	1.95
0.20	1.44	1.58	1.76	1.97
0.30	1.46	1.69	1.99	2.13
0.40(MHC)	2.48	2.77	3.11	3.42
0.50	3.19	3.87	4.01	4.94
0.60	4.06	4.71	5.38	6.22
0.70	4.94	5.88	6.85	7.71
0.80	5.92	6.72	8.23	9.50
0.90	6.38	8.10	9.85	11.21
1.00	7.67	9.32	11.60	13.12
1.10	8.54	10.61	13.22	15.20
1.20	9.52	12.28	14.96	17.20
1.30	10.64	13.52	17.11	19.73
1.40	12.03	15.41	19.02	22.66
1.50	12.82	16.84	21.47	24.91
1.60	14.32	18.41	23.33	27.78
1.70	15.20	20.08	25.24	30.28
1.80	16.86	21.22	27.73	33.21
1.90	17.25	22.20	28.47	34.59
2.00	19.01	24.25	31.41	37.41
2.20	20.57	26.25	32.93	39.61
2.40(C_{max})	21.72	27.58	34.29	41.05
2.60	21.93	27.65	34.33	41.10
2.80	21.97	27.65	34.35	41.10
3.00	21.97	27.69	34.35	41.11

Table 3. Effect of nicotinamide concentration (C) on the solubility (S) of methyl benzoate in water

C, mol/L	10^3 S, mol/L			
	T=303 K	T = 313 K	T = 323 K	T = 333 K
0.00	1.43	1.49	1.62	1.81
0.10	1.44	1.53	1.73	1.96
0.20	1.61	1.61	1.78	2.01
0.30	1.76	1.72	1.82	2.08
0.40	1.76	1.81	1.91	2.19
0.50	1.81	2.06	2.28	2.34
0.60 (MHC)	2.91	3.38	3.51	3.82
0.70	3.07	3.64	4.08	4.93
0.80	4.25	4.59	5.11	6.12
0.90	5.07	6.01	6.44	7.65
1.00	6.01	6.86	7.93	9.18
1.10	6.93	8.11	9.28	10.71
1.20	7.78	9.34	10.76	12.07
1.30	8.73	10.52	12.36	13.77
1.40	9.63	11.98	13.61	15.63
1.50	10.67	13.03	15.11	17.41
1.60	11.64	14.13	16.41	19.63
1.70	12.60	15.37	18.26	21.20
1.80	13.31	16.45	19.52	22.63
1.90	13.92	17.27	20.33	23.46
2.00	14.62	18.21	21.59	24.54
2.20(C_{max})	15.73	19.43	22.86	25.84
2.40	16.20	19.48	22.92	26.25
2.60	16.22	19.52	22.99	26.28
2.80	16.22	19.55	23.02	26.33
3.00	16.24	19.55	23.05	26.33

Table 5. MHC and C_{max} values of Hydrotropes

Hydrotrope	MHC, mol/L	C_{max}, mol/L
Citric acid	0.40	2.40
Urea	0.40	2.40
Nicotinamide	0.60	2.20

Table 6. Maximum solubilization enhancement factor of (φ_s) methyl benzoate

Hydrotrope	Maximum enhancement factor for solubility (φ_S)			
	T = 303 K	T = 313 K	T = 323 K	T = 333 K
Citric acid	16.08	21.52	24.82	26.66
Urea	15.19	18.51	21.17	22.68
Nicotinamide	11.00	13.04	14.11	14.28

Table 7. Effect of hydrotrope concentration (C) on the mass transfer coefficient (k_{La})of methyl benzoate

Hydrotrope	C, mol/L	(k_{La}), 10^5 s^{-1}	Enhancement factor for mass transfer coefficient (φ_{mtc})
Citric acid	0.00	0.92	-
	0.20	1.68	1.83
	0.40(MHC)	3.14	3.41
	0.60	5.91	6.42
	0.80	7.23	7.86
	1.00	9.44	10.26
	1.20	11.16	12.13
	1.40	12.91	14.03
	1.60	14.04	15.26
	1.80	15.16	16.48
	2.00	16.57	18.01
	2.20	19.44	21.13
	2.40(C_{max})	21.92	23.83
	2.60	22.26	24.19
	2.80	22.51	24.47
	3.00	22.87	24.85
Urea	0.00	0.92	-
	0.20	1.50	1.63
	0.40(MHC)	2.71	2.95
	0.60	4.81	5.23
	0.80	5.98	6.50
	1.00	7.84	8.52

	1.20	9.38	10.19
	1.40	10.94	11.89
	1.60	12.04	13.09
	1.80	13.16	14.30
	2.00	15.28	16.61
	2.20	17.06	18.54
	2.40(C_{max})	18.62	20.23
	2.60	18.87	20.51
	2.80	19.01	20.66
	3.00	19.32	21.00
Nicotinamide	0.00	0.92	-
	0.20	1.38	1.50
	0.40	2.19	2.38
	0.60(MHC)	3.49	3.79
	0.80	4.96	5.39
	1.00	6.03	6.55
	1.20	7.82	8.50
	1.40	9.78	10.63
	1.60	11.14	12.11
	1.80	12.28	13.35
	2.00	13.17	14.32
	2.20(C_{max})	14.42	15.67
	2.40	14.61	15.88
	2.60	14.87	16.16
	2.80	15.06	16.37
	3.00	15.39	16.73

Table 8. Setschenow Constant (K_S) of Hydrotropes with respect to methyl benzoate

Hydrotrope	Setschenow Constant (K_S)			
	T = 303 K	T = 313 K	T = 323 K	T = 333 K
Citric acid	0.481	0.513	0.539	0.565
Urea	0.471	0.499	0.521	0.539
Nicotinamide	0.458	0.475	0.508	0.518
Sodium Salicylate	0.469	0.485	0.512	0.527

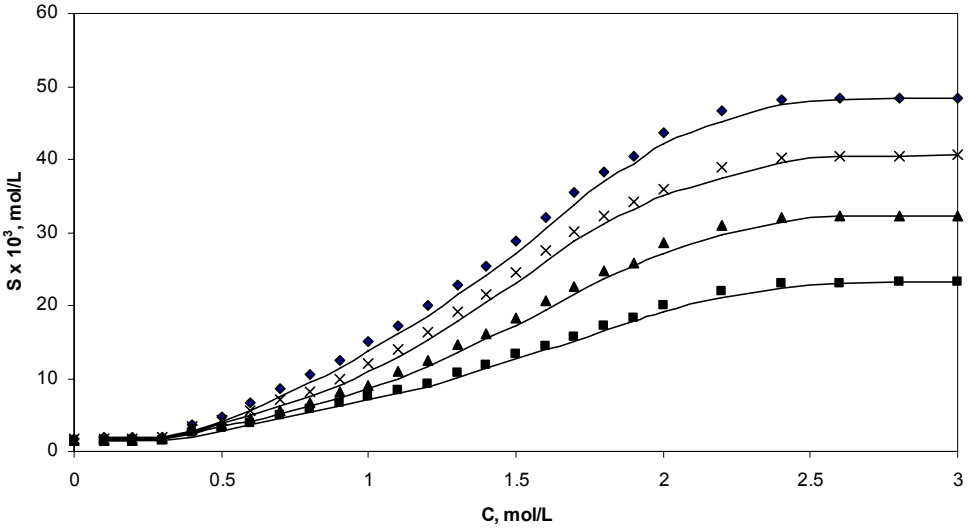

Figure 1. Effect of Citric acid concentration (C) on the solubility (S) of Methyl benzoate in water at different temperatures T=303K (♦), 313K (▲), 323K (×) and 333K (■).

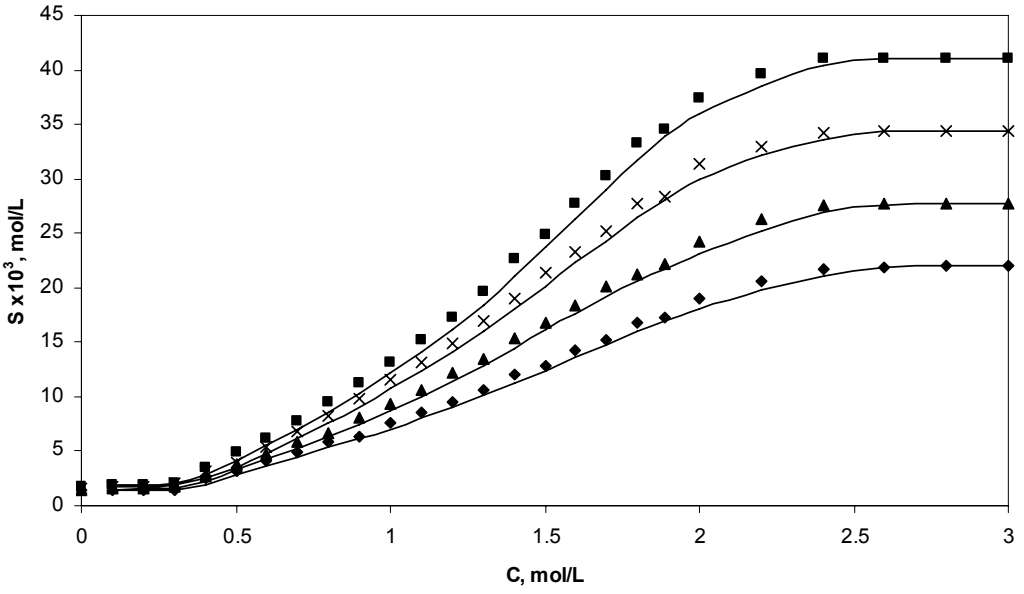

Figure 2. Effect of Urea concentration (C) on the solubility (S) of Methyl benzoate in water at different temperatures T=303K (♦), 313K (▲), 323K (×) and 333K (■).

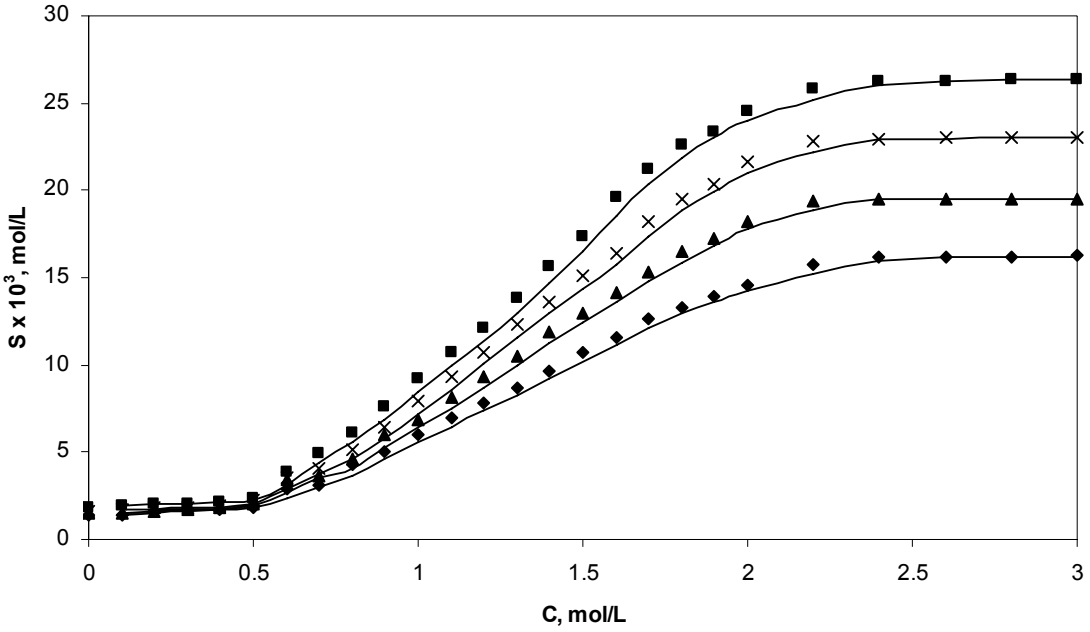

Figure 3. Effect of Nicotinamide concentration (C) on the solubility (S) of Methyl benzoate in water at different temperatures T=303K (♦), 313K (▲), 323K (×) and 333K (■).

Modern Applied Science

www.ccsenet.org/journal.html

Vol. 3, No. 3

March 2009

Curative Effect Observation of Ciprofloxacin Injection in the Treatment of Acute Mastitis on Dairy Cows

Jie Qin & Yanming Sun (Corresponding author)

College of Animal Science & Technology

Shihezi University

Shihezi 832000, China

Abstract

Effects of ciprofloxacin in the treatment of acute mastitis on dairy cows was clinically investigated, penicillin-streptomycin as control. Results showed that cure rate of ciprofloxacin and penicillin-streptomycin on dairy cows was 86.0% and 72.0%, respectively, and in two periods of treatment (6 days) was 72.0% and 30.0%, respectively. Through statistical test, there was significance in cure rate and period of treatment between treatment group and control group, which revealed that ciprofloxacin had the characters of shorter period of treatment and better clinical efficacy.

Keywords: Ciprofloxacin, Dairy cows, Acute mastitis, Curative effect observation

1. Introduction

Mastitis is the most common and most costly disease of dairy cows. Among 1363 ten thousands dairy cows in China, about 40%~70% of cows are infected with such disease. It has been estimated that mastitis costs about 3.16 hundred million yuan per annum. Acute mastitis not only results in a great economic loss, but also causes chronic mastitis subsequently, which makes galactophore tissues fibrosis and udder shrinked. Therefore, it is urgent and significant to seek a drug with high efficacy on the treatment of such mastitis. In the present paper, ciprofloxacin was applied as a drug agent to observe its curative effect.

2. Materials and methods

2.1 Drugs

Ciprofloxacin Lactate (0.5g/ml) was produced by Chengdu Ware Yuanheng Pharmaceutical Co.,Ltd with the batch number of 20070907; Benzylpenicillin sodium for injection (800, 000U) was produced by Jiangsu Nannong Gaoke Animal Pharmaceutical Co., Ltd with the batch number of 20070107; Streptomycin sulfate for injection (1000, 000U) was also produced by Jiangsu Nannong Gaoke Animal Pharmaceutical Co., Ltd with the batch number of 20070526. All these drugs above were purchased from Shihezi veterinary station without further purification.

2.2 Experimental methods

2.2.1 Animals

All dairy cows in the treatment were diagnosed as having acute mastitis in several cattle farms of Kuidun in 2008. Symptoms of cows with acute clinical mastitis were described as follows: Inflammation is characterized by gross abnormalities in the udder (swelling, heat, redness, pain) and change in composition and appearance of milk. Abnormalities in milk may include flakes, clots or a watery appearance. The flakes in the milk are congealed leukocytes, secretory cells and protein.

2.2.2 Allocation of treatment

100 cows infected during experiment were randomly divided into two groups, ciprofloxacin group (treatment group) and penicillin-streptomycin (control group), 50 per group. For ciprofloxacin group, infusion through udder at a dose of 20 ml, once a day, 3 days a period of treatment; For penicillin-streptomycin group, infusion through udder at a dose of 800,000U penicillin and 1000,000U streptomycin together (diluted by normal saline to 50 ml), twice a day, 3 days a period of treatment.

2.2.3 Criterion of curative effect

According to the criterion of Zhou Xuzheng (2007, PP. 44-47), briefed as follows:

Cure: clinical symptoms vanished and the properties, color and yield of milk all recovered to normal.

Validity: clinical symptoms basically vanished with increased milk yield and property and there were still few clots in

the milk.

Invalidation: Clinical symptoms and properties of milk failed to develop improvement apparently, or even worse.

2.2.4 Data analysis

Data were analyzed statistically by the software SPSS 3.0; Valued of $P<0.05$ were regarded as significant.

3. Results

3.1 Curative effect

Cure rate of ciprofloxacin and penicillin-streptomycin in the treatment of acute mastitis on dairy cows was 86.0% and 72.0%, respectively. Through statistical test, it showed that ciprofloxacin group got best efficacy with great significance. The detail results were listed in Table 1.

3.2 Period of treatment

Three days applied as a period treatment, according to specific curative effect, 1 to 3 periods of treatment were performed. Periods of treatment showed great significance between two groups through statistical test, which were listed in Table 2.

4. Discussions

Amongst effects of ciprofloxacin and penicillin-streptomycin in the treatment of acute mastitis on dairy cows, ciprofloxacin showed its best efficacy and penicillin-streptomycin followed. Effect of ciprofloxacin in the present paper basically conformed to the investigation of Zhang Jinhe (2007, PP.36-38).

Research showed that fluoroquinolone consumption was feasible to inhibit DNA synthesis of bacteria and have no crossing drug-resistance. Compared to other antibiotics, it was not susceptible to result in drug-resistance. Ciprofloxacin could accumulate in phagocytic cell, which achieved possibility to kill mastitis pathogens.

As far as period in the treatment of acute mastitis is concerned, the period of ciprofloxacin was shortest with great significance, compared to penicillin-streptomycin. In the present experiment, curative rate of ciprofloxacin in two periods of treatment achieved 72.0% with great significance, compared to 30% of penicillin-streptomycin. Cure rate of ciprofloxacin was 86.0%, and total validity rate was 94.0%. Ciprofloxacin had shorter period of treatment as well. Taken together, ciprofloxacin could be used as a desirable drug agent in the treatment of acute mastitis and developed to further widespread application.

References

Zhang, Jinhe, Han, Min, & Zhao, Suwei. (2007). Clinical Study of Ciprofloxacin Lactate Injection in the Treatment Acute Mastitis on Dairy Cow. *China Dairy Cattle*, 8:36-38.

Zhou, Xuzheng. (2007). The Study of "Ruyuankang" on Treatment Trial of Dairy Cow Mastitis. *Progress in Veterinary Medicine*, 28(2):44-47.

Table 1. Curative effect of two groups on acute mastitis

Curative Effect	Penicillin-streptomycin Group(50)		Ciprofloxacin Group (50)	
	Case Load	(%)	Case Load	(%)
Cure	36	72.0[a]	43	86.0 [b]
Validity	3	6.0[a]	4	8.0[a]
Invalidation	11	22.0[a]	3	6.0[b]
Total validity	39	78.0%[a]	47	94.0%[b]

Table 2. Period of treatment of two groups against acute mastitis

Period of treatment	Penicillin-streptomycin Group(50)		Ciprofloxacin Group (50)	
	Cure Case (%)		Cure Case (%)	
1 period	5	10.0[a]	16	32.0[b]
2 period	10	20.0[a]	20	40.0[b]
3 period	21	42.0[a]	7	14.0[b]

Modern Applied Science

www.ccsenet.org/journal.html

Vol. 3, No. 3

March 2009

Analysis of Malaysian Wind Direction Data Using ORIANA

Siti Fatimah Hassan (Corresponding author)

Centre for Foundation Studies in Science

University of Malaya, 50603 Kuala Lumpur, Malaysia

Tel: 6-013-2508490 E-mail: s_fatimahh@yahoo.com

Abdul Ghapor Hussin

Centre for Foundation Studies in Science

University of Malaya, 50603 Kuala Lumpur, Malaysia

Tel: 6-03-7967-5996 E-mail: ghapor@um.edu.my

Yong Zulina Zubairi

Centre for Foundation Studies in Science

University of Malaya, 50603 Kuala Lumpur, Malaysia

Tel: 6-03-7967-3241 E-mail: yzulina@um.edu.my

Abstract

Of late, analysis of circular variables or directional data have gained much attention as they describe most of the environmental phenomena such as waves, wind gust, tornados and others. Unlike linear data, the availability of statistical software dedicated to analyze of directional data is scarce. Furthermore, the analyses are limited to descriptive summary, point estimation and comparison of means. This could partly due to the difficulty in statistical analysis of circular data because of disparate topologies between circle and straight line. For example, if the angles are recorded in the range $[-\pi, \pi)$ radian or $(0°, 360°]$, then the direction close to the opposite end-points are near neighbours in a metric if we refer to the topology of circle, but maximally distant in linear metric. Thus, the "distance" between 350 and 15 angular degrees is more commonly thought as 25° opposed to the 335° as a standard calculation. In this paper, we describe the analysis of Malaysian wind direction data using the newly improved statistical software, ORIANA designed to analyze circular data. Exploratory data analysis (EDA) based on descriptive statistics, graphical display of the data and comparison of samples are discussed.

Keywords: Directional data, Circular data, ORIANA software, Wind direction

1. Introduction

We come across directional or circular data almost everywhere in applied science. They are widely used in biology, geography, astronomy, meteorology, medicine and many other areas. Data measured in the form of angles or two dimensional orientations is unlike the linear data and it cannot be treated in the same way as linear data. Furthermore, most of the methods used in statistical analysis of linear data cannot be applied in circular data due to different topology between circle and straight line. Thus, the need of analyzing directional or circular data is really indispensable. For the past few years, many new techniques for analyzing circular data have been developed, for example see Fisher (1993), Mardia (2000) and Jammalamadaka (2001). However, these are often computationally intensive and to find the suitable friendly software is always an issue. Researchers in the area of directional statistics are looking for the friendly software like SPLUS and MATLAB that have been widely used for linear data.

2. The ORIANA Software

ORIANA, the statistical software dedicated to the analysis of circular variables, was first introduced on 31st December 2003 and was further upgraded with the latest version issued on 3rd May 2007. In view of the scarcity of commercialize statistical software in the market, the software can be useful for students, researcher, scientists and also medical professional in areas which involve in analyzing circular data. It has a window-based environment with several options in the drop down menu. There are five windows in ORIANA including the main window, status window, data editor, results window, graph windows and notepad. The tutorial guide also provided in ORIANA in order to help users

become familiar with this software. It offers various graphical and analytical analysis as a well as to calculate a variety of the special types of statistics involving the data measured in degrees, time of day or other circular form. Some of the features that available in ORIANA include summary statistics for each sample, one sample test, multi sample test and also correlation between samples. As an illustration, the statistical analysis of Malaysian wind direction data is performed using this software.

3. Malaysian Wind Direction Data

In this study, the data was obtained from Malaysian Meteorological Services Department and it consists of the observations of surface wind at Kuala Lumpur International Airport (KLIA) station. The data was recorded daily in 2005 at time 1200 and was measured by anemometer at location 16.3 m above ground level, latitude 02°44´ N and longitude 101°33´ E. Two sets of data have been considered in this study known as Northeast monsoon data (January and February 2005) and Southwest monsoon data (July and August 2005).

4. Descriptive Statistics of Malaysian Wind Direction Data

4.1 Circular plot

In most exploratory data analysis, graphical representations are often used to summarize the data. ORIANA offers wide range of representation which included rose diagram, circular histogram, raw data plot, arrow data plot and linear histogram. However, the most commonly used types of graph for circular data is the rose diagram. The rose diagram is a histogram displayed in a circle, similarly to the pie chart for linear data. However, each sector represents the frequency or number of observations which falls in the range of angles. The concentric circles show the frequency of the observations for each angular value. Fig. 1 and Fig. 2 show the rose diagram of wind direction for Northeast and Southwest data set respectively. Also shown in the plots are the mean direction of the observation which denoted by thick line running from the center of the diagram to the outer edge and is given by 50° and 240° for Northeast and Southwest data set respectively together with their confidence interval which can be set either at 95% or 99% level.

Another diagrammatical representation available in ORIANA is the circular histogram. The circular histogram as shown in Fig. 3 and Fig. 4 are quite similar to the rose diagram, except that the wedge-shaped in rose diagram become parallel-sided bar that show the number of observations within that class range.

Alternatively, raw data plots are shown in Fig. 5 and Fig. 6 can be used to view the spread of the data and describe the distribution of the data.

Another graph shown in Fig. 7 and Fig. 8 are the arrow graphs and these graphs are similar to rose diagram, but instead of wedge-shaped sector they have arrows to indicate the number of observations for each class.

4.2 Basic statistics for each sample

To complement the graphical analysis, summary statistics are often deployed in the EDA. Similar to any window-based environment, the summary statistics in ORIANA can be obtained from the drop down menu. In other words, from the Analyses menu, drop down to choose Stats... and further to the Statistics dialog box, in which one can choose several summary statistics and statistical tests. For this study, the summary statistics are given as in Table 1.

The summary statistics as shown in Table 1 depicts the following:

- The numbers of observations for this study are 59 and 62 observations for Northeast and Southwest respectively.
- The mean direction (μ) is the direction of the resultant vectors with given corresponding angles and is defined by

$$\mu = \begin{cases} \tan^{-1}\left(\frac{S}{C}\right), & S > 0, C > 0 \\ \tan^{-1}\left(\frac{S}{C}\right) + \pi, & C < 0 \\ \tan^{-1}\left(\frac{S}{C}\right) + 2\pi, & S < 0, C > 0 \end{cases}$$

where $S = \sum_{i=1}^{n} \sin(\theta_i)$ and $C = \sum_{i=1}^{n} \cos(\theta_i)$. For Northeast data, the mean angle is 52.189°, while for Southwest data the mean angle is 247.019°.

- Length of mean vector is defined by $r = \frac{1}{n}\sqrt{C^2 + S^2}$. It is the length of the directions of the resultant vectors at given angles and the range is between 0 and 1. The larger value of *r* implies that the observations are closely clustered around the mean. For this data set, the value of *r* is 0.828 and 0.566 for Northeast and Southwest data set respectively. The value of *r* for Northeast is higher than Southwest and it closer to 1 meaning that the observations for Northeast is clustered closely around the mean as compared to Southwest.

- Median is defined as a direction that divides the data into two equal size groups and in ORIANA the median may be calculated by minimizing the function of $d(\theta) = \pi - \frac{1}{n}\sum_{i=1}^{n}\left|\pi - \left|\theta_i - \theta\right|\right|$. As opposed to linear data, where we can easily find the midpoint between observations as we arranged the data in increasing order. However, for circular data it is rather complicated since the data are in closed curve and can always be rotated around the circle. This has caused a problem on how to choose an appropriate axis on the circular scale. For the given data set, the calculated median is 60° for Northeast data set and 245° for Southwest data set.

- Concentration is denoted by κ and is a parameter that related to von Mises distribution. It is also related to the length of mean vector and the value of κ given by ORIANA is the maximum likelihood estimation of population concentration. A large value of *r* will imply the large value of κ. For this data set, the concentrations are 3.246 and 1.377 for Northeast and Southwest data set respectively.

- Circular variance is the measures of dispersion of circular data. Variance is related to length of mean vector and calculated by using $V = 1 - r$. The values of circular variance for the Northeast and Southwest data set are 0.172 and 0.434 respectively.

- Circular standard deviation is an analogue to linear counterpart but it is calculated in a much different way and is given by $S = \sqrt{(-2\ln(r))}$. The values are 35.236° and 61.137° for Northeast and Southwest data set respectively.

- Standard error of mean are calculated based on the length of mean vector and concentration parameters as well as assuming that the data set follows a von Mises distribution. For the given data set, the standard error of mean is 4.551° and 8.242° for Northeast and Southwest data set respectively.

- Finally, the 95% and 99% confidence intervals are derived from the standard error as for the normal distribution. It is defined as 95% or 99% probability that the true mean vector is greater and less than this value. At 95% confidence interval, the values are between 43.268° and 61.11° for Northeast data set whereas 230.861° and 263.177° for Southwest data set. While at 99% confidence interval, the value is between 40.466° and 63.913° for Northeast data set whereas 225.785° and 268.252° for Southwest data set.

4.3 Testing for uniformity

The samples can be tested whether they are uniformly distributed or otherwise, that is to test whether all directions are equal likely. By using one sample test such as Rayleigh's Uniformity Test where the Z value is calculated simply as $Z = nr^2$, with *n* is the number of observations and *r* is the length of the mean vector**.** A longer mean vector will give larger value of Z and greater concentration of the data around the mean. Thus, the likelihood of the data being uniformly distributed is less. From the test statistics, it gives a Z value of 40.42 with p-value < 0.001 for Northeast data set and 19.857 with p-value < 0.001 for Southwest data set. Hence at 5% significant level, we reject the null hypothesis that the samples were uniformly distributed.

4.4 Comparison between samples

Watson-William F-Test can be used to compare two or more samples to determine if their mean angles differ significantly. The *F* statistic is the same as Fisher's variance ratio statistic which is commonly used in linear statistics. This test assumes that the two samples are independent and drawn at random from a population with a von Mises distribution. It also assumes that the concentrations of the two samples are similar and that they are sufficiently large, normally greater than 2. For this data set, the test statistics give the value of 254.151 and the probability value associated with the null hypothesis is less than 0.001. Hence, null hypothesis can be rejected at 5% significant level implying that the mean directions for the two monsoons are not the same.

5. Conclusion

We found that ORIANA is user friendly software, and proves to be a useful package in analyzing circular data. For EDA, it offers a wide selection of graphical display and descriptive statistics which deemed sufficient in statistical analysis of circular data. Nevertheless it has some limitations. For example, other features that is available for linear data set such as measure of skewness and kurtosis. Further analysis such as statistical inference, probability distribution function and predictive modeling such as regression are also not available in the statistical package. Thus, there is much to be done in developing a more comprehensive analysis of circular data which can be incorporated into the statistical package.

References

Fisher, N. I. (1993). *Statistical Analysis of Circular Data*. Cambridge University Press.

Jammalamadaka, S.R. & SenGupta, A. (2001). *Topics in Circular Statistics*. World Scientific Publishing Co. Pte. Ltd.

Mardia, K. V. & Jupp, P.E. (2000). *Directional Statistics*. John Wiley, Chichester.

ORIANA Software Version 2.02e

Table 1. Summary statistics for each sample

Variable	**Northeast (Jan & Feb)**	**Southwest (July & Aug)**
Data Type	Angles	Angles
Number of Observations	59	62
Data Grouped?	No	No
Group Width (& Number of Groups)		
Mean Vector (μ)	52.189°	247.019°
Length of Mean Vector (r)	0.828	0.566
Median	60°	245°
Concentration	3.246	1.377
Circular Variance	0.172	0.434
Circular Standard Deviation	35.236°	61.137°
Standard Error of Mean	4.551°	8.242°
95% Confidence Interval (-/+) for μ	43.268°	230.861°
	61.11°	263.177°
99% Confidence Interval (-/+) for μ	40.466°	225.785°
	63.913°	268.252°

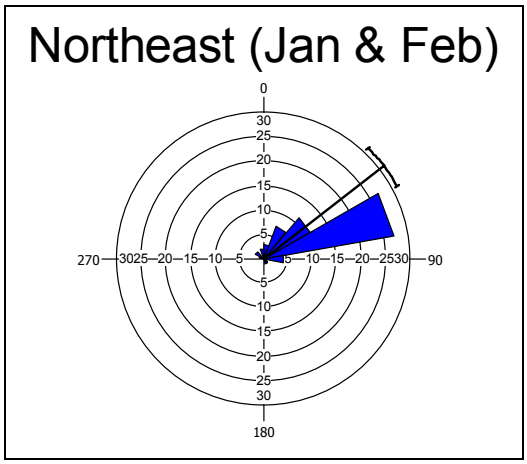

Figure 1. Rose diagram of Northeast data set.

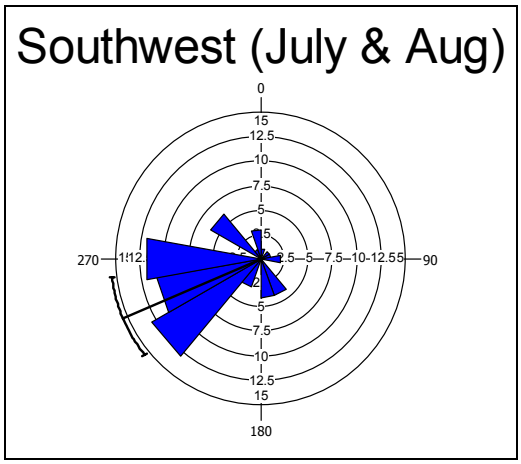

Figure 2. Rose diagram of Southwest data set.

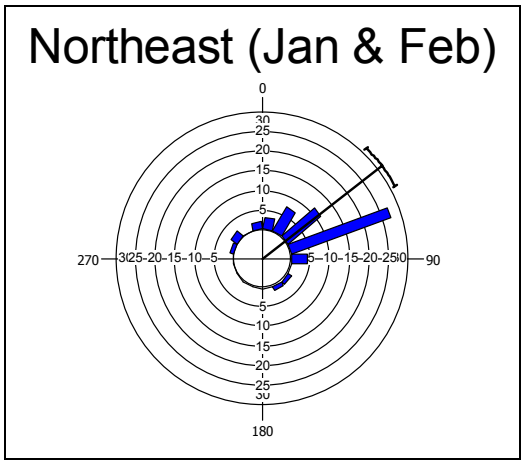

Figure 3. Circular histogram of Northeast data set.

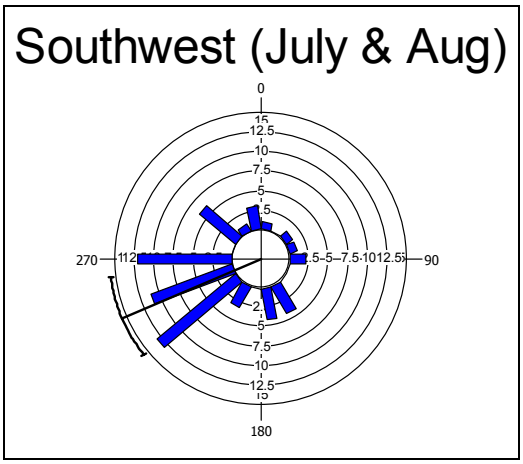

Figure 4. Circular histogram of Southwest data set.

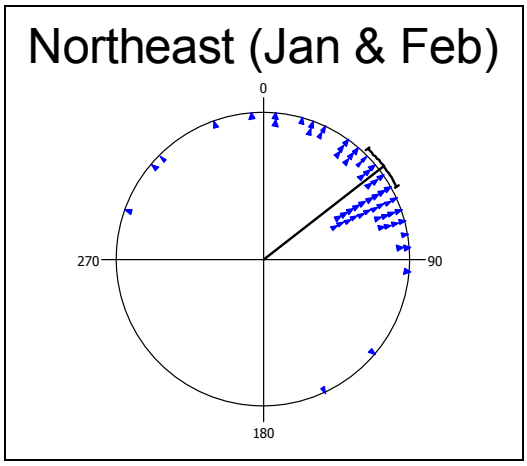

Figure 5. Raw data plot of Northeast data set.

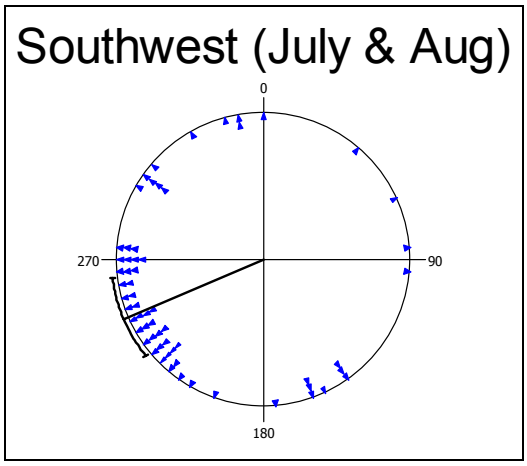

Figure 6. Raw data plot of Southwest data set.

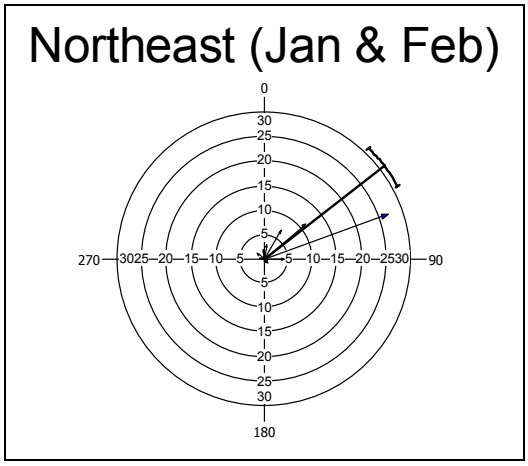

Figure 7. Arrow graph of Northeast data set.

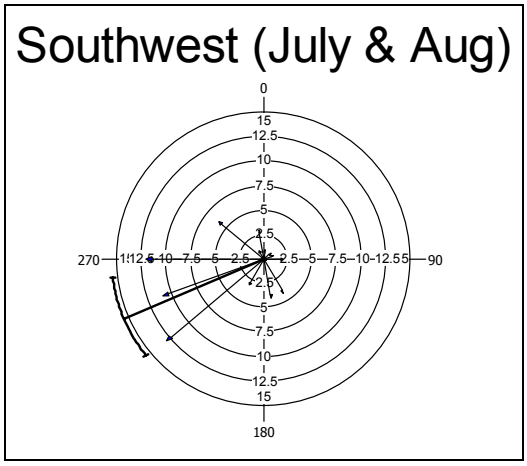

Figure 8. Arrow graph of Southwest data set.

Modern Applied Science

www.ccsenet.org/journal.html

Vol. 3, No. 3

March 2009

Evaluation Analysis on Anti-cracking Performance of Semi-rigid Base Courses Based on Grey Relational Grade

Jinpeng Zhang

Henan Zhongyuan Expressway Co. Ltd.

Zhengzhou 450052, China

Abstract

The theory of grey relational grade was applied to calculate the relational grades between the maximum dry shrinkage strain and some evaluation indices of cracking resistance to dry shrinkage, and the relational grades between the maximum thermal shrinkage strain and some evaluation indices of cracking resistance to thermal shrinkage. The study results indicate that the relation between dry shrinkage energy anti-cracking coefficient and the maximum dry shrinkage strain and the relation between thermal shrinkage energy anti-cracking coefficient and the maximum thermal shrinkage strain of base materials are much better. This paper also draws a conclusion that it is more reasonable to evaluate the anti-cracking performance of semi-rigid base courses adopting dry shrinkage energy anti-cracking coefficient and thermal shrinkage energy anti-cracking coefficient. The conclusion has great direction on the design of bituminous pavements with semi-rigid base courses, and the results also indicate that grey relational analysis is a simple and effective method in the evaluation of anti-cracking performance of semi-rigid base course materials.

Keywords: Grey relational grade, Semi-rigid base, Anti-cracking performance, Evaluation index

1. Introduction

Semi-rigid base course have been applied in high-grade highway widely in China because they have many advantages, such as high strength, better integrity, better water stability and so on. However, with more application of such base courses, their problem of cracking becomes more and more prominent and the problem has affected the performance of highway. Nowadays, great research has been done on the cracking mechanism of semi-rigid base courses all over the world. Generally, the deformation caused by dry shrinkage and thermal shrinkage of semi-rigid base course is thought to be the factor leading to their cracking. And some research has presented some methods to improve the anti-cracking performance of semi-rigid base course materials on the basis of the mechanism of cracking (Zhang, 1991, pp.16-21). Whereas, the research on how to evaluate the anti-cracking performance of semi-rigid base course materials reasonably is very rare. According to the research achievements throughout the world, there are many kinds of evaluation indexes of the anti-cracking performance of semi-rigid base courses. Commonly used evaluation indices are dry shrinkage coefficient and thermal shrinkage coefficient, dry shrinkage anti-cracking coefficient (wet endurance coefficient) and thermal shrinkage anti-cracking coefficient (temperature endurance coefficient), dry shrinkage anti-cracking index (anti dry shrinkage endurance index) and thermal shrinkage anti-cracking index (anti thermal endurance index), dry shrinkage energy anti-cracking coefficient and thermal shrinkage energy anti-cracking coefficient (Yang, 2002, pp.13-15). Among these indices, there isn't a certain answer about how to choose a more reasonable index.

Reasonable evaluation index not only should reflect the deformation ability of semi-rigid materials in tensile stress, but also should reflect the shrinkage performance of materials and it should have better relation with the maximum dry shrinkage, thermal shrinkage strain, which lead to the cracking of materials. Therefore, this essay has analyzed the relation between the anti-cracking indices on dry shrinkage and the maximum dry shrinkage strain and the relation between the anti-cracking indices on thermal shrinkage and the maximum thermal shrinkage strain. Accordingly, the more efficient evaluation indices of semi-rigid base course materials have been decided.

2. Method of grey relational analysis

2.1 Mechanism of grey relational analysis

Grey relational analysis is the important content of grey system theory and it ascertains the difference and proximity among the series through the curve formed by the reference series and the compared series (Wang, 1987). The curve with much closer geometry shape has closer change trend and its relational grade is larger. Relational grade shows how close the compared factor is to the reference factor. The most important influencing factor to the reference factor of the system, which has the largest relation with the reference factor, is found through the calculation of relational grade. Grey relational analysis doesn't need large amount of specimens and model distribution of the data and its calculation is very simple.

2.2 The approach of calculation of grey relational grade

(1) Choose reference series X_0: $X_0 = \{x_0(1), x_0(2), ..., x_0(n)\}$

Comparative series X_i: $X_i = \{x_i(1), x_i(2), ..., x_i(n)\}$, $(i = 1,2,3,..., m)$

(2) Seek for the initial values images of the series. The series , which have different units or initial values, have to be dealt with when doing relational analysis in order to make the series nil-dimension and eliminate the influence of each index dimension. This paper deals with the data applying initializing method. Then, the initial value image is as follow:

$$Y_i = \{y_i(1), y_i(2), ..., y_i(n)\} = \{\frac{x_i(1)}{x_i(1)}, \frac{x_i(2)}{x_i(1)}, ..., \frac{x_i(n)}{x_i(1)}\}, \quad (i = 0,1,2,..., m) \tag{1}$$

(3) Seek for the difference series Δ_i:

$$\Delta_i(k) = |y_0(k) - y_i(k)|, \qquad (i = 1,2,3,..., m), \quad (k = 1,2,3,..., n) \tag{2}$$

$$\Delta_i = \{\Delta_i(1), \Delta_i(2), ..., \Delta_i(n)\} \qquad (i = 1,2,3,..., m)$$

(4) Seek for the relational coefficient $\xi_i(k)$:

$$\xi_i(k) = \frac{\min\limits_i \min\limits_k \Delta_i(k) + \rho \max\limits_i \max\limits_k \Delta_i(k)}{\Delta_i(k) + \rho \max\limits_i \max\limits_k \Delta_i(k)}, \quad (i = 1,2,3,..., m), \quad (k = 1,2,3,..., n) \tag{3}$$

where $\min\limits_i \min\limits_k \Delta_i(k)$ and $\max\limits_i \max\limits_k \Delta_i(k)$ are called dipolar minimum margin and dipolar maximum margin, respectively. ρ is discrimination coefficient whose value is selected from 0 to 1 and is often selected to be 0.5.

(5) Calculating relational grade. In order to concentrate the information in every relational coefficient to be compared easily, we seek for the relational grade γ_i of curve X_i to curve X_0 applying a method of seeking average, which is as follow:

$$\gamma_i = \frac{1}{n}\sum_{k=1}^{n} \xi_i(k) \qquad (i = 1,2,3,..., m), \quad (k = 1,2,3,..., n) \tag{4}$$

3. Grey relational analysis of evaluation index of anti-cracking performance of semi-rigid base course materials

The maximum dry shrinkage strain and the maximum thermal shrinkage strain of semi-rigid base course materials are chosen as reference series to found two grey relational analysis models. The first model regards dry shrinkage coefficient, dry shrinkage anti-cracking coefficient, dry shrinkage anti-cracking index and dry shrinkage energy anti-cracking coefficient of materials as compared series. The second model regards thermal shrinkage coefficient, thermal shrinkage anti-cracking coefficient, thermal shrinkage anti-cracking index and thermal shrinkage energy anti-cracking coefficient of materials as compared series. Table 1 and Table 2 show maximum dry shrinkage strain , the maximum thermal shrinkage strain of several kinds of semi-rigid base course materials and several groups of above-mentioned evaluation index values of anti-cracking performance. The evaluation index values of anti-cracking performance are acquired through the calculating of the experimental data, which comes from reference (Jiang, 2001), by the before-mentioned calculation means. The experimental period is 90 days.

3.1 Grey relational analysis of anti-cracking indexes about dry shrinkage and maximum dry shrinkage strain

After the series in table 1 has been dealt with applying initializing method, we can get the following series of relational coefficients according to Eq. (3). (When calculating: $\rho = 0.5$. After calculating: $\min\limits_i \min\limits_k \Delta_i(k) = 0$, $\max\limits_i \max\limits_k \Delta_i(k) = 0.565$):

$\xi_1 = \{1, 0.613, 0.615, 0.545, 0.400, 0.407\}$

$\xi_2 = \{1, 0.725, 0.670, 0.559, 0.350, 0.412\}$

$\xi_3 = \{1, 0.682, 0.695, 0.712, 0.413, 0.333\}$

$\xi_4 = \{1, 0.956, 0.837, 0.688, 0.413, 0.523\}$

Take upper relational coefficients into Eq. (4), and we can get the following relational grades.

$\gamma_1 = 0.596$ (Relational grade of dry shrinkage coefficient and maximum dry shrinkage strain);

$\gamma_2 = 0.619$ (Relational grade of dry shrinkage anti-cracking coefficient and maximum dry shrinkage strain);

$\gamma_3 = 0.639$ (Relational grade of dry shrinkage anti-cracking index and maximum dry shrinkage strain);

$\gamma_4 = 0.736$ (Relational grade of dry shrinkage energy anti-cracking coefficient and maximum dry shrinkage strain).

The corresponding relational grades series is: $\gamma_4 > \gamma_3 > \gamma_2 > \gamma_1$. This indicates that dry shrinkage energy anti-cracking coefficient has best relativity with the maximum dry shrinkage strain of semi-rigid base course materials. Therefore, we can evaluate the resistance to dry shrinkage cracking of semi-rigid base course materials applying dry shrinkage energy anti-cracking coefficient.

3.2 Grey relational analysis of anti-cracking indice3 about thermal shrinkage and maximum thermal shrinkage strain

After the series of table 2 has been dealt with applying initializing method, we can get the series of relational coefficients according to Eq. (3). (When calculating: $\rho = 0.5$. After calculating: $\min_i \min_k \Delta_i(k) = 0$, $\max_i \max_k \Delta_i(k) = 0.479$):

$\xi_1 = \{1,0.589,0.582,0.348,0.508,0.361\}$

$\xi_2 = \{1,0.494,0.789,0.454,0.360,0.385\}$

$\xi_3 = \{1,0.699,0.464,0.523,0.333,0.418\}$

$\xi_4 = \{1,0.905,0.360,0.446,0.937,0.923\}$

Take upper relational coefficients into Eq. (4), and we can get the following relational grades.

$\gamma_1 = 0.565$ (Relational grade of thermal shrinkage coefficient and maximum thermal shrinkage strain);

$\gamma_2 = 0.580$ (Relational grade of thermal shrinkage anti-cracking coefficient and maximum thermal shrinkage strain);

$\gamma_3 = 0.573$ (Relational grade of thermal shrinkage anti-cracking index and maximum thermal shrinkage strain);

$\gamma_4 = 0.762$ (Relational grade of thermal shrinkage energy anti-cracking coefficient and maximum thermal shrinkage strain).

The corresponding relational grades series is: $\gamma_4 > \gamma_2 > \gamma_3 > \gamma_1$. This indicates that the thermal shrinkage energy anti-cracking coefficient has best relativity with the maximum thermal shrinkage strain of semi-rigid base course materials. Therefore, we can evaluate the resistance to thermal shrinkage cracking of semi-rigid base course materials applying thermal shrinkage energy anti-cracking coefficient.

4. Conclusions

There are many evaluation indices of anti-cracking performance of semi-rigid base course materials nowadays. This essay introduces several kinds of common evaluation index systems simply, and calculates the grey relational grades of anti-cracking indices about dry shrinkage and maximum dry shrinkage strain, and the grey relational grades of anti-cracking indices about thermal shrinkage and maximum thermal shrinkage strain through examples by applying grey relational analysis method. The analytic result shows that the evaluation index system of dry shrinkage energy anti-cracking coefficient and thermal shrinkage energy anti-cracking coefficient, witch is based on dry shrinkage energy, thermal shrinkage energy and limit anti tensile energy, can well evaluate the anti-cracking performance of semi-rigid base course materials. The same semi-rigid base course materials may have different resistance to dry shrinkage cracking or to thermal shrinkage cracking. Therefore, we should take the dry shrinkage energy anti-cracking coefficient and thermal shrinkage energy anti-cracking coefficient into account synthetically when evaluating the anti-cracking performance of semi-rigid base course materials.

References

Deng, Julong. (1987). *Elementary method of grey system*. Wuhan: Huazhong University of Technology Press.

Jiang, Yingjun. (2001). *Study on the prevention and cure measure of shrinkage crack of the stable crushed stones base course of cement*. Xi'an: Master degree dissertation of Chang'an University.

Yang, Honghui and Tang, xian, et al. (2002). Evaluation method for anti-cracking performance of semi-rigid base

course. *Journal of Chang'an University (Natural Science Edition)*, 22 (4), 13-15.

Zhang, Dengliang and Zheng, Nanxiang. (1991). On the anti-shrinkage cracking performance of semi-rigid base course materials. *China Journal of Highway and Transport*, 4 (1), 16-21.

Table 1. The values of anti-cracking indices about dry shrinkage of semi-rigid materials

Semi-rigid materials	Maximum dry shrinkage strain (10^{-6})	Dry shrinkage coefficient(10^{-6}/%)	Dry shrinkage anti-cracking coefficient (%)	Dry shrinkage anti-cracking index	Dry shrinkage energy anti-cracking coefficient (%)
Cement stabilized macadam A	120	27.27	4.95	0.87	4.33
Cement stabilized macadam B	111	30.08	4.05	0.92	3.95
Cement fly ash stabilized macadam A	141	27.22	5.13	1.13	4.85
Cement fly ash stabilized macadam B	132	23.56	4.34	0.86	4.21
Lime-fly ash macadam A	197	33.22	5.53	1.08	5.33
Lime-fly ash macadam B	185	30.84	5.64	0.85	5.56

Table 2. The values of anti-cracking indices about thermal shrinkage of semi-rigid materials

Semi-rigid materials	Maximum thermal shrinkage strain (10^{-6})	Thermal shrinkage coefficient (10^{-6}/°C)	Thermal shrinkage anti-cracking coefficient (°C)	Thermal shrinkage anti-cracking index	Thermal shrinkage energy anti-cracking coefficient (°C)
Cement stabilized macadam A	672.6	9.52	14.18	0.88	1.97
Cement stabilized macadam B	680.3	11.21	10.86	0.98	2.04
Cement fly ash stabilized macadam A	652.2	10.87	12.84	0.61	2.75
Cement fly ash stabilized macadam B	674.1	13.81	10.12	0.69	2.56
Lime-fly ash macadam A	880.2	14.67	12.53	0.73	2.61
Lime-fly ash macadam B	843.5	15.97	12.35	0.81	2.43

Modern Applied Science

www.ccsenet.org/journal.html

Vol. 3, No. 3

March 2009

Experimental Investigation on the Effects of Audible Sound to the Growth of *Escherichia coli*

Joanna Cho Lee Ying

School of Science and Technology, Universiti Malaysia Sabah

Lock Bag 2073, 88999 Kota Kinabalu, Sabah, Malaysia

E-mail: joanna_252@yahoo.com

Jedol Dayou

Vibration and Sound Research Group (VIBS), Universiti Malaysia Sabah

Lock Bag 2073, 88999 Kota Kinabalu, Sabah, Malaysia

Tel: 60-88-320-302 E-mail: jed@ums.edu.my

Chong Khim Phin (Corresponding author)

School of Sustainable Agriculture, Universiti Malaysia Sabah

Lock Bag 2073, 88999 Kota Kinabalu, Sabah, Malaysia

Tel: 60-88-325-655 E-mail: chongkp@ums.edu.my

Abstract

In this paper, we report an experimental result regarding the effects of audible sound on the growth of *Escherichia coli* (*E. coli*). Standardized *E. coli* suspensions of fixed concentration were used for inoculation throughout the experiment in nutrient agar (NA) and nutrient broth (NB). First, the samples were incubated at 37ºC for three hours in a water bath-shaker for NB and in a conventional oven for NA. The samples were then transferred to an acoustic chamber JedMark LV-1 with given sound treatment at controlled temperature of 24±2ºC for five hours for NB and 16 hours for NA. Three different tonal frequencies were selected for sound treatment in this experiment which is 1 kHz, 5 kHz and 15 kHz. The growth of E. coli was assessed by their cell number through indirect viable cell counts (*E. coli* on NA) and direct viable cell counts (*E. coli* on NB), after the incubation with sound in the acoustic chamber. We found that all selected frequencies were able to promote the growth of *E. coli*. In particular, the tonal sound of 5 kHz gave significant increase in cell number of *E. coli* for both growth media.

Keywords: *Escherichia coli*, Audible sound wave, Plate count, Direct microscopic count

1. Introduction

Mechanical waves have been shown to have effect on microbes. Ultrasound for example, has been used for sterilizing and killing unwanted bacteria due to thinning of cell membranes, localized heating and production of free radicals (Piyasena et al., 2003). Ultrasound is able to inactivate bacteria and deagglomerate bacterial clusters or flocks through a number of physical, mechanical and chemical effects arising from acoustic cavitations (Joyce et al., 2003). However, certain frequency of ultrasound was found to increase the growth rate of bacteria cells such as *E. coli, Staphylococcus epidermidis* and *Pseudomonas aeruginosa* cells adhered to and grew on a polyethylene surface (Pitt and Ross, 2003). Ultrasound technology is relatively expensive to be used for large scale microbiological decontamination or production. The consideration of the amount of energy inputs and its cost must be first carried out if this technology is put to be used (Hao et al., 2004). A more affordable alternative way using audible sound wave may sound practical, and there have been some evidences for this possibility. Matsuhashi *et al.* (1998) for example, had found that audible sound and ultrasound waves between 6 kHz to 40 kHz can induce colony formation of *Bacillus carbophilus* grown on non-permissive media. In this paper, the effect of audible sound of certain frequencies to *E. coli* is investigated as a compliment to the application of ultrasound. The effect is assessed based on the comparison in their cell number, through direct and indirect viable cell counts, with their respective control samples.

2. Materials and methods

2.1 Esherichia coli

The investigation on the effects of audible sound to *E. coli* was carried out in two modes - on the *E. coli* that was inoculated on NA and on the *E. coli* that was inoculated on NB medium. The *E. coli* on NA was used for indirect viable cell count using plate counts whereas the *E. coli* on NB was used for direct viable cell counts using a haemocytometer. *E. coli* was obtained from previous stock cultured at Microbiology Lab, Universiti Malaysia Sabah and maintained on NA plate (medium) at 37ºC for 24 hours in an oven. The medium was prepared by suspending 10g of NA in 500ml distilled water and was autoclaved to sterilize at 121ºC for two hours. This is the secondary cultured *E. coli* to be used to prepare samples in the experiment.

2.2 Innoculation

Eight NB and six NA media were prepared in this experiment. The NB medium was prepared by suspending 4g of NB in 500ml distilled water and autoclaved to sterilize at 121ºC for two hours whereas NA medium was prepared in the same way described previously. Single colony of *E. coli* from the secondary culture was transferred to each NB mediums which was prepared in screwed-capped bottles. The remainder of the secondary cultured *E. coli* was diluted ten-folds and then divided into eight for inoculation on NA which was prepared on petri dishes.

2.3 Incubation of the samples

The NB samples were incubated in water bath-shaker at 100 rotations per minute at 37^{o}C for 3 hours and the NA samples with *E. coli* were incubated in conventional oven also at 37^{o}C for 3 hours. After the incubation, the samples were then transferred to an acoustic chamber JedMark LV-1 (Figure 1) for sound treatment through the opening. The chamber which is made of thick glass, is air tight when in operation and equipped with three ultraviolet lamps for fully sterilizing the inner part of the chamber before the treatment carried out. The chamber was also installed with a loudspeaker connected to a function generator so that tonal frequency of sound can be generated. The samples were exposed to sound for five hours at frequency of 1 kHz, 5 kHz and 15 kHz for sound treatment. For each selected frequency, two NA and NB samples were exposed simultaneously whereas two control samples was maintained without sound treatment as reference as reference. During the treatment process, the temperature was maintained at 24±2ºC.

2.4 Measurements

Soon after the exposure, direct *E. coli* cell counts was performed on NB samples using haemocytometer whereas indirect cell counts was carried out on NA samples using plates counts technique. The same *E. coli* cell counting method was performed on the respective control medium type. In the direct cell counts, trypan blue (0.4% w/v) was used to stain dead cells (stained dark blue and immobile). In indirect cell counts, the number of viable colonies growth on NA plates was counted with the assumption that the number of *E. coli* cells is proportional to the number of colonies formed on the media which is measured in colony forming unit per milliter, CFU.

3. Results and discussion

3.1 Direct viable cell count

As previously mentioned, direct viable cell counts method was used to determine the number of viable *E. coli* cell on the NB samples using a hemocytometer. Throughout the experiment, less than one percent of dead cells were found in each NB samples. It was found that sound treatment at all selected frequencies have increased the number of viable cells compared to the control samples. Sound treatment at 1 kHz for example was found to increase the average number of viable cells to 3.97 x 10^8 cells per ml, 4.98 x 10^8 cells per ml for the sound at 5 kHz and 4.83 x 10^8 cells per ml for the sound at 15 kHz. These increases are equivalent to 7%, 34% and 30.5% for the sound treatment at 1 kHz, 5 kHz and 15 kHz, respectively, compared to the average number of viable cells found on the control sample which is only 3.70 x 10^8 cells per ml. The cell number for this direct viable cell counts is given in Figure 2. From the observations, sound treatment at 5 kHz found to give the most significant increases in the number of viable cells followed by the sound at 15 kHz and 1 kHz.

3.2 Indirect viable cell count

Indirect viable cell counts (or plate counts) was performed to determine the viable *E. coli* cells on NB samples using ordinary microscope. The assumption is each *E. coli* cell give rise to one colony, and therefore the indirect viable cell count is measured in colony forming unit per milliter, CFU. As in the direct viable cell count, it was found that sound treatment at all selected frequencies also have increased the CFU of *E. coli* (and so the number of *E. coli* cells). Sound treatment at 1 kHz for example increased the average CFU to 1.75 x 10^9 compared to only 1.69 x 10^9 CFU for the control sample. On the other hand, sound treatment at 5 kHz and 15 kHz gave rise to uncountable colony. However, visual inspection shows that sound treatment at 5 kHz gave higher value of CFU compared to frequency 15 kHz. The resultant increased for the sound treatment at 1 kHz is 3.5% compared to the control samples. The mean of *E. coli* CFU is shown in Table 1 whereas Figure 3 represents the visual inspection of the samples. In Table 1 and Figure 3, the mean

number of CFU for 5 kHz and 15 kHz sound treatments were simply given so that they can be distinguished.

4. Conclusion

In this paper, we presented the result of an experimental investigation on the effects of audible sound to the growth of *E. coli* inoculated on NA and NB media. We found that all selected frequencies (1 kHz, 5 kHz and 15 kHz) have increased the number of viable cells of the bacteria. This shows that the bacteria react positively to the given sound treatment which results in the growth of the number of the bacteria cells. However, the degree of their respond is different to a different sound frequency. This is consistence with the finding reported by other researchers. In this experiment, we found that *E. coli* on NA and NB responded more to sound at frequency 5 kHz compared to other frequencies. This shows that *E. coli* has selective frequency response towards sound treatment.

References

Hao, H., Wu, M., Chen, Y., Tang, J. & Wu, Q. (2004) Cavitations mechanism in cyanobacterial growth inhibition by ultrasonic irradiation. *Colloids and Surfaces*, 33(3-4):151-156.

Joyce, E., Phull, S.S., Lorimer, J.P. & Mason, T.J. (2003). The development and evaluation of ultrasound for the treatment of bacterial suspensions. A study of frequency, power and sonification time on cultured bacillus species. *Ultrasonics Sonochemistry,* 10(6):315-318.

Matsuhashi, M., Pankrushina, A.N., Takeuchi, S., Ohshima, H., Miyoi, H., Endoh, K., Murayama, K., Watanabe, H., Endo, S., Tobi, M., Mano, Y., Hyodo, M., Kobayashi, T., Kaneko, T., Otani, S., Yoshimura, S., Harata, A. & Sawada, T. (1998). Production of sound waves by bacterial cells and the response of bacterial cells to sound. *Journal of General Applied Microbiology* , 44**:** 49-55.

Pitt, W.G. & Ross, S.A. (2003).Ultrasound Increases the Rate of Bacterial Cell Growth. *Biotechnology Progress*, 19(3):1038-1044.

Piyasena, P., Mohareb, E. & McKellar, R.C. (2003). Inactivation of microbes using ultrasound: A review. *International Journal of Food Microbiology*, 87(3):207-216.

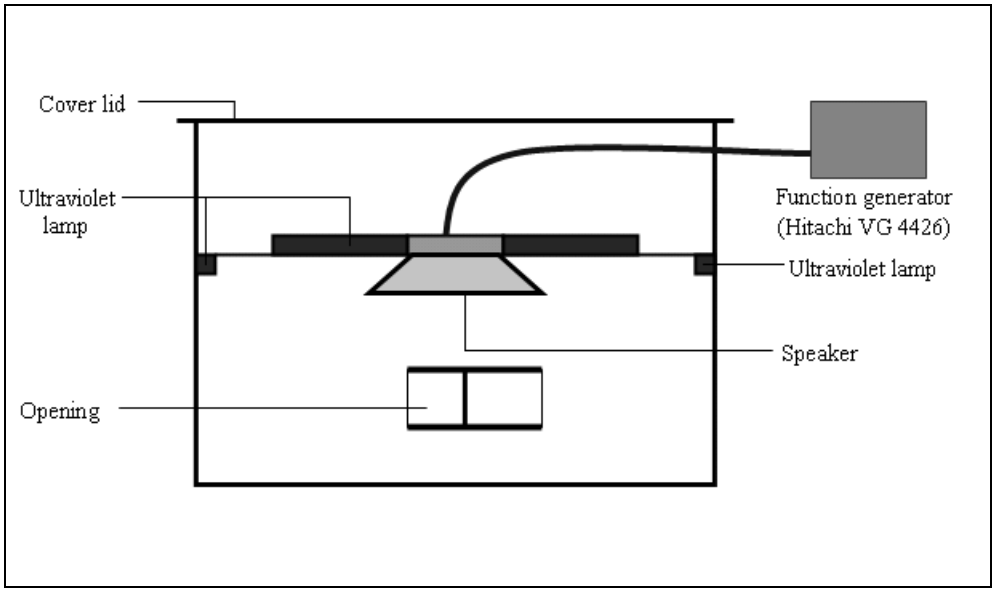

Figure1. Schematic diagram of the JedMark LV-1 acoustic chamber

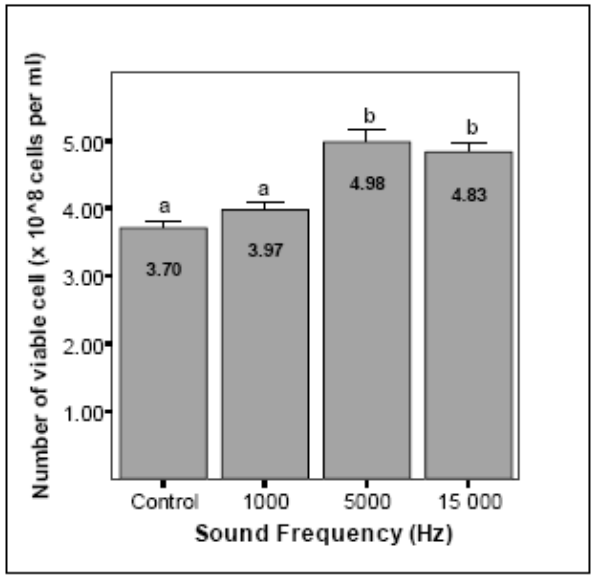

Figure 2. Viable *E. coli* cell count (x10^8 cells per ml) for different sound treatments

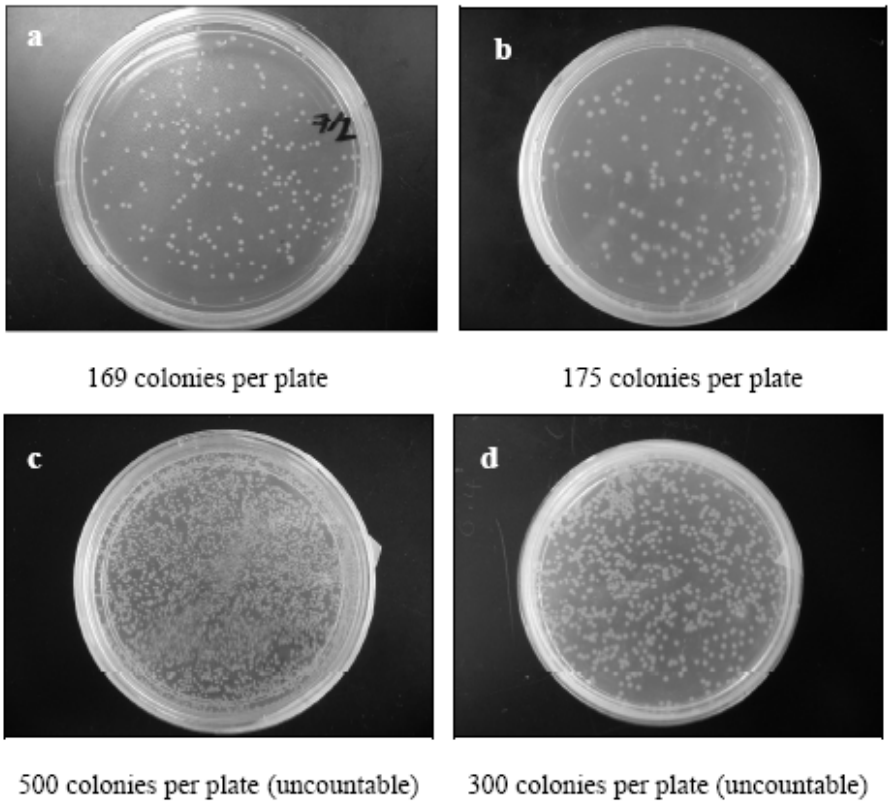

Figure 3. Number of colony per plate for the different sound treatments.
(a) Control, (b) 1kHZ, (c) 5 kHZ and (d) 15kHZ

Modern Applied Science

www.ccsenet.org/journal.html

Vol. 3, No. 3

March 2009

Study on the Free-positioning of ETS in the PDL Track Surveying System

Hongtao Zhu, Weijun Wu & Zhiyong Wang

School of Mechanical and Electrical Engineering

Nanchang University

Nanchang 330031, China

E-mail:wwjott@163.com

Abstract

The station positioning by the electric total station (ETS) is the first step which must be done for the passenger dedicated line track survey and one of the important factors which influence the final surveying precision. To enhance the surveying efficiency and surveying precision, we study the principles and methods of free positioning by ETS.

Keywords: Passenger dedicated line (PDL), Electronic total station (ETS), Free-station positioning

1. Introduction

The PDL track surveying system adopts ETS to survey the 3D coordinate of the track, and the positioning of ETS is the necessary work before the normal survey, and the resection method is generally adopted. This positioning method doesn't require the position of the ETS which can be freely set on one side of the track or the centre of the track, so it is also called the free-positioning method. When freely positioning, ETS will observe the prism on the control foundation pile point (CPIII) with compulsory centering device, and we can obtain the side length and the angle between the ETS and prism point. According to the principle of the free positioning, we only need survey two foundation pile points to confirm the station coordination and back sight direction of ETS. But according to the precision requirements of the permanent CPIII control net (the relative precision of the plane is $\pm 1mm$, and the relative precision of the altitude is $\pm 0.5mm$) (Chinese Ministry of Railway, 2006), comprehensively considering the surveying precision index of ETS (0.5″, 1+1ppm) (Fan, 2003), the surveying uncertainty can not fulfill the position precision of the track 3D coordinate surveying (the precision usually should be controlled in $\pm 1.0mm$) only through observing two foundation pile points. So in the actual project, we usually adopt the surplus surveying (such as 8~12 points), the set collection surveying and other measures to enhance the positioning precision through error compensation. The cost is to add the surveying workload and reduce the efficiency of the positioning. The research of the free positioning of ETS is to utilize the auto-collimating function of ETS, control the autorotation, object searching, auto-surveying of ETS by the software, and realize the high-efficient and precise auto-survey of ETS to the surplus observation and set collection without human operation.

2. Basic principles of ETS for free positioning

When freely positioning, after ETS levels off and achieves stable, a self surveying coordinate system has existed in ETS, but this coordinate system is not relative with the coordinate system which the control foundation pile points are located. So the precondition of free positioning is to implement cursory positioning by manual surveying and obtain the station coordinates of ETS in the control foundation pile net coordinate system and the selected horizontal reference angle Ah_0, and establish the conversion relationship between two coordinate systems and settle bases for the autorotation and collimation and survey of ETS controlled by the software.

The resection computation formulas of the station coordinates of ETS are

$$x_0 = x_1 + (x_2 - x_1) \times L + (y_2 - y_1) \times H$$

$$y_0 = y_1 + (y_2 - y_1) \times L + (x_2 - x_1) \times H$$

$$z_0 = \frac{(z_1' - z_1 + z_2' - z_2)}{2}$$

$$Ah_0 = \arctan(\frac{y_1' - y_0}{x_1' - x_0})$$

where, $L=\frac{(s_1^2+s_0^2-s_2^2)}{2\times s_0^2}$, $H=\sqrt{s_1^2/(s_0^2-L^2)}$, $s_0=\sqrt{(x_1-x_2)^2+(y_1-y_2)^2}$, $s_1=\sqrt{x_1^2+y_1^2}$, $s_2=\sqrt{x_2^2+y_2^2}$, $(x_1',\ y_1',\ z_1')$ and $(x_2',\ y_2',\ z_2')$ respectively are the surveying coordinates of the foundation pile point 1 and the foundation pile point 2 under the coordinate system of ETS, (x_1, y_1, z_1) and (x_2, y_2, z_2) respectively are the appointed coordinates of the foundation pile point 1 and the foundation pile point 2 under the geodetic coordinate system, and (x_0, y_0, z_0) is the station coordinate computed by the resection method.

The requirement of free positioning is that ETS implements automatic surveying for the surplus surveys and set collection surveys and obtains the station coordinates with high precision through strict error compensation. And its basic principle induces four aspects.

(1) The route layout of free positioning

ETS adopts the mode of P2P to survey the appointed foundation pile points when freely positioning, and its route can rotate according to certain direction or selected sequence. The precondition quickly turning from one appointed surveying point to the next surveying point is that the position of the surveyed point can be confirmed. So, the free positioning software picks up the 3D coordinates under the geodetic coordinate system in the database according to the next surveyed foundation pile number, and confirms the horizontal angle and the vertical angle of the surveyed foundation pile prism point under the survey system of ETS through coordinate conversion.

Taking the computation of the horizontal angle of the *i*'th prism point as the example, through the coordinates of the stations of ETS, the selected back sight datum mark and the searched foundation pile point, we can obtain the horizontal deflection angle of the researched point relative to the back sight datum mark Ah_i.

$$Ah_i=\arctan(\frac{y_i-y_0}{x_i-x_0})-\arctan(\frac{y_1-y_0}{x_1-x_0})\{0\le Ah_i\le 2\times\pi\}$$

Ah_i+Ah_0 is the horizontal angle of the *i*'th prism point in the coordinate system of ETS.

The computation method of the vertical angle is simple, and it needs not to compute the benchmark angle like the horizontal angle because it only needs to select the 0^0 of the zenith angle as the vertical benchmark angle, so the vertical angle Av_i is

$$Av_i=\arctan(\frac{\sqrt{(x_i-x_0)^2+(y_i-y_0)^2}}{z_i-z_0}\{0\le Av_i\le 2\times\pi\}$$

After confirming the horizontal rotation angle Ah_i and the vertical rotation angle Av_i, we can find out the surveyed point.

(2) The implementation of the manual working of ETS

We can start the automatic search function of ETS to make ETS to collimate the surveyed point and automatically complete survey and data upload.

ETS turns to the surveyed point by the mode of P2P, and considering the station coordination of the primary position of ETS is not exact enough, and the errors exist between the actual position of the foundation pile prism point and its theoretical position, we should control ETS to quickly search the prism in a small appointed search range taking the direction as the centre through orders.

To enhance the nicety of the rotation and the efficiency of the search, after survey one foundation pile point, we should add the survey result into the surveyed data, and recomputed the station coordinate of ETS through error compensation to make the coordinate precision of the station gradually enhanced.

(3) Set collection survey

To eliminate or reduce the survey error of ETS direct telescope or reverse telescope, we need to adopt one set collection survey or multiple set collections survey. When computing the error compensation, we should take the average value of the direct telescope or reverse telescope of every set collection as the final survey data. And the data formats of different brand ETS may be different, for example, the once set collection average of Topcon ETS is the half of the difference between the direct telescope survey value and the reverse telescope survey value, and the once set collection average of Leica ETS is the half of the sum of the direct telescope survey value and the reverse telescope survey value.

(4) Computation of the station coordinates

According to the results of the surplus survey and multiple set collection survey of ETS, the error equation listed through the indirect error compensation method is (You, 1991)

$$V_{si}=\cos\alpha_i dx_p+\sin\alpha_i dy_p+l_i$$

$$V_{\gamma j} = \left(\frac{\rho}{S_j} \sin \alpha_i + \frac{\rho}{S_{j+1}} \sin \alpha_{i+1} \right) dx_p + \left(\frac{\rho}{S_j} \cos \alpha_i + \frac{\rho}{S_{j+1}} \cos \alpha_{j+1} \right) dy_p + \omega_j$$

$$l_i = S_i^0 - S_i$$

$$\omega_j = \gamma_j^0 - \gamma_j$$

$$i = 1, 2 \cdots 8$$

$$j = 1, 2 \cdots 7$$

Where, α_i is the coordinate azimuth angle approximation from the point *i* to P, S_i is the survey value of the *i*'th side, S_i^0 is the approximation of the *i*'th side, γ_j is the survey value of the included angle between the *j*'th side and *j+1*'th side, γ_j^0 is the approximation of the included angle between the *j*'th side and *j+1*'th side, S_i^0 and γ_j^0 can be obtained through the back calculation of the approximate coordinates of the station.

So we can obtain the matrix equations set, $V_{n\times 1} = B_{n\times 1} \cdot \delta X_{t\times 1} + l_{n\times 1}$ (n=15, t=2), and it is the consistent equations which have two undetermined correction quantities and 15 unknowns, and there are 17 undetermined quantities and 15 equations, so the equations set has infinite groups of solution (Zhu, 2006).

$$P = \begin{pmatrix} P_{S1} & 0 & \cdots & 0 \\ 0 & \ddots & & \\ & & P_{S8} & \vdots \\ \vdots & & P_{\gamma 1} & \\ & & & \ddots \ 0 \\ 0 & \cdots & 0 & P_{\gamma 7} \end{pmatrix}$$

According to the free extremum of function, when $V^T PV = \min$, we can seek the unique solution. So we can obtain $B^T PV = 0$, and to find the solution of the equation, we must confirm the matrix P. According to the survey principle of ETS (Fan, 2003), the surveying angles and the surveying sides are independent, so the weight matrix P is a diagonal matrix of 15×15, and P_{Si} is the weight value of the surveying side.

Based on that, we can utilize the matrix inverse or the solution of Gauss equation to solute all unknown quantities such as V_{si}, $V_{\gamma i}$, dx and dy. So we can obtain the final position coordinate.

$$\begin{cases} x = x_0 + dx \\ y = y_0 + dy \end{cases}.$$

3. Intellectualization of ETS for free positioning

The intellectualization of ETS for free positioning is mainly embodied in two aspects. First, it can make the system interface to be more humanism and adopt different operation habits, and further simplify the operation. Second, the system can timely reflect the abnormal instances in the process of free positioning and implement proper disposals or offer clues for the emergency disposal.

For the system interface and the function design, the convenience of operation and the perfection of the function are two important indexes of the system, and to avoid the complexity of the operation when perfecting the function is one of the important intellectualization directions of ETS for free positioning, and we should try to reduce the operation times and approaches, strengthen the aim and navigation of the operation, and make operators more relax.

At the same time, abnormal instances will occur in the free positioning unavoidably, and if the program has not preplans for the usual abnormal instances, it will influence the precision of the station, even make the positioning failed. To ensure free positioning of ETS with high quality and high efficiency, we have to efficiently capture and dispose these abnormal instances in time.

The abnormal instances which might occur in the free positioning include following instances at least.

(1) Prism identification

Because the track foundation pile net is set along both sides of the line, so when searching the selected station prism,

other prisms might exist around the search sight line, and the wrong object always be found after searching and locking the prism. If the program could not judge this instance, though the positioning process can be completed, but the final residual error will largely exceed the anticipation, and the positioning will fail.

Another instance is that when manual surveying the former two foundation-pile points, if the actual surveying target doesn't match with the predetermined target (for example, the foundation-pile 1 and the foundation-pile 2 are selected, but the prism 1 and the prism 3 are surveyed), the prism search of ETS will fail when automatically turning to next foundation pile point and the positioning can not continue.

To solve these problems, the system should have the ability to identify the prism. ETS Trimble has a sort of special prism ID identification function, but many mainstream ETS such as Leica and Topcon have no that function. Therefore, we have to look for a sort of general solution. The simple method is to compute the difference between the theoretical position (horizontal angle, vertical angle and slop distance) after each prism survey is completed, and if the difference exceeds certain threshold value, so the prism doesn't match, we can search again or pause for the free positioning and disposal through the human-computer interaction.

(2) Bad sight line

When freely positioning, 8-12 prisms are distributed at both sides of the line of about 200m, and worker, vehicles and construction all might induce the ETS can not collimate or survey certain or some prisms, and the free positioning process will be interrupted or ceased.

When the sight line is bad, according to the feedback information from ETS, the free positioning software can clew the reason of error and the solution through the human-computer interaction, and allow operators survey again, skip or delete this point, and ensure the free positioning to go on wheels.

(3) Residual errors of positioning

Because of the loosening of individual foundation piles, the large error of the prism, the wrong database information of the foundation pile point, the instable tripod and quick changing temperature differences, the residual errors of positioning may exceed the limitation.

When the residual error of positioning exceeds the limitation, the free positioning software could clew that operators eliminate, survey again or permanently delete the data of the foundation pile point which exceeds the limitation.

4. Conclusions

The free positioning and the intellectualization of ETS can largely enhance the efficiency and the reliability of the positioning. The positioning process is mainly completed by the software, and few human-computer interactions are only operated on the remote computer, and the chance of the manual operation is reduced to the least, which can ensure the stability of the electric air bubble of ETS and various compensation values and make the surveying data more exact and reliable. At the same time, the decrease of the operation difficulty and the enhancement of the efficiency for the positioning can make the two-set-collection and multiple-set-collection possibly applied in the actual engineering.

The ETS free positioning in the PDL track surveying system has been successfully applied in the SGJ series of PDL track survey meter made by Jiangxi Everbright Industry Company, and the effect is very good.

References

Chinese Ministry of Railway. (2006). *The Tentative Specifications on PDL Ballastless Track Railway Engineering Surveying.* Beijing: China Railway Press.

Fan, Baixing. (2003). Processing Survey Data Automatically by Survey Robot. *Beijing Surveying and Mapping.* No.2.

You, Zuji. (1991). *Survey Adjustment and Tutorial.* Beijing: Press of Surveying and Mapping. May of 1991.

Zhu, Baoxun, Liu, Chenglong & Yang, Tianyu. (2006). Method of Resection and the Precision Estimation. *Railway Investigation and Surveying.* No.4.

Modern Applied Science

www.ccsenet.org/journal.html

Vol. 3, No. 3

March 2009

Synthesis Porous GaN by Using UV-assisted Electrochemical Etching and Its Optical Studies

Khalid Omar, Z. Hassan, K. Goh, H. Teh & H. Abu Hassan

School of Physics, Universiti Sains Malaysia

11800 Penang, Malaysia

E-mail: khalhadithi@yahoo.com

The authors are grateful to School of Physics, Universiti Sains Malaysia, 11800 Penang, Malaysia for financial supporting of this work under the project No. 304/PFIZIK/637040.

Abstract

The PL of porous GaN sample shows higher intensity with smaller FWHM and red-shifting relative to the as-grown sample. The energy gap for porous GaN sample was smaller compare to the as-grown sample. The SEM surface image of UV-assisted electrochemical etching process is shown a shape and size of pore which was formed on the surface of the GaN, therefore the shape of pores formed was in spherical shape. The size of the pores formed has diameter as small as 85 nm. Two PL peaks were observed in the as-grown and porous GaN sample. For the as-grown GaN, the higher peak was observed at "361.946 nm" and the other at "723.739 nm" which is in UV and red luminescence region respectively. The FWHM is "8.198 nm" at "361.946 nm". For the porous GaN, the higher peak was observed at "364.235 nm" and at "728.039 nm", so their FWHM are "4.244 nm" and "8.926 nm" respectively. The peaks of porous sample were red-shifted at "2.289 nm and 4.30 nm" respectively compare to the peaks of the as-grown GaN. PL intensity of the porous samples was observed to be increased. Raman peaks representative to the wurtzite GaN crystal, namely E_2 (low) at 142.426 cm^{-1}, E_2 (high) at 568.771 cm^{-1}, and A_1 (LO) at 736.769 cm^{-1} were clearly observed.

Keywords: GaN, Porous, Semiconductor, Photo-electrochemical etching

1. Introduction

The most interesting property of "III-Nitride" semiconductors is their wide direct band gaps which enable the fabrication of highly efficient optoelectronic device operating in the blue and ultraviolet part of the spectrum. The direct band gap for wurtzite structure of InN, GaN, and AlN are "1.9 eV, 3.4 eV, and 6.2 eV" respectively [H. Sohn et al, 2000]. The "III-Nitride" semiconductors cover a part of the electromagnetic spectrum that is not covered by conventional semiconductor technology. Current semiconductor technology covers the spectrum from infra-red "IR" to green. GaN has a direct band gap of "3.4 eV"; this property makes it the best candidate for devices operating in the blue or UV part of the electromagnetic spectrum [V.S.Y. Lin et al, 1997]. In addition, piezoelectricity is another property of GaN. The piezoelectric properties of GaN can be utilized to fabricate high frequency surface acoustic wave "SAW" devices.

There are many applications for "III-Nitride" semiconductors including blue LED's, efficient full color flat panel displays, blue lasers, UV detectors, and high temperature sensors [P.M. Fauchet et al, (1995)]. Ultraviolet (UV), high brightness, and long-life LEDs are under development to replace incandescent bulbs [L. Beji, 2006]. Full color flat panel displays with low power consumption are desirable for lab-top computers, whose battery life is severely limited by the displays in use today. Blue lasers with their shorter wavelength will permit higher recording densities of all media based on laser technology, including CD-ROM and magneto-optical "MO" disk drives. UV detectors have a variety of military and civil applications and high temperature sensors are desirable under extreme conditions like inside jet engines. The high thermal conductivities of GaN "210 W/m K" and AlN "340 W/m K" make them suitable for high power applications, where the heat generated by these devices must be efficiently dissipated [L. Beji, 2003].

Experimental optical study of low dimensional semiconductor such as nanoporous GaN received enormous attention for the past few years due to its attractive properties which is useful particularly in optoelectronics and sensing devices.

Porous semiconductors show various important optical features compare to normal crystalline semiconductors such as higher intensity of photoluminescence emission, better photoresponce and shift of band gap [H. Hasagawa et al, 2005].

One of the most undesired problems in growing quality GaN is the unintentionally doped GaN. Most material grown so far had been *n*-type of values typically in the range from "10^{19} to 10^{16} cm^{-3}" [http://en.wikipedia.org/wiki/Gallium_nitride]. Unintentionally n-type dopant in GaN is said due to the nitrogen vacancies in it's crystalline since no impurities have so far been observed to account for such a large background carrier concentrations [N.G. Weimann, et al (1998)].

Most of the GaN-based devices realized up to date are deposited by heteroepitaxy, mostly on sapphire "Al_2O_3" or silicon carbite (SiC) substrates. Sapphire features a relatively low cost and it is the most commonly used substrate material for optoelectronic devices. These material have a lattice mismatch of approximately 16%, however it is one of the closest commercially produced lattice type to that of GaN [H. Hasagawa et al, 2005]. The mismatch in the lattice constants and thermal expansion coefficients between the GaN and its substrates gives rise to a high density of dislocations "between 10^8 and $10^{10}cm^{-2}$" and stress, limiting e.g. the electron mobility, doping efficiency and lifetime of devices [M. Dudley et al (2000) and K.E. Miyano et al, 1997].

2. Basic properties of crystalline and nanocrystalline GaN

GaN is one of the III-V compound semiconductors, where Ga is a trivalent element and N is a pentavalent element. The crystal structure of GaN can be in two types, wurtzite and zinc-blende crystal structure. The GaN sample used is the type of wurtzite structure, therefore, in the following, only wurtzite type of GaN will be discussed. In solid, the atoms of Ga and N are bonded to each other by strongly covalent covalent bands. The covalent bonds are formed between tetrahedral "s^1p^3"- hybrid orbitals at the angles of "109.5^o". The equation for the forming of covalent bonds of GaN may be written as following [Hartmut Haug et al (1993)]:

$$Ga\ (4s^2 4p^1) + N\ (2s^2 2p^3) \rightarrow Ga\ (4s^1 4p^3)^+ + N\ (2s^1 2p^3)^- \quad (1)$$

2.1 Vibrational property

The atom can undergoes oscillation about that point. Furthermore we assume that all atoms in a plane oscillate together. The planes can move either transverse with respect to each other in two possible ways or longitudinally in one way. For *N* atoms, there are 2*N* modes of vibration from the transverse motion and *N* modes of vibration from the longitudinal motions, thus giving total 3*N* modes of vibration. The elastic vibrations of a crystal can be considered in the form of elastic wave and we can find the frequency of the elastic wave in term of wave vector and elastic constants [Charles Kittel, (2005)].

2.2 Electronic energy band structure

Electrons are restricted to sets of discrete energy levels within atom. Large gaps exist in the energy scale in which no energy states are available. In a similar fashion, electrons in solids are restricted to certain energies and are not allowed at other energies. The different between an electron in an isolated atom and an electron in a solid is that in solid the electron has a range, or band. In a solid, many atoms are brought together and the wave functions of electrons in neighboring atoms overlap, and an electron is not necessarily localized at a particular atom so that the energy levels form essentially continuous bands of energy [Ben G. Streetman (1990)]. One important feature of the band gap of semiconductors is that the value of band gap varies with temperature. For wurtzite structure GaN, the direct band gap value at temperature 300 K is 3.39 eV while at 0K is 3.47 eV.

2.3 Properties of nanocrystalline

Following the reduction in dimensions to nanometer size, various changes of properties had been observed, such as the optical, electronic and vibrational properties in nanocrystalline compare to bulk crystalline. In low dimension system, the free charge carriers are confined in different type of confinement systems depend upon the dimensionality of carries confinement. The movement of electrons can be confined in three ways; one directional confinement "quantum well", two directional confinement "quantum wire" and three directional confinement "quantum dot" [M. Jaros (1989)].

3. Characterization of GaN semiconductor

3.1 Photoluminescence

In PL characterization, a laser is normally used an excitation source. A variation of frequencies of excitation laser beam will be subjected to the sample of study. Different frequency of laser beam will gives different value of excitation energy to the subjected sample. No absorption will occurred if the energy of subjected laser beam is lesser than the band edge energy gap of the sample. Therefore, the energy of subjected laser beam is equal or more than the energy gap, the sample will absorbs the laser energy and through radiative recombination. The corresponding wavelength at the peak of PL spectra can be used to calculate the band gap energy of the sample [M. Jaros (1989)].

3.2 Raman spectroscopy

Raman Effect is a type of inelastic scattering with the creation or annihilation of a phonon. In Raman scattering, the incident photon may gives part of its energy to the lattice in the form of phonon "phonon creation" and emerges out with lower energy photon. This interaction is known as Stokes scattering. On the other hand, Anti-Stokes scattering happens when the photon absorbs phonon energy (phonon annihilation) and emerges out as higher energy photon. The Raman Effect comprises a very small fraction, about "1 in 10^7", of the incident photons [R. Loudon (1964)]. Since the Raman scattering is not very efficient, a high power excitation source such as a laser is normally used. Raman spectroscopy is used to measures the vibrational (phonon) energies of molecules. For a transition to be Raman active there must be a change in polarizability of the molecule which means the polarizability of the molecule must change with the vibrational motion [H. P. Maruska et al (1969)].

4. Nanostructure fabrication

There are several ways can be used to fabricate nanostructure semiconductors. The standard approach for semiconductor nanostructure formation is to use fine crystal growth techniques such as molecular beam epitaxy (MBE) and metalorganic vapor phase epitaxy (MOVPE). Various standard etching and metal deposition techniques are used together to fabricate the devices with standard lithography techniques. However, these techniques possess few disadvantages such as high processing cost and complexity of processes. On the other hand, dry and wet etching techniques are more popular methods used in nanostructure fabrication mainly due to its low processing cost and simple experimental procedure and versatility of processes [D. Zhuang, et al (2005)]. Generally, dry etching processes such as reactive ion etching (RIE) can be highly anisotropic, an ideal characteristic for producing vertical profiles. However, due to the strong physical component in dry etching, it has low etch-selectivity between materials and can cause subsurface damage by ion bombardment. In contrast, wet etching, produces negligible damage, can be highly selective, is relatively inexpensive, and can be done with simple equipment.

4.1 UV-assisted electrochemical etching

UV-assisted electrochemical etching is one of the photo-assist electrochemical (PEC) etching techniques and it is also categorized under wet etching techniques. Wet etching of semiconductors involves oxidation of the semiconductor surface and subsequent dissolution of the resulting oxides. Oxidation requires holes that can be supplied either chemically or via an electrochemical circuit in anodic etching, the semiconductor and an inert electrode are attached to the positive and negative terminals of a direct voltage source, respectively. Both electrodes are put inside an electrolyte, e.g. aqueous potassium hydroxide (KOH). The semiconductor is oxidized by removal of bonding electrons (injecting holes) from the surface bonds via an external voltage source. The resulting oxides subsequently dissolve into the electrolyte [D. Zhuang, et al (2005)].

In PEC etching, the supply of holes to the oxidation process is further enhanced by illumination of photons in the etching process. Electron–hole pairs are generated by photons from an illumination source with energy equal to or greater than the band gap energy (E_g) of the semiconductor. The photogenerated holes assist in the oxidation of the semiconductor surface and the excess electrons are consumed by the reduction reaction on the counter electrode. Increasing the absorption of incident optical radiation with energy greater than band gap energy increases the supply of holes at the surface, thereby enhancing the etch rates.

The GaN oxidation process in the photo-assisted electro-chemical reaction mechanisms was explained in detail as follows [J. W. Seo, et al (2002)]:

$$2GaN_{(s)} \xrightarrow{h\nu} 2GaN_{(s)} + 2e^- + 2h^+ \quad (2)$$

$$2GaN_{(s)} + 2e^- + 2h^+ \xrightarrow{V} 2GaN_{(s)} + 2h^+ \quad (3)$$

$$2GaN_{(s)} + 2h^+ + 3H_2O_{(l)} \longrightarrow Ga_2O_{3\,(s)} + N_{2\,(g)} + 3H_{2\,(g)} \quad (4)$$

The electron-hole pairs are generated on the GaN film by UV illumination as shown in "equation 2". In "equation 3", the photo-generated holes are confined in the potential well formed by biasing at the surface of n-GaN while the extra electrons are swept out to the electrode. The holes accumulated at the surface of n-GaN assist the activation of Ga, and the oxidation reaction in "equation 4" take places.

The oxidation reaction in "equation 4" is in agreement with the interpretation of [Li et al, (2002)] who performed etching in aqueous KOH solutions. According to "Li et al, (2002)", the hydroxide ion "OH^-" is first adsorbed on the sample surface and subsequently react with Ga atoms following the reaction [D. Zhuang, et al, (2005)]:

$$2GaN + 3H_2O \xrightarrow{KOH} Ga_2O_3 + 2NH_3 \quad (5)$$

The "equation 5" is a simplified equation of oxidation reaction of GaN compare to the oxidation reaction in "equation 4". The KOH electrolyte here works as a catalyst and is also a solvent for the resulting Ga_2O_3.

5. Sample preparation

The UV assisted electrochemical etching set up is shown in "figure 1". In this technique, silver "Ag" was first deposited at one corner of the GaN surface for front contact by using thermal evaporator. The silver coated area is then contacted with copper washer and tightened with a bolt. In the anodic etching process, platinum is used as electrode, the GaN sample was connected by a copper wire to power supply and biased positive. The fabrication conditions were 30 minutes etching duration, 10V applied voltage and KOH electrolyte concentration of 1.0% and the sample illuminated with ultra-violet "UV" light source with "500 W".

6. Results and Discussion

The SEM surface image of the untreated as-grown GaN shows in "figure 2" that is smooth surface. No pores or any significant surface defects. The smooth surface is shown the single-crystallite layer of GaN deposited on sapphire substrate. However, some relatively dark spots were observed all over the surface of as-grown GaN. These dark regions may be the micro-defects of the as-grown GaN. The oxidation rate of GaN depends mainly on the photo-generated holes supply rate. Thus the larger pores formed may be attributes to higher holes concentration at that surface area. Although the movement of holes in semiconductor was predicted to be random, but since the etching rate depends solely on the parameters of the etching process (the applied voltage and illumination of UV lights were constant through out the etching process), the different etching rate at different concentration of holes through out the surface of GaN. It is believed that the concentration of holes through out the semiconductor surface area may be selective where holes may be more concentrated at certain area such as at the micro-defect area. Since the movement of holes in semiconductors is uncertain, so it is difficult to conclude that the holes concentration is higher at defect areas. However, it is known that the surface etching pattering has relation with the defects in the semiconductors.

The SEM surface image of UV-assisted electrochemical etching process is shown a shape and size of pore which was formed on the surface of the GaN as shown in "figure 3", therefore the shape of pores formed was in spherical shape. The size of the pores formed has diameter as small as 85 nm.

The room temperature PL spectra of as-grown and porous GaN samples were illustrated in "figure 4". The peak position, Full Width at Half Maximum (FWHM), peak shift and the peak intensity of the PL are summarized are shown in "table 1". The energy band gap, E_g was calculated based on $E_g=hc/\lambda$, where c and λ are speed of the nature light and selected wavelength, respectively. The wavelengths were obtained from the peak positions of near band edge of PL. Two PL peaks were observed in the as-grown and porous GaN sample. For the as-grown GaN, the higher peak was observed at "361.946 nm" and the other at "723.739 nm" which is in UV and red luminescence region respectively. The FWHM is "8.198 nm" at "361.946 nm". For the porous GaN, the higher peak was observed at "364.235 nm" and at "728.039 nm", so their FWHM are "4.244 nm" and "8.926 nm" respectively. The peaks of porous sample were red-shifted at "2.289 nm and 4.30 nm" respectively compare to the peaks of the as-grown GaN. PL intensity of the porous samples was observed to be increased. The intensity of emitted lights is proportional to the number of photons emitted. This means that the number of photons emission is much higher for porous GaN than as-grown GaN. The amplification of porosity-induced PL intensity could be explained by the extraction of strong PL by light scattering from the sidewalls of the GaN crystallites. Since the surface area per unit volume is higher in porous GaN, the larger surface area of porous GaN provide much more exposure of GaN molecules to the illumination of PL excitation lights. This would results higher number of electrons to take part in the excitation and recombination process in porous GaN compares to the smaller surface area of as-grown GaN. As a result, the number of emitted photon due to radiative recombination process is higher in porous GaN.

The Raman spectra of the both as-grown and porous GaN exhibit phonon mode E_2 (high), A_1 (LO), E_2 (low) and an additional peak which are shown in "figure 5, (a), (b)". However, A_1 (TO) phonon mode only observed in the porous GaN. All the phonon modes in porous GaN observed to be shifted to lower frequency relative to the as-grown GaN with the exception of the additional peak which remain the same. On the other hand, the Raman intensity of porous sample was found to be decreased except the additional peak. "Table 2" compiles all the peak position of the observed phonon mode together with its intensity. Three allowed Raman peaks representative to the wurtzite GaN crystal, namely E_2 (low) at "142.426 cm^{-1}", E_2 (high) at "568.771 cm^{-1}", and A_1 (LO) at "736.769 cm^{-1}" were clearly observed. In addition, a peak from the sapphire substrate was also seen at "415.971 cm^{-1}". All the phonon mode peak positions of the as-grown GaN observed in our Raman study is in good agreement compare with the value obtained It should be noted that all the GaN samples above were grown on sapphire and the entire phonon mode values are in cm^{-1}. For porous GaN, all the peaks of E_2 (low), E_2 (high), and A_1 (LO) were observed to be shifted to lower frequency compare to the as-grown GaN. However, the peak attributed to sapphire was observed to be at the same position "415.971 cm^{-1}" for both as-grown GaN and porous GaN but with higher intensity for porous GaN. The same peak position for both samples shows that the sapphire substrate was not subjected to the chemical etching process. The higher intensity observed for

porous GaN may be due to reduction of GaN thickness in the dissolution process during etching. With lower thickness of GaN in porous GaN, the argon ion laser beam may penetrate deeper to sapphire, hence higher intensity of Raman scattering. The red shifting in Raman spectral has further confirmed the compressive stress relaxation in porous GaN compare to as-grown GaN. It is interesting to note that the forbidden modes A_1 (TO) were present in our Raman spectral. The forbidden modes, i.e. A_1 (TO) and E_1 (TO) were absent in the as-grown sample but present in some of the etched samples. The forbidden peaks in the porous samples shows that the porosity, indeed, could change the optical properties of the material, this could be ascribed to the crystal disordering in the films, in which the increase of the scattering from the sidewalls of the porous structure eventually may change the light polarization.

Finally, it is hoped with better understanding of the optical properties of GaN, the potential of GaN semiconductor in optoelectronics devices can be fully utilized. The optical properties of the stress-free GaN, porous GaN and as-grown GaN can be compared and leads to a more understanding on the influence of residual stress in GaN on its optical properties.

References

Ben G. Streetman. (1990). *Solid State Electronic Devices*, 3rd Edition, Prentice-Hall International, Inc,

C. Kittel (2005). *Introduction to Solid State Physics,* 8th Edition, John Wiley & Sons, Inc.

D. Zhuang and J. H. Edgar. Wet etching of GaN, AlN, and SiC: a review, Material Science and Engineering: R: Reports, V 48, Issue 1 (2005). p.p.1-46

Hartmut Haug, Stephen W. Koch. (1993). Quantum theory of the Optical and Electronic properties of Semiconductors, *World Scientific,* Singapore.

H. Sohn, S. Letant, M.J. Sailor and W.C. Trogler, "Detection of Fluorophosphonate Chemical Warfare Agents by Catalytic Hydrolysis with a Porous Silicon Interferometer". *J. Am. Chem. Soc.* 122, 22 (2000). p.p.5399.

H. Hasagawa, and T. Sato, Electrochemical processes for formation, processing and gate control of III–V semiconductor nanostructures, *Electrochimica Acta,* 50, (2005), p.p. 3015-3027

H. P. Maruska and J. J. Tietjen, The preparation and properties of vapor-deposited single-crystal-line GaN, *Appl. Phys. Lett.* 15, 327 (1969).

http://en.wikipedia.org/wiki/Gallium_nitride, available March 2007

J. W. Seo, C. S. Oh, H. S. Cheong, J.W. Yang, C. J. Youn and K. Y. Lim, UV-Assisted Electrochemical Oxidation of GaN, *Journal of the Korean Physical Society,* V 41, No. 6 (2002),1017-1020.

K.E. Miyano, J.C. Woicik, Lawrence H. Robins, C.E. Bouldin, and D.K. Wickenden, Extended x-ray absorption fine structure study of $Al_xGa_{(1-x)}N$ films, *Appl. Phys. Lett.* 70 (1997). p.p.2108-2110

L. Beji, A. Missaoui, A. Fouzri, H. Ben Ouada, H. Maaref and A. Bouazizi, Nanostructurale nature of the porous GaAs layer formed on p^+-GaAs substrate by electrochemical anodization, *Microelectron. J.* 37 (2006), p.p. 783.

L. Beji, L. Sfaxi, B. Ismail, S. Zghal, F. Hassen and H. Maaref, Morphology and Photoluminescence studies of electrochemically etched heavily doped p-type GaAs in HF solution, *Microelectron. J.* 34 (2003), p.p. 969.

M. Dudley and X. Huang, Characterization of SiC using synchrotron white beam X-ray topography, Mater. Sci. Forum 338–342 (2000), p.p. 431.

M. Jaros. (1989). *Physics and Applications of Semiconductor Microstructures*, Clarendon Press, Oxford.

N.G. Weimann, L.F. Eastman, D. Doppalapudi, H.M. Ng, and T.D. Moustakes, Scattering of electrons at threading dislocations in GaN, *J. Appl. Physics.* 83, 3656 (1998).

P. M. Fauchet, L. Tsybeskov, C. Peng, S.P. Duttagupta, J. Von Behren, Y. Kostoulas, J.M.V. Vandyshev and K.D Hirschman, *Light-emitting porous silicon: materials science, properties, and device*

R. Loudon, Raman scattering from crystals, Adv. Phy, 14, 423 (1964).

V.S.Y. Lin, K. Motesharei, K.P.S. Dancil, M.J. Sailor and M.R. Ghadiri, A Porous Silicon-Based Optical Interferometric Biosensor, *Science* 278 (1997), p.p. 840.

X. Li, Y.W. Kim, P.W. Bohn and I. Adesida, In-plane band gap control in porous GaN through electroless wet chemical etching, Appl. *Phys. Lett.* 80 (2002), p.p. 980.

Table 1. PL spectra peaks position

	As-Grown GaN		Porous GaN	
	Peak 1	Peak 2	Peak 1	Peak 2
Peak position (nm)	361.946	723.739	364.235	728.039
Energy, E_g (eV)	3.425	1.713	3.404	1.703
Peak intensity, (a.u)	3297.19	540.005	57206	6193
Relative intensity	1.00	1.00	17.34	11.47
FWHM (nm)	8.198	-	4.244	8.926
Peak shift (nm)	-	-	2.289	4.30

Table 2. The phonon modes detected in the Raman spectra

Sample / Phonon mode	As-grown GaN		Porous GaN		
	Peak position (cm^{-1})	Intensity (a.u)	Peak position (cm^{-1})	Intensity (a.u)	Peak shift (cm^{-1})
E_2(high)	568.771	5094	567.1750	2284.2	-1.596
A_1(TO)	-	-	536.7740	767	-
A_1(LO)	736.769	859	713.126	421.8	-23.643
E_2(low)	142.426	286	143.5590	247.4	-1.133
Additional peak	415.971	205	415.971	303.4	0

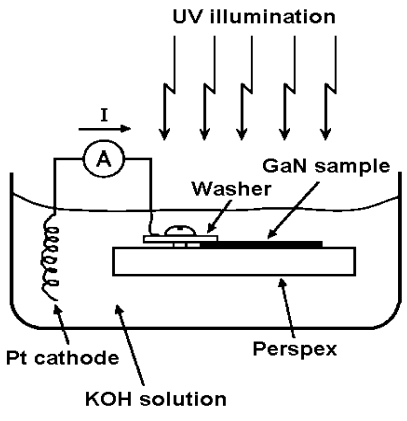

Figure 1. The electrochemical etching set up

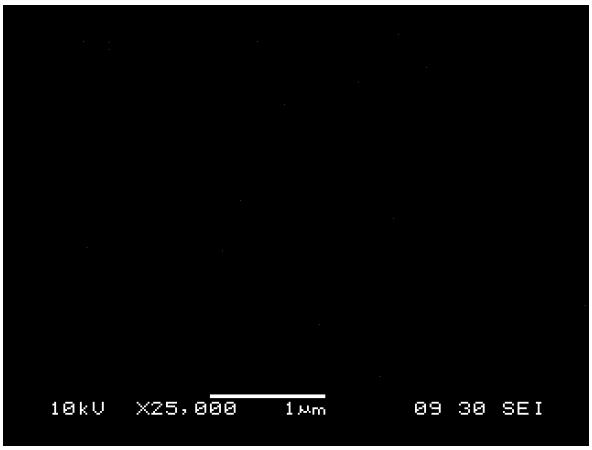

Figure 2. SEM surface image of as-grown GaN

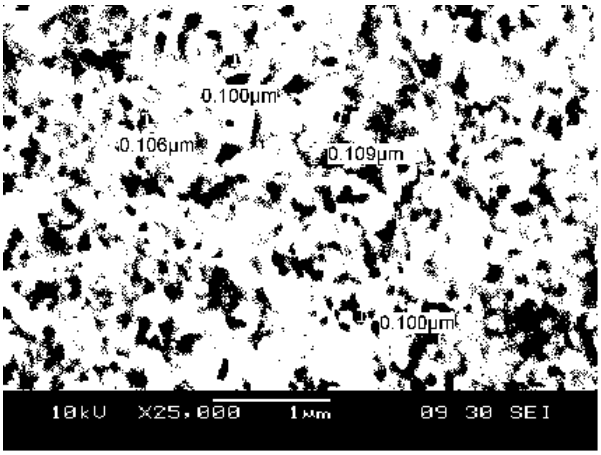

Figure 3. SEM surface images of porous GaN

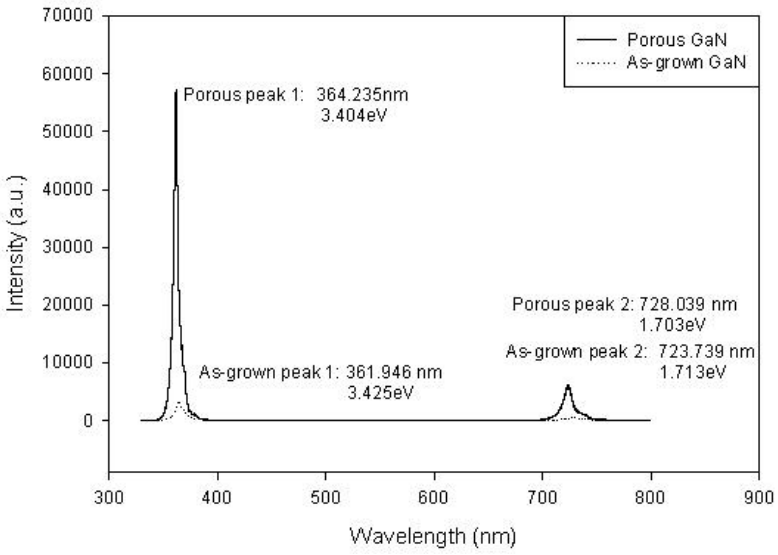

Figure 4. Room temperature PL spectra of the as-grown and porous GaN

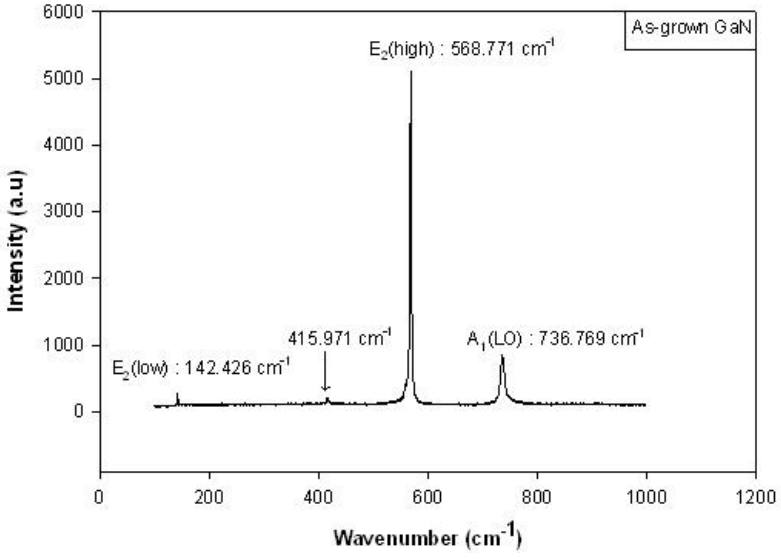

(a)

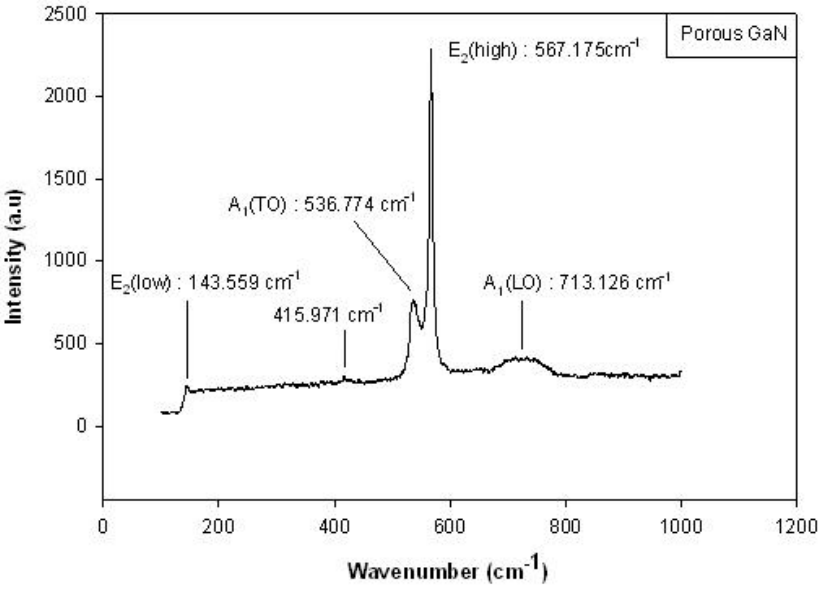

(b)

Figure 5. Raman spectra of (a) as-grown GaN (b) porous GaN

Modern Applied Science

www.ccsenet.org/journal.html

Vol. 3, No. 3

March 2009

Performance Improvement of Weaving and Penetrability for 4mm Hollow Fabric of PHAs

Xishan Wang & Xingfeng Guo

School of Textiles, Tianjin Polytechnic University

Tianjin 300160, China

E-mail: bmt0123@163.com

Abstract

This article introduces the advantages of new material PHAs (Polyhydroxyalkanoates) and its application in the medical domain, expatiates on the weaving method and machining technology of weaving the tube blank of 4mm artificial blood vessel by this material, and the measures to improve the penetrability according to the porosity.

Keywords: PHAs, Hollow fabric, Penetrability

PHAs is a sort of new macromolecule material arisen in recent years, and it possesses not only the materialized character of synthetic plastic, but the biodegradability, bio-compatibility, optical activity and piezoelectricity which are not possessed by synthetic plastic and many excellent performances such as large proportion of reproducible materials, low oxygen permeability, anti-ultraviolet radiation and anticoagulation, so it has wider application foreground in many domains such as textile, medicine, agriculture, food packaging and electron (Zhu, 2003, p.61-64 & Yang, 2005, p.1015-1021).

PHAs can be used as the implant of histology for animal and human being, and it can be made as the bracket of some organizations to implant into human body, and it can be made as the bone nail and bone stick in the orthopedic operation to fix the framework material. It has strengthening function, and it coarse surface could promote the growth of Human Tissues, and its holes could be used to penetrate and exchange. When new tissue forms, PHAs will gradually decompose, the results of decomposition could be absorbed by human body and would not produce bad reaction (Jiao, 2003, p.15-20).

1. Materials and apparatuses

1.1 Materials

PHAs filament includes the chip made by Tsinghua University and the spinning made by Tianjin Polytechnic University. Because PHAs spinning technology is not mature, so the diameter differences are large but the plasticity distortion is very good. The parameter means include the breaking strength is 286.2cN, the breaking tension if 4.5cN/T, the extension rate is 47.40%, the breaking power is 258.8mJ, and the average diameter is 0.25mm.

1.2 Apparatuses

The weaving adopts the WCS-03 computer sample weaving machine, and the long silk is tested by HD021 electric single yarn strength meter (made by Jiangsu Nantong Hongda Experiment Instruments CO., LTD).

2. Design

Use the method of "staving-weaving-reverting", first stave the 3D tube preform to make it a sort of plane fabric with multiple layers structure, then wave this fabric by the weaving principle of multiple layers fabric, and finally revert the multiple layers fabric to the solid shape of tube preform (Yi, 2002, p.7-8).

2.1 Confirmation of tube blank basic weave

The tube weave should select same weave as the basic weave of surface layer and inner layer. Under the premise to fulfill the requirement of fabric, the basic weaves should possibly select simple weaves such as plain weave, twill weave and satin weave to simplify the machining work, for example, if the weave is required to be successive on the folded place of the fabric, so the weave which latitudinal S is constant should be adopted as the basic weave, and the total amount of longitude yarn is fixed, and it can not increase or reduce optionally (Zhu, 2004, p.5-7). Therefore, two sorts of weave such as 2/2 twill and 1/1 plain are adopted.

2.2 Confirmation of total longitude yarn amount

First, confirm the tube diameter R of the fabric, compute the tube breadth W according to the tube diameter, and compute the total longitude yarns M_J on the upper and lower layers according the tube breadth.

$$W = \pi \times R$$

$$M_J = 2 \times W \times P_J = \pi \times D \times P_J \quad (1)$$

To keep the continuity of fabric brim weave, the total longitude amount through computation must be modified by following formula.

$$M_j = R_J \times Z \pm S_w \quad (2)$$

Where, R_J is the longitude circle amount of the basic weave, Z is the circle amount of the inner layer and the surface layer of the basic weave, S is the latitude amount of the basic weave (coefficient-constant), and when the latitude direction is from right to left, S is positive sign, and when the latitude direction is from left to right, S is negative sign (Zhu, 2004, p.5-7).

3. Weaving

3.1 Confirmation of parameters

According to formula (1) and (2), compute and adjust the parameters, the longitude yarn amount takes 47, the reed number is 80, 8 penetrates, so the actual tube blank diameter is little bigger than the design diameter, and it is convenient to be treated.

3.2 Machining figure

Figure 1 is the machining figure of 2/2 twill weave, and it only needs modify the twill figure when weaving 1/1 plain weave (Cai, 1979, P.124-127).

4. Results and discussion

4.1 Practicality figure

In figure 2, the first part is the 2/2 twill part and the second part is the 1/1 plain weave (two longitude yarns are thick).

4.2 Performance analysis

From Table 1, two sorts of weaves have better porosity, and it offers advantageous conditions for the successive disposal.

Because the warp and weft yarns are interlaced each other, so the holes must exist on the surface of the fabric, and if the density of the fabric is not high, too large spacing among yarns will induce the effusion of blood when it is directly used in clinic, but too high density could not be achieved under certain conditions of materials and equipments (Zhao, 2002, p.2-22).

Therefore, the successive disposal method to the fabric could make it achieve proper penetrability. The successive disposal method could strengthen and densify the fabric to stabilize the structure, increase the density of the fabric, reduce the opening rate and prevent blood penetrability. And it can reduce the stress J on the seam place after implant to certain extent, make the blood vessel possess stronger anti-drawn ability and small avulsion transfer property, and improve the stress on the seam place and the anti-extrusion performance (Ling, 2003, p.49-52).

5. Conclusions

The method proved that it was feasible to weave the artificial blood vessel tube blank of 4mm by the machine, and the better penetrability effect could be achieved after disposal according to the porosity, and the study in the article was the helpful attempt for the production and improvement of the artificial blood vessel with the diameter less than 6mm.

References

Cai, Bixia. (1979). *Structure and Design of Fabrics.* Beijing: Textile Industry Press. P.124-127.

Jiao, Ningning. (2003). Synthesis and Application of Polyhydroxyalkanoates. *New Chemical Materials.* No.10. P.15-20.

Lingkai, Wanglu & Jia, Lixia. (2004). Design and machining technology of artificial Vascular Prostheses. *Shanghai Journal of Biomedical Engineering.* No. 24(2). P.49-52.

Yang, Yijin, Li, Zhizhang & Zhang, Xueqiao. (2007). Present Research of Using PHAs Synthesized by Microbes. *Chemical Research and Application.* No.9. P.1015-1021.

Yaomu & Zhou, Jinfang. (1990). *Textile Materials.* Beijing: China Textile Press. P.492-494.

Yi, Honglei, Yewei & Wang, Hongli. (2002). The Structural Design and Weaving Technology of the Tubular Woven Preforms. *Journal of Textile Research.* No.2. P.7-8.

Zhao, Shuyao, Li, Liuling & Chen, Xuwei. (2003). Study on the Weaving and Infiltration of the Fabrics Used in Artificial Vascular. *Technical Textile.* No.10. P.2-22.

Zhu, Bochao et al. (2003). Research Advance in Synthesis and Application of Polyhydroxyalkanoates. *Modern Plastics Processing and Applications.* No.10. P.61-64.

Zhu, Meinan & Yu, Fapeng. (2004). Small-diameter Textile Weaving on the Silk Weaving Machine. *Silk Textile Technology Overseas.* No.6. P.5-7.

Table 1. The tightness of two sorts of weaves (Yao, 1990, P.492-494)

weave	Total tightness (%)	Longitude tightness (%)	Latitude tightness (%)	Longitude and latitude tightness proportion
2/2	98.9	98	43.6	2.2:1
1/1	96.2	90.5	60	2:1

Note: 2/2 weave: P_T= 392/10cm, P_w= 178/10cm, d_T= d_w= 0.25mm.

1/1 weave: P_T= 362/10cm, P_w= 240/10cm, d_T= d_w= 0.25mm.

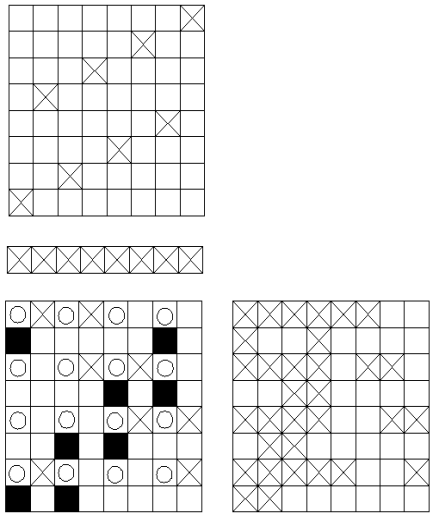

Figure 1. Machining Figure of 2/2 Twill Weave

Figure 2. The first part is the 2/2 twill part and the second part is the 1/1 plain weave (two longitude yarns are thick)

Modern Applied Science

www.ccsenet.org/journal.html

Vol. 3, No. 3

March 2009

A Study on Cold Forging Die Design Using Different Techniques

Khaleed Hussain M.T.(Corresponding author)

School of Mechanical Engineering, University Science Malaysia

Engineering Campus, 14300 Nibong Tebal, Pulau Pinang, Malaysia

Samad. Z

School of Mechanical Engineering, University Science Malaysia

Engineering Campus, 14300 Nibong Tebal, Pulau Pinang, Malaysia

A.R.Othman

School of Mechanical Engineering, University Science Malaysia

Engineering Campus, 14300 Nibong Tebal, Pulau Pinang, Malaysia

S.C.Pilli

School of Mechanical Engineering, K.L.E.C.E.T,Karnataka, India

Salman Ahmed N.J

School of Mechanical Engineering, University Science Malaysia

Engineering Campus, 14300 Nibong Tebal, Pulau Pinang, Malaysia

Irfan Anjum Badruddin

Department of Mechanical Engineering

University of Malaya

Kuala Lumpur, Malaysia

Hakim SS

Department of Mechanical Engineering

University of Malaya

Kuala Lumpur, Malaysia

Quadir GA

School of Mechatronics Engineering

Kolej Univesiti Kejuruteraan Utara Malaysia, MALAYSIA

A.B. Abdullah

School of Mechanical Engineering, University Science Malaysia

Engineering Campus, Seri Ampangan, 14300 Nibong Tebal, Malaysia

Abstract

It is becoming increasingly essential to predict the exact behavior of cold forging die during the forging process and it is also important to optimize the die design for its durability and to reduce the production cost of the die. Optimization of cold forging die design is required to reduce the production cost of die as well as the forged part and also to increase the accuracy of the die and the forged part. Since the past few years computer aided engineering (CAE) techniques have been widely used for research in metal forming. Amongst them finite element analyses (FEA) have been greatly successful to provide the understanding of metal flow and die stresses for different forming processes. The present work is a review of the existing die design techniques which are used in forging process to enhance the die design and to optimize die design process which will improve the performance of die. In cold forging the die will under go high loads, hence it is essential to know Fatigue behavior and Fatigue Failure of the die when it has been under go cyclic loading. The study end up with future challenges of the die design and its processes, the approaches adopted to develop an optimum system that can fulfill the customer demand.

Keywords: Cold forging die design, Stress, Deformation, Optimization, Forged part

1. Introduction

The forging is a process in which the work piece is shaped by compressive forces applied through various die and tools. It is one of the oldest methods in metalworking operations, dating back at least 4000 B.C. Forging were first used to make jewelry, coins and various implements by hammering metal tools made of stone. Many researchers have worked on cold forging, this paper emphasizes on cold forging die design and cold forged part. Different authors made an attempt to optimize the die design and to achieve the quality of forged part, for that they have used different techniques, like FEM, Nuaral Network, etc.

2. Literature Review

2.1 CAD/CAE used for modeling and analysis

FEM (Finite Element Method) has been adopted by many researchers for optimization of die design and die design process. This tool has been used to perform analysis of the die design parameters, and to get the accurate results without damaging any physical structure. The physical structure can easily be modeled in CAD package and then can be transferred to FEA package where the various analysis can be done. To optimize the product, one can easily change the geometry in CAD model to get the optimize geometry. Similarly the material properties also can be change. The researchers have excellently used these tools for the simulation. Many researchers made an attempt to give the solution for problem using the FEM, like Castro et al.(C. F. Castro , C. A. C. António and L. C. Sousa, 2004) made an attempt to obtain an optimal design in forging. The design problem is formulated as an inverse problem incorporating a finite element thermal analysis model and an optimisation technique conducted on the basis of an evolutionary strategy. A rigid viscoplastic flow-type formulation was adopted, valid for both hot and cold processes. In industrial forming processes most of the deformation energy is transformed into thermal energy. The generated heat causes the increase in temperature. External friction losses raise the temperature at the die–work-piece interface. To obtain optimal solutions Castro, C. A. C. António et al, used a developed numerical algorithm based on a genetic search supported by an elitist strategy. They chose design variables are work-piece preform shape and work-piece temperature. In order to demonstrate the efficiency of the inverse evolutionary search, specific forging cases are presented and they have consider the optimization of the process parameters aiming the reduction of the difference between the realised and the prescribed final forged shape under minimal energy consumption and restricting the maximum temperature.

Hyunkee Kim, Kevin (Hyunkee Kim, Kevin Sweeney and Taylan Altan, 1994) Sweeney have summarized the results of industrially relevant work in progress research with the DEFORM and DEFORM-3D FEM systems. They have been also studied a new tool design for cross groove inner race for a constant velocity joint, the flashless forging of an aluminum connecting rod, design of cold forgings and forming sequences, die wear in warm forging extrusion, and examples of DEFORM-3D simulations of a connecting rod, blade coining.

Hyunkee Kim and Taylan Alfan(Hyunkee Kim and Taylan Alfan, 1996) have given several examples of cold forged parts collected from literature and cold forging industry. For the example parts, forming process sequences, including the dimensions of the workpiece at each forming station, are given. They have been verified forming sequences generated by FORMEX with FE simulation program such as DEFORM.

T. Petersen and P. S. Frederiksen (T. Petersen and P. S. Frederiksen, 1994) have presented the results of two-dimensional finite element analysis with special emphasis on the effects of plasticity. The geometry treated concerns a die with rather sharp fillets, as found for example in a bolt-head die. They mainly examine stress concentration and propagation of the plastic zone in the fillet area as applied forging pressure increases. An automatic mesh generation routine is used in order to investigate different fillet designs and results of an optimization study are presented.

J.-H. Song Y.-T. Im (J.-H. Song and Y.-T. Im, 2007) have studied the process design for closed-die forging of a bevel gear used for a component of automobile transmission was made using three-dimensional finite element simulations. Process variables of the closed-die forging of the bevel gear were selected to be the pressing type, punch location, and billet diameter. Based on FE simulation results, appropriate process design without causing under-filling and folding defect was determined. In addition, with design of a die set including die insert and stress ring, cold forging of the bevel gear was experimented to estimate effectiveness of the designed process, the design process for the closed die forging of the bevel gear for the 3D FE analysis.

From experiments, they found that bevel gear with complete formation of the teeth was obtained without making any forming defects although flash in a forged product and punch fracture was occurred due to a slight difference in the punch stroke during formation. Through comparison of results between experiments and FE simulations, it was found that die clamping device clamping force and improvement of the die safety.

Chengliang Hu, Kesheng Wang et,al (Ravi Duggirala, Rajiv Shivpuri, Satish Kini, Somnath Ghosh and Subir Roy, 1994) have found three design schemes with different die shape. Firstly, finite element method is used to simulate the cold forging process of the spur gear with two-dimensional axisymmetrical model, and the strain distributions and velocity

distributions are investigated through the post processor. Radial-flow-velocity distribution is an important indicator to be evaluated, and a relatively better scheme is selected. Secondly, three-dimensional simulation for the relatively better scheme is further performed considering the complicated geometric nature of gear, and the results show that the corner filling is improved and well-shaped gear is forged. Finally, a corresponding experiment is done, which is mainly utilized for supporting and validating the numerical simulation and theoretical investigation.

Young Suk Kim, Hyun Sung Son et,al, (Young Suk Kim, Hyun Sung Son and Chan Il Kim, 2003) have used rigid–plastic finite element simulation to analyze the deformation characteristic of the whole impeller hub forming processes and to optimize the process. As a result, two kinds of improvement for the impeller hub forming process satisfying the limit of the machine's load capacity and the geometrical quality are suggested and they verified their results with experimental results.

Takahiro Ohashi, Satoshi Imamura,et,al, (Takahiro Ohashi, Satoshi Imamura, Toru Shimizu and Mitsugu Motomura, 2003) have given the system which will designs one forging process and preform, and after then, it also does the internal profiles of dies and exports them as point line into general purpose CAD systems. Repeating the above procedures, the system generates process plans and die profile design from the product's shape to its raw materials. Multiple plans and profiles are designed by repeating the procedure recursively.

P. B. Hussain, J. S. Cheon,et,al, (P. B. Hussain, J. S. Cheon, D. Y. Kwak, S. Y. Kim and Y. T. Im, 2002) has used an inner gear component, clutch-hub, as an object for a numerical study investigating the usefulness and effectiveness of employing numerical simulations in the design process of metal forming parts. They have used CAMP*form* as computer-aided design simulation tool .They studied effect of shear friction factor on the forming process and it was examined using the most suitable die and workpiece geometries. They also, studied an aluminum alloys Al1100-O, Al2024-T3, Al6061-T4 and Al7075-T4 with respect to their defect factors of work hypothesis. They found that only Al6061-T4 could be considered as a substitute material of steel for cold forging of the clutch-hub.

T. Ishikawa, N. Yukawa,et,al, (T. Ishikawa, N. Yukawa, Y. Yoshida, H. Kim and Y. Tozawa, 2000) have discussed analytically the effects of forming stresses and generated heat on the dimensional change of punch die and work piece during forging. They have change in outer and inner diameter of backward extruded cup is investigated numerically using thermo-elastic-plastic FEM code according to the actual forging sequence, namely extruding, unloading of punch force, and ejection and air cooling of extruded cup. They got results of outer and inner diameters of product which are in good agreement with the experimental results. They have used the simulation to determine the initial tool dimensions for precision parts in the tool design process of cold forging.

C. S. Im, S. R. Suh, (C. S. Im, S. R. Suh, M. C. Lee, J. H. Kim and M. S. Joun, 1999) have worked on a computer aided process design technique, based on a forging simulator and commercial CAD software, has been presented together with its related design system for the cold-former forging of ball joints. The forging sequence design and its detail designs are generated through user–computer interaction using templates, design databases, knowledge-based rules and some basic laws. The forging simulation technique has been used to verify the process design. It has been shown that engineering and design productivity is much improved by the presented approach from the practical standpoint of process design engineers. Rong-Shean Lee, Quang-Cherng Hsu et, al, (Rong-Shean Lee, Quang-Cherng Hsu and Saint-Len Su, 1999) have worked to develop a computer-aided die design system using Auto-Lisp. The design characteristics of the die elements and the die assembly has been expressed in parametric form and programmed. They have proposed a system which has an open architecture, therefore, according to the system structure, die-design engineers can extent the die element design data base and programs. With the aid of the proposed system, the functions of die element design, die assembly design, automatic graphics and dimensions generation, redesign, dimension constraint correlations and bill of materials will provide efficiency and convenience of die.

B. Falk, U. Engel and M. Geiger (B. Falk, U. Engel and M. Geiger, 1998) have emphasized in their work to assess the applicability of different failure concepts for a closed cold forging die. The critical, process-dependent load is quantified and localized by using a finite element method. Based on the resulting stress–strain distributions, the damage parameters have been calculated yielding different estimates of tool life that are compared with practically experienced data.

D. J. Kim, B. M. Kim (D. J. Kim, B. M. Kim and J. C. Choi, 1997) have used neural networks to determine the initial billet geometry for the forged products using a function approximation. They have been used three-layer neural network and the back-propagation algorithm has employed to train the network. They have used simulated data to determine the aspect ratios that fill the die cavity. Hence the number of simulations has been reduced. By using the neural network they have predicted the unfilled volume for some aspect ratios they would not explored in the finite element simulation. They reduced the number FEM simulation in process planning.

W. L. Xu and K. P. Rao, (W. L. Xu and K. P., 1997) have carried out an analysis of isothermal axisymmetric spike-forging using an integrated FEM code. Simulations has been conducted to investigate the influence of different

geometric parameters, processing variables and interfacial conditions on the instantaneous spike height. Their results of the simulations are discussed along with comparisons with available experimental results. They have given some guidelines for the design of this test has been drawn up.

Quang-Cherng Hsu and Rong-Shean Lee(Quang-Cherng Hsu and Rong-Shean Lee, 1997) have given a cold forging process design method based on the induction of analytical knowledge has proposed. They used analysis engine, which is a finite-element-based program, to analyze various multi-stage cold forging processes based on pre-defined process condition parameters and tooling geometry. Method which has been proposed by these authors is useful for the shop floor to decide the cold forging process parameters for producing a sound product within the required minimum quantity of the die set.

Hyunkee Kim, Kevin Sweeney et, al, (Hyunkee Kim, Kevin Sweeney and Taylan Altan, 1994) have summarized the results of industrially relevant "work-in-progress" research with the DEFORM and DEFORM-3D FEM systems. They also worked on a new tool design for cross groove inner race for a constant velocity joint, the flashless forging of an aluminum connecting rod, design of cold forgings and forming sequences, die wear in warm forging extrusion, and examples of DEFORM-3D simulations of a connecting rod, blade coining, and wire drawing of shapes.

Béla Lengyel, Ijaz A. Chaudhry,et,al, (Béla Lengyel, Ijaz A. Chaudhry and R. D. Hibberd, 1994) have worked on a new developments in the expert system COFEX ,for process planning in the cold forging of flanged round steel hollows. It has been written in PROLOG for IBM personal computers, implemented in modular form and linked to a finite element program. The finite element results show the development of the fold and indicate the boundary between conditions leading to acceptable and defective flange geometries.

In recent years, computer aided engineering (CAE) techniques have been increasingly applied with great success in metal-forming research, as well as in the cold- and hot-forging industry. Taylan Altan and Markus Knoerr (Taylan Altan and Markus Knoerr, 1992) have been adapted for cold-forging applications from an earlier publication (*J. Mater. Process. Technol.*, 33 (1992) 31–55) summarizes industrially relevant research results obtained with DEFORM. It has been reported on an investigation of a suck-in type extrusion defect, forging of bevel gears, stress analysis of forging tooling, design of multi-stage cold-forging operations, design of a net-shape cold-forging operation for pipe fittings and development of a new test to evaluate lubrication in cold forging.

S. I. Oh, W. T. Wu and J. P. Tang (S. I. Oh, W. T. Wu and J. P. Tang, 1992) have worked on features required to simulate cold forging operations are discussed. Example solutions are also presented to demonstrate the capabilities of the DEFORM system. It has been also shown that the automatic mesh generation and remeshing capability is an essential feature for industrial applications.

Markus Meidert, Markus Knoerr,et,al, (Markus Meidert, Markus Knoerr, Knut Westphal and Taylan Altan, 1992) have worked on, two modelling techniques, finite element (FE) based numerical modelling and physical modelling with plasticine, are being presented as process design tools in cold forging. They have developed a strategy to allow successful 2D FE modelling of bevel gear forging. They used the results from the process simulation then that they used it as a load input data for a punch stress analysis. Thus it has been possible to modify the punch geometry in order to reduce the punch stresses. They have been applied Physical modelling to verify the results of the 2D FE simulations.

Armin Buschhausen Klaus Weinmann (Armin Buschhausen, Klaus Weinmann, Joon Y. Lee and Taylan Altan, 1992) have worked on a friction test, based on a double backward-extrusion process, is proposed and examined in order to obtain information on lubrication quality. They have been used the program DEFORM, for FEM analysis conducted for different area reduction ratios and billet heights. They have been got simulated results are very close to the experimental results which has been performed in Germany some years ago. The reduction ratio that gives the greatest differences in extruded cup heights was selected for the test design and the influence of friction shear factors between $m = 0.08$ and $m = 0.20$ was investigated

Aly A. Badawy, P. S. Raghupathi,et,at, (Aly A. Badawy, P. S. Raghupathi, David J. Kuhlmann and Taylan Altan, 1992) have described a computer-aided system called "FORMING" for designing the forming sequence for multistage forging of round parts. FORMING can handle only solid round parts without protrusions. However, the program can be expanded to design forming steps for hollow parts and parts with internal protrusions that are forged without flash in upsetters, automatic forging machines, and vertical presses

Natsume,and Y., Miyakawa (Natsume, Y., Miyakawa, S. and Muramatsu, 1989) have studied systematically to understand the dimensional difference between forging tools and forged components has been tried by both experimental and FEM analysis. They have found that the difference is mainly influenced by the elastic deflections of the die and the elastic recovery of the forged part. The FEM analysis results from the consideration of the die as a deformable body are well agreed with the experimental results. They have been considered shrink-fitting factor. They have come know that when the shrink-fitting factor has adequately compensated, the analyzed dimensional difference results are well fitted to the measured data within the range of 1 μm.

Since the dimensional accuracy of forged parts are largely influenced by elastic behaviors of the tool material. Young-Seon Lee, Jung-Hwan Lee, et,al, (Young-Seon Lee, Jung-Hwan Lee, Jong-Ung Choi and T. Ishikawa, 2002) have evaluated the characteristics of elastic deformation at a forming tool for a cold forged alloyed steel by experimental and FEM analysis. Y. Qin, R. Balendra and K. Chodnikiewicz (Y. Qin, R. Balendra and K. Chodnikiewicz, 2000) have worked to combine coupled thermo-mechanical FE plastic simulation and heat transfer analysis to define heat-flux-density functions across die/workpiece interfaces. The functions were then used for initiating heat transfer analysis on the die with the repeated heat-loading for the given cycles. Since only heat transfer analysis was required for the die for the multi-cycle analysis, high-efficiency of the computation has achieved.

2.2 Micro Genetic Algorithm

To optimize the cold forging design design process some the authors have been used the Micro Genetic Algorithm like Ravi Duggirala, Rajiv Shivpuri,et,al, (Chengliang Hu, Kesheng Wang and Quankun Liu, 2007) have used the finite element analyses for providing the successful understanding of metal flow and die stresses for different forming processes. To minimize the possibility of the initiation of tensile fracture in the outer race preform of a constant velocity joint manufactured by cold forming operations, an adaptive Micro Genetic Algorithm has implemented. The chosen design variables were the preform diameter, the maximum number of forming operations, the number of extrusion and upset operations, the amount of area reduction in each pass, the amount of upset in each upset, and the included angles in the extrusion and upset dies. Significant reduction in the maximum damage value was achieved as a result of this optimization process.

A new method have been described by S. Roy, S. Ghosh, et,all, (S. Roy, S. Ghosh and R. Shivpuri, 1997) for design optimization of process variables in multi-stage metal forming processes. The selected forming processes are multi-pass cold wire drawing, multi-pass cold drawing of a tubular profile and cold forging of an automotive outer race preform. An adaptive micro genetic algorithm (μGA) scheme has been implemented for minimizing a wide variety of objective-cost functions relevant to the respective processes. The chosen design variables are die geometry, area reduction ratios and the total number of forming stages. Significant improvements in the simulated product quality and reduction in the number of passes has been observed as a result of the micro genetic algorithms-based optimization process.

2.3 Inverse Approach

Some of the researchers have been applied an inverse approach to the preform shape optimization problem. R. Di Lorenzo and F. Micari (R. Di Lorenzo and F. Micari, 1998) made an attempt to ensure that in the finishing step to obtain the desired product without shape defects such as underfilling or folding and with a minimum material loss into the flash in closed die forging. The preform design plays a critical role for the success of the process. They have been applied an inverse approach to the preform shape optimization problem. The method permits to evaluate a response function which links the set of parameters defining the preform shape with the fulfillment of the product design specifications. They have been applied their approach to a closed die forging process aimed to the production of a C-shape component, and has allowed to determine the optimal preform geometry which ensures the complete filling of die cavity . R. Di Lorenzo and F. Micari (V. Maegaard, 1985) have applied an inverse approach to the preform shape optimization problem: the method permits to evaluate a response function which links the set of parameters defining the preform shape with the fulfillment of the product design specifications. They have been applied their approach to a closed die forging process to the production of a C-shape component, and has allowed to determine the optimal preform geometry which ensures the complete filling of the die cavity.

Researchers have worked on cold forging die design and the die design process to achieve the optimal die design and the optimal die design process, they have adopted different techniques and methods like model-material technique, least squares, physical modeling slab-analysis method upper-bound technique, and matrix method.

Upper-bound technique Boundary Element Methods, finite difference method and some researchers have used the experimental approach and numerical methods which have been discussed. V. Maegaard (V. Maegaard, 1985) has studied the parameters which limit the forging process are the maximum press force available and the contact pressure between the workpiece and the tool. Researchers can make use of this knowledge for a better understanding of the prevailing process mechanics and for improvement of the forging process, whilst the production engineer can use this knowledge for the selection and allocation of process steps. Furthermore, determination of contact pressure facilitates understanding of tool wear and fracture, of the plastic flow behaviour of the materials, and of the necessary radial and/or axial splitting and pre-stressing of the tooling. The different design parameters for a rod/cup component are discussed and experimental results are presented, particularly for the contact pressure on the die surface in forward/backward extrusion, using the model-material technique. T. Ohashi, A. Nakata, et,al, (T. Ohashi, A. Nakata, 2001) have intended to use a to analyze the qualitative accuracy of a multi-body machine system, part of which receives a large changing external load, the Improvement in process of cold forging die design with analyzing qualitative accuracy.

Jens Groenbaek and Torben Birker (Jens Groenbaek and Torben Birker, 2000) have studied the demand of the market to the major industrial cold forgers for the development and production of complicated net shape parts at fairly low unit costs which requires an innovative new die designs for the optimisation of die deflections. They reduce the die deflection by 30–50% in critical dies so that die lives can be improved by factors of 3–10.they applied the high-stiffness STRECON E^+ containers influence the stresses, strains, and deflections in critical dies. They showed how the STRECON® E^+ containers can be applied to such critical dies like bevel gear dies, planetary gear wheel dies, and spline dies in an innovative way.

Chen, R. Balendra, et, al, (Chen, R. Balendra, and Y. Qin, 2004) have used relevant technologies depend on tools in which error-compensation can be affected. To minimise the component errors have presented the novel die-design approach, known as the least squares approach, has been used and Shrink-fitting compensating die structure has been employed. The errors caused by die-elasticity, secondary yielding, springback and temperature were considered in the process of minimisation.

The main factors that may influence the accuracy of the optimisation procedure has analysed. The final component errors have been controlled to within a few micrometers ie 1 μm. The approach has been illustrated using axisymmetric closed-die forging. H.S. Kim, (H.S. Kim, 2007) has proposed a cold forging process sequence in order to produce the terminal pin as one piece. The plate-shaped head section requires an upsetting in the lateral direction of a ylindrical billet, which is followed by a blanking process.The intermediate forgings obtained by experiments of the preform forging stage and the final forging stage, respectively, by using the proposed cold forging process sequence, the head and the body section could be produced as one piece without any defects.

K. D. Hur, Y. Choi,et,al, (K. D. Hur, Y. Choi and H. T. Yeo, 2003) have found that the use of high stiffness materials to the first stress ring of forging dies can reduce the elastic deformation of die insert without failure. Yi-Che Lee and Fuh-Kuo Chen (Yi-Che Lee and Fuh-Kuo Chen, 2001) have selected four die materials commonly used in the cold-forging process which has been examined to obtain the relationship between the hardness and the die fatigue life. They first heat-treated die materials by a developed process to obtain different values of hardness, and the ductility has been retained at a favorable level. The material properties of these die materials were then obtained from tension and impact tests. The relationship between the mechanical properties and the hardness has established. They also worked to build up theoretical model which will predict the die fatigue life.

W. G. Cho and C. G. Kang (W. G. Cho and C. G. Kang, 2000) have studied the filling behavior and various defects of products has observed, and microstructures and mechanical properties were investigated along with parameters such as pressure and die temperature. The porosity, which is an internal defect, has observed by the researchers particularly at lower die temperatures. A dense microstructure has been found at lower die temperature and higher applied pressure. In a tensile test, they have observed that the higher the applied pressure, the higher the ultimate strength, yield strength, and elongation. In a hardness test, it has been observed that the hardness decreased gradually from the center to the periphery of the specimen.

John Walters, Wei-Tsu Wu, et,al, (John Walters, Wei-Tsu Wu, Anand Arvind, Guoji Li, Dave Lambert and Juipeng Tang, 2000) have worked on Recent development of process simulation for industrial applications. The application of process simulation, as applied to the forging, cold heading and heat treatment has been discussed. Several applications are presented, with an emphasis on industrial cases.

Victor Vazquez and Taylan Altan (Victor Vazquez and Taylan Altan, 2000) have summarized the results of industrially relevant work-in-progress they have done research with numerical and physical modeling systems. They worked on a tool design for the forging of a cross groove inner race for a constant velocity joint, and the design of a tooling to forge a connecting rod without flash. Hong-Seok Kim and Yong-Taek Im (Hong-Seok Kim and Yong-Taek Im, 1999) have worked on a methodology of applying the searching technique for process sequence design. The flexibility of the introduced searching technique has been evaluated by generating design examples of a shaft part, a wrench and hexagonal bolts of AISI 1045.

B. I. Tomov and V. I. Gagov (B. I. Tomov and V. I. Gagov, 1999) have given comprehensive description of some die forging operations selected as representative steps for the near-net-shape forging of spur gears. The main results are obtained on the basis of quasi-static model material experiments that have been applied to collect data needed for statistical processing or to verify some analytical solution and computer simulations. These results could be helpful in engineering practice for simple calculations in process planning design.

P.F. Bariani, G. Berti**,** (P.F. Bariani, G. Berti, L. D'Angelo and J.J. 1998) have done research on an integrated approach to the computer-assisted design of the tooling systems and identification of appropriate setting conditions and timing for multi-station presses to be used in cold, warm and hot forging.

Their approach is based on (i) the classification of possible configurations of punch- and die-side tool subassemblies, (ii) the automatic retrieval of the tool-holder assembly configuration for the specific station of the press, (iii) the assembly

rules and automatic scaling and fitting of individual tool components and (iv) the animation -with check for interference- of die, punches, slugs, grippers and ejectors according to the kinematic model of the press.

L. S. Nielsen, S. Lassen ,et,al, (L. S. Nielsen, S. Lassen, C. B. Andersen, J. Grønbæk and N. Bay, 1997) have described a flexible tool system, which makes it possible to operate with the eight basic cold forging processes, forward rod extrusion, backward can extrusion, forward tube extrusion, open die reduction, ironing, coining, upsetting and heading by changing only a few component specific tool parts like punch, die and ejector, whereas all other tool parts are standard, applicable for many different tool set-ups, thus minimizing the tool costs and the design lead time. The tool exchange time has been minimized by developing special quick tool change systems for punches and dies and a tool positioning system of the hard stop type.

S. Choi, K. H. Na and J. H. Kim (S. Choi, K. H. Na and J. H. Kim, 1997) have worked on rotary forging an incremental forming processes, is a cost-effective forming method for the cold forging of intricate parts to net shape. They have been conducted the experiments which are carried out with carbon steel (AISI1020, AISI1045) and aluminium (6061) and the results then compared with theoretical results. Their analysis seems to be available for the prediction of the forming force and to investigate the influence of the forming parameters on the design of the forging process. Yuichi Nagao , Markus Knoerr et,al, (Yuichi Nagao, Markus Knoerr and Taylan Altan, 1994) have been analyzed the stress states that exist in the inserts during the forming operation and determines the causes of the fatigue failures. They have verified design concept by a specially designed laboratory forging test. They concluded from the test results which show that the stress state in a die can be reduced with the new tooling concept and that the fatigue failure can be avoided.

J. M. Monaghan (J. M. Monaghan, 1993) has worked on an experimental and theoretical analysis of the metal deformation arising during the cold forging of countersunk headed fasteners. The author has derived the expression for the punch—workpiece interface and the mean forging pressure using the slab-analysis method. He had been found that the slab-analysis expressions predicted results are very closer with experimental results.

T. Nagahama and S. Enomae (T. Nagahama and S. Enomae, 1992) have concentrated on the hardware aspects of forging technology in Japan, relating in particular to the automotive industry. They have been studied the market trends in forming methods and press capacity, the requirements for cold- and warm-forging presses, the design and performance characteristics of a number of different types of commercially available forging presses; the process and main features of warm forging, including die life and die lubrication; and different types of forging systems and forging devices, including a die lubricating device, a quick die changing system, and an enclosed-die forging system. Examples of parts produced by cold and warm forging are presented and discussed.

John A. Pale Rajiv Shivpuri et,al**,** (John A. Pale, Rajiv Shivpuri and Taylan Altan, 1992) have reviewed the recent developments in cold forming tooling, machines and processing. They have primary focused on forming complex parts which often required a combination of forward, backward and radial extrusion, using novel multi-action tooling and forming equipment. G. Maccarini, C. Giardini**,** (G. Maccarini, C. Giardini, G. Pellegrini and A. Bugini, 1991) have particularly concerned the results obtained when the fillet radius of the die was varied and then tested in a process of extrusion forging. The rake angle of the extrusion hole provides a solution similar to the devices actually in use. They have been used the well-known matrix method which has first introduced by professor Kobayashi to study theoretically the problem of filling the die cavity during cold forging of copper.

J. M. Monaghan (J. M. Monaghan, 1988) has investigated the coining stage of a closed-die axisymmetric cold-forging operation. He had used an upper-bound technique to establish a generalised expression capable of being used in conjuction with a small computer or programmable calculator for the calculation of forging loads. He had also investigated an influence of preform geometry on die corner fill-out, the results shows that while initial preform geometry does not significantly influence the material flow at the final stages of fill-out, it does influence the maximum loads required to achieve complete die-filling. K. Sevenler, P. S. Raghupathi (K. Sevenler, P. S. Raghupathi and T. Altan, 1987) have been described the development of a prototype expert system for forming-sequence design in cold and warm forging of axisymmetric parts. The different design parameters for a rod/cup component are discussed by V. Maegaard (V. Maegaard, 1985) and he had presented experimental results, particularly for the contact pressure on the die surface in forward/backward extrusion, using the model-material technique.

S. A. Tobias (S. A. Tobias, 1984) has reviewed the field of high energy rate bulk forming, considering the machine advantages and the process advantages in relation to conventional machines; the different types of HERF machines and their respective industrial roles; the economics of HERF hammers; and finally HERF processes. He had reviewed on both the machines and the processes which are illustrated by numerous figures, and there is extensive reference to relevant published literature. (S. K. Biswas and K. Mallikarjuna Rao, 1984) S. K. Biswas and K. Mallikarjuna Rao have been investigated; flow in plane-strain extrusion-forging has investigated. They have been chosen dies so as to allow lateral flow in only the inward direction.The modelling of this elementary process by the present method is simple in

concept and execution. The demonstrated overall validity of this approach recommends its use for predicting flow in more complex configurations and ultimately as a tool of the practising engineer for industrial die and process design.

T. Tran-Cong and N. Phan-thien (T. Tran-Cong and N. Phan-thien, 1988) have worked on simple technique to design extrusion dies for three dimensional profiles based on Boundary Element Methods has reported. They have applied this technique to design a few dies for triangular and square Newtonian extrudates. They have been compared the obtained results with the available data on common design practice. Mingwang Fu and Baozhong Shang (Mingwang Fu and Baozhong Shang, 1995) havebeen developed a boundary-element method (BEM) program used to assess a doubly-reinforced die for the precision forging of a bevel gear. According to their program, the characteristics of the BEM program are given. On the basis of the results calculated by the use of the BEM, the region of dangerous stress has been determined and the effect of the amount of interference on the distribution of stress is revealed. S. Shamsundar, A. G. Marathe et,al, (S. Shamsundar, A. G. Marathe and S. K. Biswas, 1984) have wrought a computer code using finite difference method to estimate temperature histories and validated by comparing the predicted cooling of an integral die-billet

Liu Qingbin, Fu Zengxiang, Yang He,et,al, (Liu Qingbin, Fu Zengxiang, Yang He and Wu Shichun, 1997) have employed a numerical simulation technique to study the thermal behavior of the high-speed forging of an AISI1045 disk. They have been found that die-chilling and some forging parameters have a key effect on the forging process and even on the final product shape. They also found that through the optimization of the forging parameters, an optimum forming processing can be selected before the component is put into production. Heon-Young Kim, Joong-Jae Kim ,et,al, (Heon-Young Kim, Joong-Jae Kim and Naksoo Kim, 1994) have been worked to obtain quantitative information regarding hot closed-die forging, especially in respect of the material flow, the die pressure, and the temperature. For the study of the flow, layered plasticine was used in physical modeling with a half-scale die set. For the numerical simulation, a thermoviscoplastic finite-element program has been developed. Pressure and temperature distributions are obtained at each stage. The temperature changes in the workpiece and the dies per process cycle are simulated. It has been expected that the information can be used in the design of preforming operations to reduce the forging load and to enhance the die life.

Yuichi Nagao, Markus Knoerr (Yuichi Nagao, Markus Knoerr and Taylan Altan, 1994) have analyzed the stress states that exist in the inserts during the forming operation and determines the causes of the fatigue failures. They have been verified the design concept by a specially designed laboratory forging test. Then they found that the test results shows the stress state in a die can be reduced with the new tooling concept and that can be avoid fatigue failure. G. Sutradhar, A. K. Jha et,al, (G. Sutradhar, A. K. Jha and S. Kumar, 1995) have reported on an investigation into various aspects of cold forging of iron-powder preforms. An upperbound solution has constructed for determining the die pressures developed during the cold forging of iron powder under axisymmetric and plane-strain condition. They have been discussed critically obtained results to illustrate the interaction of the various parameters involved and are presented graphically.

Mark RobinsonHoward A. Kuhn (Mark Robinson and Howard A. Kuhn, 1978) have worked on workability analysis that can predict the surface cracking which has been applied to the types of deformation that would occur during cold forging of a gear. They have been applied the workability analysis to both stages to determine the effect of process variables on the likelihood of surface cracking. They have considered process variables in their study are preform geometry, die geometry and die-workpiece friction.Results have been used to formulate preform-design guidelines for different types of gears, including pinions, ring gears, and spur gears. A criterion to predict wall instability during upsetting of a ring has also presented.

M. Arentoft, T. Wanheim, et,al, (M. Arentoft, T. Wanheim, M. Lindegren and S. Lassen, 2005) have worked on Reversed straining in axisymmetric compression test .Because of reversed plastic deformation of the work-piece will effect on the resulting diameter of the work-piece. In order to simulate these conditions a reversed axisymmetrical material tester has designed and constructed. They have been tested three different materials, aluminum alloy AA6082, technically pure copper (99.5%) and cold forging steel Ma8, at different temperatures found during cold forging.

P. Huml, D. Zonghai et,al, (P. Huml, D. Zonghai and Y. Wei, New, 1997) have aimed at describing a new model of strain hardening applied in metal forming analysis. Their model allows better prediction of flow stress under cold forming conditions. The application of the incrementally formulated flow stress model is exemplified for prediction of metal flow, loads and temperature distribution in cold forming processes like cold rolling, wire drawing, cold forging.

3. Conclusions

This paper gives a review of optimization of cold forging die design and dies design process. Cold forging die design and die design process optimization has been done by many authors using different techniques excellently. Still it is require getting the higher accuracy in the results, which can be achieved by optimizing the meshing and finding out the optimal aspect ratio of the elements by using Nueral Network for CAD/CAE die models. Secondly the couple field

analysis has to be done to know the exact behavior of die when it has been undergo various types of loads. In cold forging the die will under go high loads, hence it is essential to know Fatigue behavior and Fatigue Failure of the die when it has been under go cyclic loading.

References

Aly A. Badawy, P. S. Raghupathi, David J. Kuhlmann and Taylan Altan. (*1992).* Computer-aided design of multistage forging operations for round parts, *Journal of Mechanical Working Technology*, Volume 11, Issue 3, July 1992, Pages 259-274.

Armin Buschhausen, Klaus Weinmann, Joon Y. Lee and Taylan Altan, (*1992).* Evaluation of lubrication and friction in cold forging using a double backward-extrusion process,*Journal of Materials Processing Technology*, Volume 33, Issues 1-2, August 1992, Pages 95-108.

B. Falk, U. Engel and M. Geiger (*1998*). Estimation of tool life in bulk metal forming based on different failure concepts,*Journal of Materials Processing Technology*, *Volumes 80-81, 1 August 1998, Pages 602-607.*

B. I. Tomov and V. I. Gagov. (*1999)*. Modelling and description of the near-net-shape forging of cylindrical spur gears,*Journal of Materials Processing Technology*, Volumes 92-93, 30 August 1999, Pages 444-449.

Béla Lengyel, Ijaz A. Chaudhry and R. D. Hibberd, (1994). A consultative system for cold forging with finite element predictions, *Journal of Materials Processing Technology*, Volume 45, Issues 1-4, September 1994, Pages 93-98.

C. F. Castro , C. A. C. António and L. C. Sousa(2004 **).** Optimization of shape and process parameters in metal forging using genetic algorithms, *Journal of Materials Processing Technology*, Volume 146, Issue 3, , Pages 356-364.

C. S. Im, S. R. Suh, M. C. Lee, J. H. Kim and M. S. Joun, (1999), Computer aided process design in cold-former forging using a forging simulator and a commercial CAD software, *Journal of Materials Processing Technology*, Volume 95, Issues 1-3, 15 October 1999, Pages 155-163.

Chen, R. Balendra and Y. Qin, (2004). A new approach for the optimisation of the shrink-fitting of cold-forging dies**.** *Journal of Materials Processing Technology*, Volume 145, Issue 2, 15 January 2004, Pages 215-223.

Chengliang Hu, Kesheng Wang and Quankun Liu, (2007), Study on a new technological scheme for cold forging of spur gears, *Journal of Materials Processing Technology*, *Volumes 187-188*, *12 June 2007*, *Pages 600-603.*

D. J. Kim, B. M. Kim and J. C. Choi, (1997). Determination of the initial billet geometry for a forged product using neural networks, *Journal of Materials Processing Technology*, Volume 72, Issue 1, 1 December 1997, Pages 86-93.

Fatigue abstract Analysis on the fracture surface and cold forging die set using the X-ray fractography Natsume, Y., Miyakawa, S. and Muramatsu*, T. J. Soc. Mater. Sci., Jpn.* June 1989 **38**, (429), 612–616 (in Japanese)

G. Maccarini, C. Giardini, G. Pellegrini and A. Bugini, (1991). The influence of die geometry on cold extrusion forging operations: FEM and experimental results, *Journal of Materials Processing Technology*, Volume27,Issues1-3, August1991,Pages227-238.

G. Sutradhar, A. K. Jha and S. Kumar, (1995). Cold forging of sintered iron-powder performs, *Journal of Materials Processing Technology*, Volume 51, Issues 1-4, April 1995, Pages 369-386.

H.S. Kim, (2007). A study on cold forging process sequence design of terminal pins for high-voltage capacitors, *Journal of Materials Processing Technology*, Volume2000s 187-188, 12 June 2007, Pages 604-608.

Heon-Young Kim, Joong-Jae Kim and Naksoo Kim, (1994). Physical and numerical modeling of hot closed-die forging to reduce forging load and die wear, *Journal of Materials Processing Technology*, Volume 42,Issue4, May1994,Pages401-420.

Hong-Seok Kim and Yong-Taek Im, (1999). An expert system for cold forging process design based on a depth-first search ,*Journal of Materials Processing Technology*, Volume 95, Issues1-3, 15October1999,Pages262-274.

Hyunkee Kim and Taylan Alfan, (1996). Cold forging of steel — practical examples of computerized part and process design,*Journal of Materials Processing Technology*, Volume 59, Issues 1-2, 15 May 1996, Pages 122-131.

Hyunkee Kim, Kevin Sweeney and Taylan Altan, (1994). Application of computer aided simulation to investigate metal flow in selected forging operations,*Journal of Materials Processing Technology*, Volume 46, Issues1-2, October1994,Pages127-154.

Hyunkee Kim, Kevin Sweeney and Taylan Altan, (1994). Application of computer aided simulation to investigate metal flow in selected forging operations,*Journal of Materials Processing Technology*, Volume 46, Issues 1-2, October1994,Pages 127-154.

J. M. Monaghan, (1988). An upper-bound analysis of an axisymmetrical coining process, *Journal of Mechanical WorkingTechnology*, Volume16,Issue2, April1988,Pages175-192.

J. M. Monaghan, (1993). Stress analysis of a cold forging process applied to a countersunk headed fastener, *Journal of Materials Processing Technology*, Volume 39, Issues 1-2, October1993,Pages191-211.

J.-H. Song and Y.-T. Im, (2007), Process design for closed-die forging of bevel gear by finite element analyses ,*Journal of Materials Processing Technology*, Volumes 192-193, 1 October2007,Pages1-7.

Jens Groenbaek and Torben Birker, (2000), Innovations in cold forging die design, *Journal of Materials Processing Technology*, Volume 98, Issue 2, 29 January 2000, Pages 15-161.

John A. Pale, Rajiv Shivpuri and Taylan Altan, (1992). Recent developments in tooling, machines and research in cold forming of complex parts,*Journal of Materials Processing Technology*, Volume 33, Issues 1-2, August 1992, Pages 1-29.

John Walters, Wei-Tsu Wu, Anand Arvind, Guoji Li, Dave Lambert and Juipeng Tang, (2000), Recent development of process simulation for industrial applications, *Journal of Materials Processing Technology*, Volume98,Issue2, 29January2000,Pages205-211.

K. D. Hur, Y. Choi and H. T. Yeo, (2003). A design method for cold backward extrusion using FE analysis, *Finite Elements in Analysis and Design*, Volume 40, Issue 2, December 2003, Pages 173-185.

K. Sevenler, P. S. Raghupathi and T. Altan, (1987). Forming-sequence design for multistage cold forging ,*Journal of Mechanical Working Technology*, Volume 14, Issue 2, March 1987, Pages 121-135.

L. S. Nielsen, S. Lassen, C. B. Andersen, J. Grønbæk and N. Bay, (1997). Development of a flexible tool system for small quantity production in cold forging, *Journal of Materials Processing Technology*, Volume 71, Issue 1, 1November1997,Pages36-42.

Liu Qingbin, Fu Zengxiang, Yang He and Wu Shichun, (1997). Coupled thermo-mechanical analysis of the high-speed hot-forging process,*Journal of Materials Processing Technology*, Volume 69, Issues 1-3, September 1997,Pages190-197.

M. Arentoft, T. Wanheim, M. Lindegren and S. Lassen, (2005), Reversed straining in axisymmetric compression test,*Journal of Materials Processing Technology*, Volume 159, Issue 1, 10 January 2005, Pages 62-68.

Mark Robinson and Howard A. Kuhn, (1978). A workability analysis of the cold forging of gears with integral teeth,*Journal of Mechanical Working Technology*, Volume 1, Issue 3, February 1978, Pages 215-230.

Markus Meidert, Markus Knoerr, Knut Westphal and Taylan Altan, (1992). Numerical and physical modelling of cold forging of bevel gears, *Journal of Materials Processing Technology*, Volume 33, Issues 1-2, August 1992,Pages75-93.

Mingwang Fu and Baozhong Shang, (1995). Stress analysis of the precision forging die for a bevel gear and its optimal design using the boundary-element method, *Journal of Materials Processing Technology*, Volume53,Issues3-4, September1995,Pages511-520.

P. B. Hussain, J. S. Cheon, D. Y. Kwak, S. Y. Kim and Y. T. Im, (2002). Simulation of clutch-hub forging process using CAMP*form ,Journal of Materials Processing Technology*, Volume 123, Issue 1, 10 April 2002, Pages 120-132

P. Huml, D. Zonghai and Y. Wei, New, (1997). Model of Flour Stress under Cold-Forming Conditions,*CIRP Annals - Manufacturing Technology*, Volume 46, Issue 1, 1997, Pages 163-166.

P.F. Bariani, G. Berti, L. D'Angelo and J.J. (1998*).* Yang (,An Integrated Approach in Design Tooling, Setting Up and Timing of Forging Transfer-Machines,*CIRP Annals - Manufacturing Technology*, Volume 47, Issue 1, 1998,Pages203-206.

Quang-Cherng Hsu and Rong-Shean Lee, (1997). Cold forging process design based on the induction of analytical knowledge,*Journal of Materials Processing Technology*, Volume 69, Issues 1-3, September 1997, Pages 264-272.

R. Di Lorenzo and F. Micari, (1998). An Inverse Approach for the Design of the Optimal Preform Shape in Cold Forging *CIRP Annals - Manufacturing Technology*, Volume 47, Issue 1, 1998, Pages 189-192.

Ravi Duggirala, Rajiv Shivpuri, Satish Kini, Somnath Ghosh and Subir Roy, (1994). Computer aided approach for design and optimization of cold forging sequences for tomotive parts,*Journal of Materials Processing Technology*, Volume 46, Issues 1-2, October 1994, Pages 185-198.

Rong-Shean Lee, Quang-Cherng Hsu and Saint-Len Su, (1999). Development of a parametric computer-aided die design system for cold forging,*Journal of Materials Processing Technology*, Volume 91, Issues 1-3, 30 June 1999,Pages 80-89.

S. A. Tobias, (1984). The state of the art of high energy rate bulk forming, *Journal of Mechanical Working Technology*, Volume9,Issue3, May1984,Pages237-277.

S. Choi, K. H. Na and J. H. Kim, (1997). Upper-bound analysis of the rotary forging of a cylindrical billet,*Journal of Materials Processing Technology*, Volume 67, Issues 1-3, May 1997,Pages78-82.

S. I. Oh, W. T. Wu and J. P. Tang, (1992). Simulations of cold forging processes by the DEFORM system, *Journal of Materials Processing Technology*, Volume 35, Issues 3-4, October 1992, Pages 357-370.

S. K. Biswas and K. Mallikarjuna Rao, (1984). Flow of metal in constrained plane-strain extrusion-forging: Part I, *Journal of Mechanical Working Technology*, Volume 9, Issue 2, March 1984, Pages 161-179.

S. Roy, S. Ghosh and R. Shivpuri, (1997). A new approach to optimal design of multi-stage metal forming processes with micro genetic algorithms, *International Journal of Machine Tools and Manufacture*, Volume37,Issue1, January1997,Pages29-44.

S. Shamsundar, A. G. Marathe and S. K. Biswas, (1984). Development of a computer code to predict cooling of die and billet in forging ,*International Journal of Machine Tool Design and Research*, Volume 24, Issue4, 1984,Pages311-320.

T. Ishikawa, N. Yukawa, Y. Yoshida, H. Kim and Y. Tozawa, (2000), Prediction of Dimensional Difference of Product from Tool in Cold Backward Extrusion,*CIRP Annals - Manufacturing Technology*, Volume 49, Issue 1, 2000,Pages169-172.

T. Nagahama and S. Enomae, (1992). Cold- and warm-forging press developments and applications,*Journal of Materials Processing Technology*, Volume 35, Issues 3-4, October 1992, Pages 415-427.

T. Ohashi, A. Nakata, (2001), Y. Saotome and S. Imamura ,Analysis on accuracy of forging die sets by disassembly planning algorithm with multiple agents, *Journal of Materials Processing Technology*, Volume 119, Issues 1-3, 20 December 2001, Pages 140-145.

T. Petersen and P. S. Frederiksen, (1994), Fillet design in cold forging dies,
Computers & Structures, Volume 50, Issue 3, 3 February 1994, Pages 393-400.

T. Tran-Cong and N. Phan-thien, (1988). Die design by a boundary element method,*Journal of Non-Newtonian Fluid Mechanics,* Volume 30, Issue 1, 2 October 1988, Pages 37-46.

Takahiro Ohashi, Satoshi Imamura, Toru Shimizu and Mitsugu Motomura, (2003). Computer-aided die design for axis-symmetric cold forging products by feature elimination ,*Journal of Materials Processing Technology*, Volume 137, Issues 1-3, 30 June 2003, Pages 138-144.

Taylan Altan and Markus Knoerr, (1992). Application of the 2D finite element method to simulation of cold-forging processes,*Journal of Materials Processing Technology*, Volume 35,Issues3-4, October1992,Pages275-302.

V. Maegaard, (1985). The use of the model technique in the prediction of the pressure distribution over the tool surfaces in cold forging,*Journal of Mechanical Working Technology*, Volume 12, Issue 2, December 1985,Pages173-192.

V. Maegaard, (1985). The use of the model technique in the prediction of the pressure distribution over the tool surfaces in cold forging, *Journal of Mechanical Working Technology*, Volume 12, Issue 2, December 1985, Pages 173-192.

V. Maegaard, (1985). The use of the model technique in the prediction of the pressure distribution over the tool surfaces in cold forging,*Journal of Mechanical Working Technology*, Volume 12, Issue 2, December 1985, Pages 173-192.

Victor Vazquez and Taylan Altan. (2000). New concepts in die design — physical and computer modeling applications, *Journal of Materials Processing Technology*, Volume 98, Issue2, 29January2000,Pages212-223.

W. G. Cho and C. G. Kang, (2000). Mechanical properties and their microstructure evaluation in the thixoforming process of semi-solid aluminum alloys, *Journal of Materials Processing Technology*, Volume 105,Issue3, 29Septembe2000,Pages269-277.

W. L. Xu and K. P. (1997). Rao,Analysis of the deformation characteristics of spike-forging process through FE simulations and experiments,*Journal of Materials Processing Technology*, Volume70,Issues1-3, October1997,Pages122-128.

Y. Qin, R. Balendra and K. Chodnikiewicz, (2000). A method for the simulation of temperature stabilisation in the tools during multi-cycle cold-forging operations,*Journal of Materials Processing Technology*, Volume 107, Issues 1-3, 22 November 2000, Pages 252-259.

Yi-Che Lee and Fuh-Kuo Chen, (2001). Fatigue life of cold-forging dies with various values of hardness, *Journal of Materials Processing Technology*, Volume 113, Issues 1-3, 15 June 2001,Pages539-543.

Young Suk Kim, Hyun Sung Son and Chan Il Kim, (2003). Rigid–plastic finite element simulation for process design of impeller hub forming,*Journal of Materials Processing Technology*, Volumes 143-144, 20 December 2003, Pages 729-734.

Young-Seon Lee, Jung-Hwan Lee, Jong-Ung Choi and T. Ishikawa, (2002). Experimental and analytical evaluation for elastic deformation behaviors of cold forging tool ,*Journal of Materials Processing Technology*, Volume 127, Issue 1, 20 September 2002, Pages 73-82.

Yuichi Nagao, Markus Knoerr and Taylan Altan, (1994). Improvement of tool life in cold forging of complex automotive parts,*Journal of Materials Processing Technology*, Volume 46, Issues 1-2, October 1994, Pages 73-85.

Yuichi Nagao, Markus Knoerr and Taylan Altan, (1994). Improvement of tool life in cold forging of complex automotive parts, *Journal of Materials Processing Technology*, Volume 46,Issues1-2, October1994,Pages73-85.

Modern Applied Science

www.ccsenet.org/journal.html

Vol. 3, No. 3

March 2009

Kinematics and Dynamics of a Master Maipulator

Yechu Hu

College of Mechanical and Electronic Engineering

Tianjin Polytechnic University

Tianjin 300160, China

E-mail: hyc820815@yahoo.cn

Abstract

I analyze the kinematics and Dynamics of Phantom Premium 1.5 made and sold by SenSable Technologies Inc., which is widely-used as the master manipulator in telerobotic systems. The forward kinematics is studied using Denavit-Hartenberg method, the manipulator Jacobian is also presented. The dynamic equations incorporating frictional effects of Premium 1.5 are derived.

Keywords: Master manipulator, Kinematics analysis, Dynamic model, Frictional effects

1. Introduction

The first telerobotic system was developed by Raymond C. Goertz in 1940s to let an operator handle radioactive materials behind a shielded wall, at National Argonne Laboratory in the US. In the past decades, teleoperation has found applications in many areas including space technologies, underwater explorations and assistance, surgery and rehabilitations, nuclear/toxic material handling and waste disposal, military/firefighting operation, mining. Recently, the applications of teleoperation systems have been extended to training, education, entertainment, and virtual reality areas as well.

As can be seen in figure 1, a teleoperation system generally has five components: operator, master, control system, slave, and environment. The main function of the system can be explained as follows: a control command is sent through the control system to the slave to make the remote manipulator perform a task as desired; to prevent damage, to reduce task completion time and to enhance performance, contact interaction from the remote site has to be transmitted to the operator.

As shown in figure 1, throughout an interaction, the master mechanism must perform the dual task of position measurement and force display. The kinematics especially the forward kinematics is of great importance for the control of the telerobotic system. While, when dealing with the dynamics of robotic manipulators, frictional effects is often neglected. This paper mainly discusses the forward kinematics using Denavit-Hartenberg method, and derives the dynamic equations incorporating frictional effects in the joints.

2. Kinematics analysis

Figure 2 is the photo and structural sketch of a typical master manipulator (PHANToM Premium 1.5), which can provide the operator with 3 DOF motion and three dimensional force feedbacks. As shown in figure 2(b), Premium 1.5 consists of three rotational joints, zero configuration of Premium 1.5 is shown in figure 2(b), spatial frame and tool frame are superposed in zero configuration. Figure 3 depicts the side and top views of the configuration of Premium 1.5. And, the reference frames are shown in figure 4, the D-H parameter is listed in table 1, where

a_i represents the distance from Z_i to Z_{i+1} measured along X_i,

α_i represents the angle from Z_i to Z_{i+1} measured about X_i,

d_i represents the distance from X_{i-1} to X_i along Z_i,

θ_i represents the angle from X_{i-1} to X_i measured about Z_i.

The general transformation matrix 1 comes directly from the D-H parameters (Craig, 2005 & Murray, 1998).

$$ {}^{i-1}_{i}T = \begin{bmatrix} \cos\theta_i & \sin\theta_i & 0 & a_{i-1} \\ \sin\theta_i\cos\alpha_{i-1} & \cos\theta_i\cos\alpha_{i-1} & -\sin\alpha_{i-1} & -\sin\alpha_{i-1}d_i \\ \sin\theta_i\sin\alpha_{i-1} & \cos\theta_i\sin\alpha_{i-1} & \cos\alpha_{i-1} & \cos\alpha_{i-1}d_i \\ 0 & 0 & 0 & 1 \end{bmatrix} \quad (1) $$

And the final transformation matrix can be written in equation 2 with some mediated matrixes from ${}^{w}_{0}T$ to ${}^{3}_{t}T$ omitted.

$$ {}^{s}_{t}T = {}^{w}_{0}T_1^0 T_2^1 T_3^2 T_t^3 T = \begin{bmatrix} \boldsymbol{R}(\theta) & \boldsymbol{p}(\theta) \\ \boldsymbol{0} & 1 \end{bmatrix} \tag{2} $$

Where

$$ \boldsymbol{R}(\boldsymbol{\theta}) = \begin{pmatrix} \cos\theta_1 & -\sin\theta_1 \sin\theta_3 & \sin\theta_1 \cos\theta_3 \\ 0 & \cos\theta_3 & \sin\theta_3 \\ -\sin\theta_1 & -\cos\theta_1 \sin\theta_3 & \cos\theta_1 \cos\theta_3 \end{pmatrix} \tag{3} $$

$$ \boldsymbol{p}(\boldsymbol{\theta}) = \begin{pmatrix} \sin\theta_1 (l_1 \cos\theta_2 + l_2 \sin\theta_3) \\ l_2 + l_1 \sin\theta_2 - l_2 \cos\theta_3 \\ -l_1 + \cos\theta_1 (l_1 \cos\theta_2 + l_2 \sin\theta_3) \end{pmatrix} \tag{4} $$

Except the forward kinematics of the manipulator, the velocity relationship between the rotational joints and the end effector is often concerned. So, the spatial and body manipulator Jacobian is written here, moreover, they can be used to describe the relationship between the end point wrench and the joint torque.

$$ \boldsymbol{J}^s(\boldsymbol{\theta}) = \begin{pmatrix} l_1 & -l_1 \sin\theta_1 \sin\theta_2 & \sin\theta_1 (l_2 + l_1 \sin\theta_2) \\ 0 & l_1 \cos\theta_2 & l_1 (\cos\theta_1 - \cos\theta_2) \\ 0 & -l_1 \cos\theta_1 \sin\theta_2 & \cos\theta_1 (l_2 + l_1 \sin\theta_2) \\ 0 & 0 & -\cos\theta_1 \\ 1 & 0 & 0 \\ 0 & 0 & \sin\theta_1 \end{pmatrix} \tag{5} $$

$$ \boldsymbol{J}^b(\boldsymbol{\theta}) = \begin{pmatrix} l_1 \cos\theta_2 + l_2 \sin\theta_3 & 0 & 0 \\ 0 & l_1 \cos(\theta_2 - \theta_3) & 0 \\ 0 & -l_1 \sin(\theta_2 - \theta_3) & l_2 \\ 0 & 0 & -1 \\ \cos\theta_3 & 0 & 0 \\ \sin\theta_3 & 0 & 0 \end{pmatrix} \tag{6} $$

3. Dynamic Model of the Master Manipulator

M. C. Cavusoglu (Cavusoglu, 2001) identified the mechanical structure of Premium 1.5 into seven segments A through G shown on figure 5. Note that the spatial frame used in dynamic calculations is centered at the intersection point of three axises of rotational joints.

And he calculated the kinetic and potential energy of each segment in the spatial frame, then wrote the dynamic equation of the system using Lagrange method.

$$ M(\boldsymbol{\theta})\ddot{\boldsymbol{\theta}} + C(\boldsymbol{\theta}, \dot{\boldsymbol{\theta}})\dot{\boldsymbol{\theta}} + N(\boldsymbol{\theta}) = \boldsymbol{\tau} \tag{7} $$

In equation 7, $M(\boldsymbol{\theta})\ddot{\boldsymbol{\theta}}$ is inertial force, $C(\boldsymbol{\theta}, \dot{\boldsymbol{\theta}})\dot{\boldsymbol{\theta}}$ is Coriolis and centrifugal force, $N(\boldsymbol{\theta})$ is gravitational force, $\boldsymbol{\tau}$ is the vector of joint torque, each element of the matrix of $\boldsymbol{M}$, $\boldsymbol{C}$, and $\boldsymbol{N}$ is listed in Cavusoglu's paper (Cavusoglu, 2001). Note that the inertial force, Coriolis and centrifugal force and gravitational force are highly non-linear, making it difficult for dynamic parameter identification and controller algorithm design (McJunkin, 2007).

So, equation 7 could be linearly parameterized as follows:

$$ \boldsymbol{\tau}_d = \boldsymbol{Y}_d \left(\boldsymbol{\theta}, \dot{\boldsymbol{\theta}}, \ddot{\boldsymbol{\theta}} \right) \boldsymbol{\pi}_d \tag{8} $$

where $\boldsymbol{Y}$ is the regressor matrix and $\boldsymbol{\pi}$ is the vector 12 dynamic parameters defined as:

$$
\begin{aligned}
y_{12} &= (1+\cos 2\theta_3)\ddot{\theta}_1 - 2\sin 2\theta_3\dot{\theta}_1\dot{\theta}_3 \\
y_{13} &= (1-\cos 2\theta_3)\ddot{\theta}_1 + 2\sin 2\theta_3\dot{\theta}_1\dot{\theta}_3 \\
y_{15} &= (1+\cos 2\theta_2)\ddot{\theta}_1 - 2\sin 2\theta_2\dot{\theta}_1\dot{\theta}_2 \\
y_{16} &= (1-\cos 2\theta_2)\ddot{\theta}_1 + 2\sin 2\theta_2\dot{\theta}_1\dot{\theta}_2 \\
y_{17} &= \ddot{\theta}_1 \\
y_{18} &= (1+\cos 2\theta_2)\ddot{\theta}_1 - 2\sin 2\theta_2\dot{\theta}_1\dot{\theta}_2 \\
y_{19} &= (1-\cos 2\theta_3)\ddot{\theta}_1 + 2\sin 2\theta_3\dot{\theta}_1\dot{\theta}_3 \\
y_{10} &= 2\cos\theta_2 \sin\theta_3\ddot{\theta}_1 - 2\sin\theta_2 \sin\theta_3\dot{\theta}_1\dot{\theta}_2 \\
&\quad + 2\cos\theta_2 \cos\theta_3\dot{\theta}_1\dot{\theta}_3
\end{aligned} \tag{9a}
$$

$$
\begin{aligned}
y_{24} &= \ddot{\theta}_2 \\
y_{25} &= \sin 2\theta_2\dot{\theta}_1^2 \\
y_{26} &= -\sin 2\theta_2\dot{\theta}_1^2 \\
y_{28} &= 2\ddot{\theta}_2 + \sin 2\theta_2\dot{\theta}_1^2 \\
y_{210} &= -\sin(\theta_2-\theta_3)\ddot{\theta}_3 + \sin\theta_2 \sin\theta_3\dot{\theta}_1^2 \\
&\quad + \cos(\theta_2-\theta_3)\dot{\theta}_3^2 \\
y_{211} &= \cos\theta_2
\end{aligned} \tag{9b}
$$

$$
\begin{aligned}
y_{31} &= \ddot{\theta}_3 \\
y_{32} &= \sin 2\theta_3\dot{\theta}_1^2 \\
y_{33} &= -\sin 2\theta_3\dot{\theta}_1^2 \\
y_{39} &= 2\ddot{\theta}_3 - \sin 2\theta_3\dot{\theta}_1^2 \\
y_{310} &= -\sin(\theta_2-\theta_3)\ddot{\theta}_2 - \cos\theta_2 \cos\theta_3\dot{\theta}_1^2 \\
&\quad + \cos(\theta_2-\theta_3)\dot{\theta}_2^2 \\
y_{312} &= \sin\theta_3
\end{aligned} \tag{9c}
$$

and

$$\pi_1 = I_{axx} + I_{efxx} \tag{10a}$$

$$\pi_2 = \frac{1}{2}\left(I_{ayy} + I_{efyy}\right) \tag{10b}$$

$$\pi_3 = \frac{1}{2}\left(I_{azz} + I_{efzz}\right) \tag{10c}$$

$$\pi_4 = I_{bxx} + I_{cdxx} \tag{10d}$$

$$\pi_5 = \frac{1}{2}\left(I_{byy} + I_{cdyy}\right) \tag{10e}$$

$$\pi_6 = \frac{1}{2}\left(I_{bzz} + I_{cdzz}\right) \tag{10f}$$

$$\pi_7 = I_{gyy} \tag{10g}$$

$$\pi_8 = \frac{1}{2}m_a l_1^2 + \frac{1}{8}m_b l_1^2 \tag{10h}$$

$$\pi_9 = \frac{1}{8}m_a l_2^2 + \frac{1}{2}m_b l_3^2 \tag{10i}$$

$$\pi_{10} = \frac{1}{2}m_a l_1 l_2 + \frac{1}{2}m_b l_1 l_3 \tag{10j}$$

$$\pi_{11} = m_a g l_1 + \frac{1}{2} m_b g l_1 - m_{cd} g l_4 \tag{10k}$$

$$\pi_{12} = \frac{1}{2} m_a g l_2 + m_b g l_3 - m_{ef} g l_5 \tag{10l}$$

The physical and geometric parameters I_{axx}, I_{ayy}, I_{azz}, I_{bxx}, I_{byy}, I_{bzz}, I_{cdxx}, I_{cdyy}, I_{cdzz}, I_{efxx}, I_{efyy}, I_{efzz}, I_{gyy}, m_a, m_b, m_{cd}, m_{ef}, l_1, l_2, l_3, l_4, l_5 can be found in the literature (Cavusoglu, 2001), while g is the acceleration gravity.

4. Inclusion of Frictional Effects

Friction effect in the joints of Premium 1.5 is neglected in Equation 7 and 8, as a matter of fact, the friction effect should not be ignored. Here I use Coulomb friction plus viscous damping (Armstrong, 1994 & Olsson, 1998) to include friction effect in the dynamic model of the device (Tahmasebi, 2005).

$$\boldsymbol{\tau}_f = \boldsymbol{\pi}_{fc} \operatorname{sgn}(\dot{\boldsymbol{\theta}}) + \boldsymbol{\pi}_{fv} \dot{\boldsymbol{\theta}} \tag{11}$$

or

$$\boldsymbol{\tau}_f = \begin{bmatrix} \tau_{f1} \\ \tau_{f2} \\ \tau_{f3} \end{bmatrix} = \begin{bmatrix} \tau_{fc1} \operatorname{sgn}(\dot{\theta}_1) + \tau_{fv1} \dot{\theta}_1 \\ \tau_{fc2} \operatorname{sgn}(\dot{\theta}_2) + \tau_{fv2} \dot{\theta}_2 \\ \tau_{fc3} \operatorname{sgn}(\dot{\theta}_3) + \tau_{fv3} \dot{\theta}_3 \end{bmatrix} = \boldsymbol{Y}_f \boldsymbol{\pi}_f \tag{12}$$

where

$$\boldsymbol{Y}_f = \begin{pmatrix} \operatorname{sgn}(\dot{\theta}_1) & 0 & 0 & \dot{\theta}_1 & 0 & 0 \\ 0 & \operatorname{sgn}(\dot{\theta}_2) & 0 & 0 & \dot{\theta}_2 & 0 \\ 0 & 0 & \operatorname{sgn}(\dot{\theta}_3) & 0 & 0 & \dot{\theta}_3 \end{pmatrix} \tag{13}$$

$$\boldsymbol{\pi}_f = \begin{bmatrix} \pi_{fc1} & \pi_{fc2} & \pi_{fc3} & \pi_{fv1} & \pi_{fv2} & \pi_{fv3} \end{bmatrix}^T \tag{14}$$

$\boldsymbol{Y}_f$ is the regressor matrix, $\boldsymbol{\pi}_f$ is 6 dimensional parameter vector.

Including the friction effect of the device and combing equation 8 with 12, I could write

$$\boldsymbol{\tau} = \boldsymbol{Y}\left(\boldsymbol{\theta}, \dot{\boldsymbol{\theta}}, \ddot{\boldsymbol{\theta}}\right) \boldsymbol{\pi} \tag{15}$$

where

$$\boldsymbol{Y} = \begin{bmatrix} \boldsymbol{Y}_d \vdots \boldsymbol{Y}_f \end{bmatrix} \tag{16}$$

$$\boldsymbol{\pi} = \begin{bmatrix} \boldsymbol{\pi}_d \vdots \boldsymbol{\pi}_f \end{bmatrix}^T \tag{17}$$

Equation 15 is named the dynamic model of Premium 1.5 with joint friction. Each of the element of the parameter vector is identified as shown in table 2.

5. Conclusion

In telerobotic systems, the kinematics especially the forward kinematics is of great importance for the control of teleoperaton, frictional effects is often neglected in dynamic equations. This paper mainly discusses the forward kinematics using D-H method, the manipulator Jacobian is also presented. And I derive the dynamic equations incorporating frictional effects in the joints.

References

Armstrong Brian, Dupont Pierre, Canudas de Wit C. (1994). A Survey of Models, Analysis Tools and Compensation Methods for the Control of Machines with Friction[J]. *Automatica*, 30(7): 1083-1138.

Cavusoglu M C, Feygin D. (2001). Kinematics and Dynamics of Phantom(TM) Model 1.5 Haptic Interface. [R]. Berkeley: University of California at Berkeley, Electronics Research Laboratory Memo M01/15.

Craig J J. Introduction to Robotics. (2005). *Mechanics and Control* (3_{rd} Editon)[M]. Upper Saddle River: Addison-Wesley.

Haptic Device. [A]. Proceedings of the 2005 IEEE Conference on Control Applications[C]. Toronto, Canada: IEEE, 1251-1256.

McJunkin S T. (2007). Transparency Improvement for Haptic Interfaces. [D]. Houston: Rice University.

Murray R M, Li Z X, Sastry S S. (1994). *A Mathematical Introduction to Robotic Manipukation.* [M]. Boca Raton:

CRC Press.

Olsson H, Astrom K J, Canudas de Wit C, et al. (1998). Friction Models and Friction Compensation[J]. *European Journal of Control,* 4(3): 176-195.

Tahmasebi A M, Taati B, Mobasser F, et al. (2005). Dynamic Parameter Identification and Analysis of a PHANToM(TM)

Table 1. D-H parameter of Premium 1.5

Frame	α_{i-1}	a_{i-1}	θ_i	d_i
0	$-\pi/2$	0	$-\pi/2$	0
1	0	$-l_1$	θ_1	l_2
2	$\pi/2$	0	θ_2	0
3	0	l_1	$-\pi/2-\theta_2+\theta_3$	0
tool	$-\pi/2$	l_2	$\pi/2$	0

Table 2. Dynamic Parameter of Premium 1.5($\times 10^{-4}$)

π_1	π_2	π_3	π_4	π_5	π_6
7.5784	0.3154	3.3572	12.0490	5.5095	0.2981
π_7	Π_8	π_9	π_{10}	π_{11}	π_{12}
11.8700	6.1644	0.8572	4.5693	-160	-739
π_{13}	π_{14}	π_{15}	π_{16}	π_{17}	π_{18}
707	251	248	-57	-35	-5

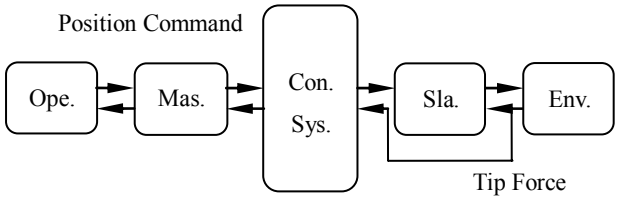

Figure 1. Diagram of the master-slave teleoperation system

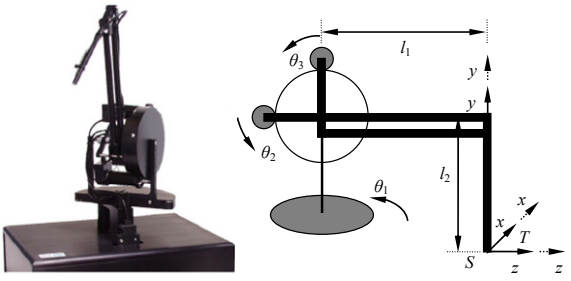

Figure 2. Photo and structural sketch of Premium1.5

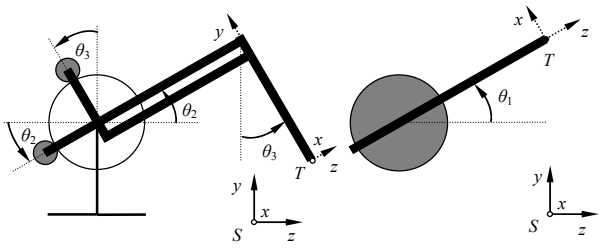

Figure 3. Configuration of Premium 1.5

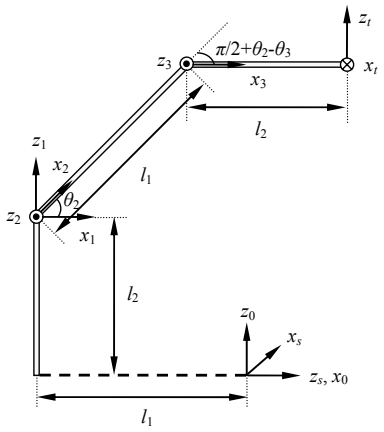

Figure 4. Reference frames of Premium1.5

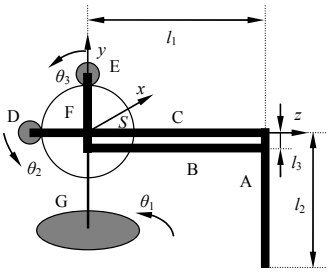

Figure 5. Segments of Premium 1.5

Modern Applied Science

www.ccsenet.org/journal.html

Vol. 3, No. 3

March 2009

Antioxidant Properties of Water Extracts for the Iraqi Plants *Phoenix Dactylifera, Loranthus Europeas, Zingiber Officinalis and Citrus Aurantifolia*

Sundus Hameed Ahmed

Radio biology center, Ministry of science and Technology

Baghdad, Iraq

E-mail: hams_63@yahoo.com

João Batista .Rocha

Departamento de Química ,Universidade Federal De Santa

Maria(UFSM), Campus Universitário-Camobi, 97105-900 Santa

Maria RS,Brasil

Abstract

In the present study, the antioxidant activities (%AA) of the water extract for *Phoenix dactylifera, Loranthus europeas, Zingiber officinalis, Citrus aurantifolia* was measured by the TBARS method. Total phenol content, DPPH scavenger free radical activity and the iron chelation capacity of these extracts were also quantified. The results revealed that *Phoenix dactylifera, Citrus aurantifolia* had a significantly ($P < 0.05$) higher total phenol, and iron chelation ability, DPPH scavenging activity, and (%AA) than *Loranthus europeas* and *Zingiber officinalis*. Meanwhile the water extracts of *Phoenix dactylifera* and *Citrus aurantifolia* had the highest protective ability and this probably due to its higher antioxidant activity (AA%), total phenol content, iron chelation and DPPH scavenging activity.

Keywords: Antioxidant activity, Polyphenol, Pro-oxidant, $Fé^{+2}$, DPPH, Iron chelation

1. Introduction

The common free radicals are oxygen reactive species (ROS) namely superoxide radical, hydroxyl radical, and peroxyl radical which can be internally produced by cellular metabolism, inflammaiton by immune cells and externally by radiation, pharmaceuticals, hydrogen peroxide, toxic chemicals, smoke, alcohol, oxidized polyunsaturated fats and cooked food. Free radicals can cause damage to parts of cells such as proteins, DNA, and cell membranes by stealing their electrons through a process called oxidation. Free radicals may cause heart damage, cancer, and a weak immune system (Feinman 1988; Esterbauer *et al*. 2006; Maharaj et al., 2006; Puntel et al., 2007). Farther more, a strong relationship between atherosclerosis and acetaldehde formed from lipid peroxidation hás been reported (Glavind *et a*l.; 1992). Most living organisms possess enzymatic and nonenzymatic defence systems against excess production of reactive oxygen species. may be of great. However, different external factors such as smoke, diet, alcohol and some drugs and aging could decrease the capability of such protective systems resulting in disturbances of the redox eqilibrium that is established in healthy conditions. Therefore, antioxidants that scavenge reactive oxygen species may be of great value in preventing the onset and / or the propagation of oxidative systems resulting in disturbances of redox equilibrium that is established in healthy conditions. There for, antioxidant that scavenge reactive oxygen species may be of great value in preventing the onest and or the propagation of oxidative disease (Whilet, 1994; Olalye and rocha, 2007). Antioxidants are also compounds that scavenge reactive oxygen species may be of great value in preventing the onset and or the propagation of oxidizing chain reaction (REF). Of late, more attention hás been paid to the role of natural antioxidants mainly phenolic compounds, which may have more antioxidant activity than vitamins C, E, β- carotene (Vinson *et al*., 1995; Haslam 2006). The antioxidative effects of natural phenolic compounds in pure formes or in thier extracts from different model systems of oxidation (Gazani *et al*., 1998; Heinonen, *et al*., 2003) . Therefore, antioxidants, which can neutrlize free radicals, may be of central importance in the prevention of carcinogenicity, cardiovascular and neurodegenerative changes associated with aging (Halliwell 1994; Yu 1994; Houghton 2003; _Felter 2008). Epidemiological studies show that the consumption of plants can protect humans against oxidative damage by inhibiting or quenching free radicals and reactive oxygen species (Ames *et al*., 1993; Chu *et al*., 2002; Materska and perucka 2005).

The aim of the present work is to evaluate in vitro the antioxidant activities of water extracts for *Phoenix dactylifera, Loranthus europeaus, Zingiber officinalis, Citrus aurantifolia* in relation to their Antioxidant activity measured by the TBARS method, total phenol content, Iron chelation,and DPPH

2. Material and methods

2.1 Materials

Thiobarbituric acid (TBA), malonaldehyde- bis-dimethyl acetal(MDA) 2,2-diphenyl-1-picrylhydrazyl (DPPH_), quercetin, rutin and phenanthroline were purchased from Sigma (St. Louis, MO,USA). Sodium nitroprusside (SNP) was obtained from Merck(Darmstadt, Germany) and iron (II) sulphate from Reagen (Rio de Janeiro, RJ, Brazil).

2.2 Preparation of plant extract

The plant was purchased from Iraq and authenticated by a botanist at University of baghdad/ Iraq. Dried plant material (25 g) was soaked in boiling water (250 ml) for 15 min, allowed to cool and filtered using Whatman filter paper.The obtained residues were further extracted, twice, and then concentrated using a rotary evaporator. Filtrates were dried to a powder in an oven at 40–50 _C.

2.3 Phenolics content

The total phenol content was determined by adding 0.5 ml of the aqueous extract to 2.5 ml, 10% Folin–Ciocalteau's reagent (v/v) and 2.0 ml of 7.5% sodium carbonate. The reaction mixture was incubated at 45 _C for 40 min, and the absorbance was measured at 765 nm in the spectrophotometer. Gallic acid was used as a standard phenol (Singleton, Orthofer R, & Lamuela-Raventos, 1999). The mean of three readings was used and the total phenol content was expressed as milligrammes of gallic acid equivalents/ g extract.

2.4 Antioxidant activity toward lipid peroxidation in brain homogenate

Production of TBARS was determined using a modified method of Ohkawa, Ohishi, and Yagi (1979). The rats were killed by anaesthetizing them mildly in ether and the brain tissues were quickly removed and placed on ice. One gramme quantities of tissues were homogenised in cold 100 mM Tris-buffer Ph 7.4 (1:10 w/v) with ten up and down strokes at approximately1200 rev/min in a Teflon glass homogenizer. The homogenates were centrifuged for 10 min at 1400g to yield a pellet that was discarded and a low-speed supernatant (S1) used for the assay. The homogenates (100 µl) were incubated with or without 50 µl of the various freshly prepared oxidants (Fé SO_4) and different concentrations of the plant extracts, together with an appropriate volume of deionized water, to give a total volume of 300 µl at 37 _C for 1 h. The colour reaction was carried out by adding 300 µl of the 8.1% sodium dodecyl sulphate(SDS), acetic acid (pH 3.4) and 0.6% TBA, respectively. The absorbance was read after cooling the tubes at a wavelength of 532 nm in a spectrophotometer (TBARS 1). As the control, the homogenate was peroxidized by Fé SO_4 without the antioxidants (TBARS2). The reaction without Fé SO_4 were carried out for each of the test substance as the blank (TBARS3 is the blank for test and TBARS4 is the blank for control). The antioxidant potential of the sample was calculated by using the following equation: Antioxidant activity (%) = (1-(TBARS1 – TBARS3) / (TBARS2 – TBARS4) × 100. All tests were done in triplicate and the results averaged .

2.5 Iron chelation assay

The ability of the aqueous extract to chelate $Fé^{+2}$ was determined using a modified method of Puntel, Nogueira, and Rocha(2005). Briefly, 150 of freshly prepared 2 mM FeSO4 were added to a reaction mixture containing 168 of 0.1 M Tris–HCl (pH 7.4), 218 saline and the aqueous extract of the plant (3.5 -16.9 mg /ml). The reaction mixture was incubated for 5 min, before the addition of 13 of 0.25% 1,10-phenanthroline (w/v). The absorbance was subsequently measured at 510 nm in the spectrophotometer

2.6 DPPH radical-scavenging

Scavenging of the stable radical, DPPH, was assayed in vitro(Hatano, Kagawa, Yasuhara, & Okuda, 1988). The extract (2.5 - 50 µg/ ml) was added to a 0.5 ml solution of DPPH (0.25 mM in 95% ethanol). The mixture was shaken and allowed to stand at room temperature for 30 min and the absorbance was measured at 517 nm in a spectrophotometer. Percent inhibition was calculated from the control. Vitamin C was used as a standard compound in the DPPH_ assay

2.7 Analysis of data

Quantitative data would be expressed as mean ± standard deviation. Statistical evaluation of the data would be performed by using one – way analysis of variance (ANOVA) followed by Duncan's multiple range test (Zar,1984).

3. Results and discussion

The yield and total phenolics content of the different plants extracts, *Phoenix dactylifera, Loranthus europeas, Zingiber officinalis, Citrus aurantifolia Showed in* table 1. The amount of extractable components expressed as percentage by weight of dried material . The results revealed that the yield of *Phoenix dactylifera (101.3* ± 1.0^{a}), *Citrus aurantifolia*

(94.2 ± 2.2 [d]) had a significantly (P<0.05) higher yield content than *Loranthus europeas* (86.8 ± 1.2[b]) *and Zingiber officinalis* (69.7 ± 2.3[c]). However, the total phenol content of *Phoenix dactylifera (498.9* ± 1.8[a]), *Citrus aurantifolia* (404.2 ± 2.8 [d]) had a significantly higher (P<0.05) total phenolic content than *Loranthus europeas* (335.5 ± 2.3 [b]) and *Zingiber officinalis* (266.3 ± 1.2 [c]). The results revealed that the yield and total phenol content of *Phoenix dactylifera* was higher than the yield and total phenol content reported by

Alfarisi, Morris and Baron (2007), while that of *Loranthus europeas* was within the same range with the value reported by Chopra, Nayar and Chopra (1997). The yields and phenol content of *Citrus aurantifolia* and *Zingiber officinalis ,* was higher than phenol content of some tropical leafy vegetable (Oboh , 2005). This study showed that the antioxidant activity (% AA) of *Phoenix dactylifera* (46.7 – 92.2%), *Citrus aurantifolia* (42.6 – 88.3%) had a significantly (P< 0.05) highest anti oxidant activity (% AA) than *Loranthus europeas* (25 – 73.7 %) and *Zingiber officinalis* (32.9 – 64.8) at the concentration (3.5 – 16.9 mg/ ml) (table2). The increasing of antioxidant acivity for each plant related with increasing plant extract concentration could be attributed to the presence of antioxidants, especially phenols (Chu *et al*., 2002; Matsufuji et al., 1998). Numerous studies have conclusively shown that the majorty of the anti oxidant activity May be from compounds such as flavanoids, catechin and isocatechin (Marin et al., 2004; Materska and Perucka, 2005). The $Fé^{+2}$ - chelating ability of the water extractable phytochemicals in the plants (*Phoenix dactylifera, Citrus aurantifolia , Loranthus europeas and Zingiber officinalis*) were determined and the results showed in table 3. The water extract of *Phoenix dactylifera* (81.5 – 96.8 %), *Citrus aurantifolia (*61.7 – 83.9 %) had a higher $Fé^{+2}$ - chelating ability than *Loranthus Europeas* (62.3 –75.8 %) and *Zingiber officinalis* (54.7- 64.1 %) at the concentration tested (3.5-16.9 mg/ml). However, the water extract of the *Phoenix dactylifera, Citrus aurantifolia* had a significantly higher (P<0.05) chelating ability than the water extract of *Loranthus europeas and Zingiber officinalis* . The use of iron chelation is a popular therapy for the management of $Fé^{+2}$ -associated oxidative stress in brain. The iron chelating ability of the plants under study was an indicator of the neuroprotective property of the plant because iron is involved in the pathogenesis of Alzeimer's and others diseases by multiple mechanisms(Elise & James, 2002). There was an agreement between table 1, 2, 3 extracts with the highest total phenol content had a highest $Fé^{+2}$ chelating ability and a higher antioxidant activity (AA%). Some authors (Katsube *et al.,* 2004; Djeridane et al., 2006; Katalin *et al.,* 2006) have demonstrated a linear correlation between the content of total phenolic compounds and thier antioxidant capacity. The results obtained in our study showed a good correlation between (% AA) and phenolic content. However, the DPPH radical scavenging activity of plant extract under study as shown in table 4. *Phoenix dactylifera* (21.7- 81.3 %), *Citrus aurantifolia* (15.4 -73.8 %), *Loranthus europeas* (10- 61.8%) *Zingiber officinalis* (6.4 – 54.8) at the concentration (2.5-50 µg/ ml). The water extract of *Phoenix dactylifera and Citrus aurantifolia* significantly (P<0.05) have the highest scavenging activity than *Loranthus europeas and Zingiber officinalis* at the highest concentration (50 µg/ ml). A high correlation between free radical scavenging and the phenolic contents hás been reported for creals (Peterson, 2001) fruits (Gao, 2000) and culinary herbs (Zheng and Wang, 2000). The results of DPPH radical scavenging assay revealed that the extracts by hydrogen and / or electron donation, might prevent reactive radical species from reaching biomolecules such as lipoproteins , poly unsaturated fatty acids (PUFA) , DNA,amino acids, proteins and food systems (Halliwell et al., 1995). Therapies developed along the principles of modern medicine are often limited in their efficacy, carry the risk of adverse effects, and are often too costly, especially for the developing world. Therefore, treating diseases with plant-derived compounds, such as *Phoenix dactylifera, Loranthus europeas, Zingiber officinalis, Citrus aurantifolia*, which are easily available and do not require laborious pharmaceutical synthesis seems highly attractive. Phytochemical analysis of the plant showed the presence of high contents of phenolics content which may be responsible for the activity of the plant, beside other phytochemicals. Herbals and herbal extracts, which contain different classes of polyphenols, are very attractive, not only in modern phytotherapy, but also for the food industry, due to their use as preservatives. It has been reported (Calliste, Trouillas, Allais, Simon,& Duroux, 2001) that phenolic acids and their glycosides,aglycones, and monoglycosyl or diglycosyl flavonoids are distributed in the different solvents as a function of polarity and water extracts contain the most polar compounds. These facts might explain the strong scavenging and antioxidant activity of water extracts of *Phoenix dactylifera, Citrus aurantifolia*. In conclusion, the results of this study demonstrated the high efficacy of the crude aqueous extracts of *Phoenix dactylifera and Citrus aurantifolia* in free radical scavenging, inhibition of reactive oxygen species and lipid peroxidation, which may be associated with its high medicinal use as a functional food and effectiveness in treatment of different diseases, among brain and liver disease is the most important.

Acknowledgments

The Authors wish to acknowledge the Conselho Nacional de Desenvolvimento Cientifico e tecnológico (CNPq) Brasil, third world Academy of Science (TWAS),Trieste Italy, UNESCO, IAEA and ICTP, for granting the auther Post-Doctoral fellow ship tenable at Biochemical Toxicology Unit of the Department of Chemistry, Federal University of Santa Maria, Brasil.

References

Alfarisi, M., Morris, K. and Baron, M. (2006). Functional properties of omani dates (Phoenix dactylifera L.).III International Date palm conference (International sociaty for horticultural science.

Ames BM, Shigena MK. And Hagen TM (1993). Oxidants, antioxidants and the degenerative disease of aging. *Proc. Nat. Acad, Sci.USA,* 90, 7915 – 7922.

Calliste, C. A., Trouillas, P., Allais, D. P., Simon, A., & Duroux, J. L. (2001). Free radical scavenging activities measured by electron spin resonance spectroscopy and B16 cell antiproliferative behaviours of seven plants. *Journal of Agriculture and Food Chemistry*, 49, 3321–3327.

Choi,C.W., Kim, S.C., Hwang, S.S., Choi, B. K. , Ahn, H.J. , Lee, M. Y., Park, S. H., Kim, S. K. (2002). Antioxidant activity and free radical scavenging capacity between Korean medicinal plants and flavonoids by assay – guided comparsion. *Plant Sci.*, 153, 1161-1168.

Chu, Y.,Sun, J., Wu, X., & Liu, R. (2002) . Antioxidant and antiproliferative activity of common vegetable .*J. of Agric. and food chem.* , 50, 6910 – 6916.

Chopra, R. N., Nayar. S. L. and Chopra. I. C**.** (1997). Glossary of Indian Medicinal Plants (Including the Supplement). *Council of Scientific and Industrial Research,* New Delhi.

Djeridane, A., Yousif, M., Nadjemi, B., Boutassouna, D., Stocker, P., and Vidal, N. (2006). Antioxidant activity of some Algerian medical plants extracts containing phenolic copmounds. *Food Chem.,* 97,654-660.

Elise, A. M., and James, R. C. (2002). The case of iron chelation and or Antioxidant therapy in Alzheimer's disease. Drug Development Research, 56, 520–526.

Esterbauer GH, Schaur RJ and Zollner H (1991). Chemistry and biochemistry of 4- hydroxynonental, malonldehyde and related aldehydes. *Free Radical Biol Méd,* 11, 81-128.

Freeman, B. A, Crapo, J. D. (1996). Biology of Diseases. Free radicals and tissue injury. *Lab Invest.,* 47, 412–426.

Feinman, SE (1988). Structure – activity relationship of formaldehyde. In: *Formal. Sensit. and Toxicity* . Feinman SE (ed),PP., 197-204.CRC press, Boca Raton FL.

Felter, H. W. and Lloyd J. U.(2008. Viscum.—Mistletoe, *http://www.henriettesherbal.com/eclectic/kings/viscum.html*

Gao, M. (2000). Changes in antioxidant effects and thier relationship to phytonutrients in fruits of sea buckthrn during maturation, *J. of Agri. and Food Chem.,* 48, 1485- 1490.

Gassani, G., Papetti A., Daglia M., (1998). Anti- and pro- oxidant activity of water soluble components of some common diet vegetables on rats liver microsome and the effect of thermal treatment. *J Agric. Food Chem*., 46, 4123 -4127.

Glavind, J., Hartmann S., Clemmessen J., Jessen KE, Dam H (1992). Studies on the role of lipoperoxides in human pathology. II. The presence of peroxidised lipids in the atherosclerotic arota. *Acta Pathol Microbiol Scand.,* 30, 1-6.

Halliwell, B., and Gutteridge, J. M. C. (1981). Formation of a thiobarbituric-acid- reactive substance from deoxribose in the presenc of iron salts:The role of superoxide and hydroxyl radicals . *FEBS Lett.*, 128, 347-352 .

Haslam, E. (2006). Natural polyphenols (vegetable tannins) as drugs: possible modes of action. *J. Natur. Produc.*, 59, 205-215.

Hatano, T., Kagawa, H., Yasuhara, T., & Okuda, T. (1988). Two new flavonoids and other constituents in licorice root; their relative astringency and radical scavenging effects. Chemical and Pharmaceutical Bulletin, 36, 2090–2097.

Katsub, T., Tabata. H., Ohta, Y., Yamasaka, Y., Anuurad, E., Shiwaku, K. (2004). Screening for antioxidant activity in edible plant products: Comparison of low – density lipoprotein oxidation assay, DPHH radical scavenging assay, and Foline – Ciocalteu assay. *J. Agricultural and Food Chem*., 52, 2391 – 2396.

Katalin, V., Milos, M., and Jukic, M., (2006). Screening of 70 medicinal plan extracts for antioxidant capacity and total phenolis . *Food Chem*., 94, 550 – 557.

Maharaj, H., Maharaj D., Daya s., (2006). Acetylsalicylic acid and acetaminophen protect against oxidative neurotoxicity(Metab Brain Dis., 16, 855 – 872.

Marin, N., Ferreres, F., Tomas-Barberan , F., and Gill, M. I. (2004).Characterization and quantitation of antioxidant constituents of Sweet peper.*J. Agr.l and Food chem*. , 53, 1750-1756

Materska, M., and perucka, I. (2005). Antioxidant activity of the main phenolic compounds isolated from Hot pepper fruit. *J. Agric. and Food Chem*., 53, 1750- 1756.

Matsufuji, H., Nakamura, H., Chino, M., and Takeda, M. (1998). Antioxidant activity of capsantin and the fatty acid esters in parprika (Capsicum annuum). *J. Agric. and Food chem*., 46, 3468 - 3472.

Mozdzan, M., Szemraj J., Rysz J., Stolarek R., Nowak D.,(2006). Anti-oxidant activity of spermine and spermidine re-evaluated with oxidizing systems involving iron and copper ions. Int J Biochem. Cell Biol. 38, 69 - 81.

Oboh, G., Puntel, RL.. Rocha, J.B. (2005). Hot pepper (Capsicum annuum, Tepin and capsicum chinese, Hahanero) Prevents Fe^{+2} –induuced lipid peroxidation in brain –in vitro. *Food chem*., 102, 178-185.

Ohkawa, H., Ohishi, N., and Yagi, K. (1979). Assay for lipid peroxides in animal tissues by thiobarbiturate acid reaction. *Analytical Biochem*., 95, 531 – 358.

Olalye, M., Rocha J., (2007). Commonly used tropical medicinal plants exhibt distinct in vitro antioxidant activities against hepatotoxins in rat liver. *Exp Toxicol Pathol.* 17395447 (P,S,E,B,D)

Peterson, D., (2001). Phenolic antioxidants and antioxidant activity in pearling fractions of oat groats, *J. of Cer. sci*., 33, 97- 103.

Puntel, R., Roos D., Paixão, M., Braga A., Zeni G., Nogueira C., Rocha J., (2006). Oxalate modulates thiobarbituric acid reactive species (TBARS) production in supernatants of homogenates from rat brain, liver and kidney: Effect of diphenyl diselenide and diphenyl ditelluride. *Chem Biol Interact*. 17188671 (P,S,E,B,D)

Vinson, JÁ., Hão Y., Su X. (1998). Plant polyphenols exihibit lipoprotien- bond antioxidant activity using an invtro oxidation model for heart disease. *J Agric. Food Chem.,* 43, 2798- 2799.

Willet, WC. (1994). Diet and health – what should we eat. *Science*, 264, 532 – 537.,

Yu, BP. (1994). Cellular defences against damage from reactive oxygen species.*Physiol Ver*. 76 , 139 – 162.

Zar, J. H. (1984). Biostatistical Analysis, *Parentice – Hall,Inc, USA* ,pp.,620.

Table 1. Characterization of the plants material and extraction yield for water extracts.

PLANTS	Botnical Family name	Yield of extraction (mg/g)	Phenolic compounds (mg GA/100G)
Phoenix dactyliefera	Arecaceae	101.34±1.02[a]	498.97± 1.89[a]
Loranthus europeas	Loranthaceae	86.82±1.22 [b]	335.5± 2.37 [b]
Zingiber officinalis	Zingiberaceae	69.7±2.23 [c]	266.3±1.20 [c]
Citrus aurantifolia	Rutaceae	94.2±2.24 [d]	404.27±2.89 [d]

Values represent means of triplicate.
Values with the different alphabet along the same column are significantly different (P>0.05).

Table 2. Antioxidant activity (AA %) of water extract for *Phoenix dactylifera, Loranthus europeas, Zingiber officinalis, Citrus aurantifolia.*

Conc. mg/ml	*Phoenix dactylifera*	*Citrus aurantifolia*	*Loranthus Europeas*	*Zingiber officinalis*
3.5	46.7±6.3 [a]	42.6±5.4 [a]	25±4.9 [a]	32.9±7.1 [a]
6.9	51.1±4.6 [b]	55.4±1.4 [b]	29±3.2 [b]	45.1±4.6 [b]
10	67.3±3.4 [c]	73.8±5.5 [c]	40.8±2.4 [c]	49.3±6.6 [c]
13.5	78.7±6.8 [d]	79.2±3.7 [d]	60.3±3.5 [d]	56.7±4.1 [d]
16.9	92.2±4.8 [e]	87.8±5.4 [e]	73.7±4.7 [e]	64.8±5.1 [e]

Values represent means of triplicate.
Values with the different alphabet along the same column are significantly different (P>0.05).

Table 3. $Fé^{+2}$ chelating ability of aqueous extracts of *Phoenix dactylifera, Loranthus europeas, Zingiber officinalis, Citrus aurantifolia*

Conc. mg/ml	*Phoenix dactylifera* %	*Citrus aurantifolia* %	*Loranthus europeas* %	*Zingiber officinalis* %
3.5	81.5 ± 2.4 [a]	61.7 ± 4.1 [a]	62.3 ± 5.3 [a]	54.7 ± 1.4 [a]
6.9	92.2 ± 3.7 [b]	80.3 ± 3.4 [b]	71.7 ± 3.3 [b]	61.3 ± 3.2 [b]
10	93.7 ± 1.4 [c]	82.5 ± 1.3 [c]	73.8 ± 1.3 [c]	62.2 ± 4.2 [c]
13.5	94.1 ± 1.9 [d]	83.1 ± 3.4 [d]	74.1 ± 4.6 [d]	63.8 ± 3.8 [d]
16.9	96.8 ± 4.3 [e]	83.9 ± 2.2 [e]	75.8 ± 3.1 [e]	64.1 ± 1.6 [e]

Values represent means of triplicate.

Values with the different alphabet along the same column are significantly different (P>0.05).

Table 4. DPPH radical scavenging activity of water extract of *Phoenix dactylifera, Loranthus europeas, Zingiber officinalis, Citrus aurantifolia.*

Conc.(µg/ml)	*Phoenix dactylifera* %	*Citrus aurantifolia* %	*Loranthus europeas* %	*Zingiber officinalis* %
2.5	21.7±2.4 [a]	15.4±3.1 [a]	10±6.0 [a]	6.4±3.3 [a]
5.0	37.4±4.5 [b]	21.6±5.4 [b]	17.3±2.6 [b]	13.8±4.8 [b]
12.5	51.8±3.8 [c]	43.5±3.2 [c]	27.8±1.4 [c]	25.4±5.2 [c]
25.0	67.2±4.1 [d]	52.3±4.7 [d]	49.5±3.7 [d]	37.2±4.7 [d]
50	81.3±2.8 [e]	73.8±22.4 [e]	61.8±3.4 [e]	54.8±1.8 [e]

Values represent means of triplicate.
Values with the different alphabet along the same column are significantly different (P>0.05).

Modern Applied Science

www.ccsenet.org/journal.html

Vol. 3, No. 3

March 2009

The Deficiencies of Flame Retardant Standard in Chinese Textiles as Viewed from Tent Flame Retardant Standard

Shuhua Yuan & Jiqun Li

Tianjin Polytechnic University

Tianjin 300160, China

E-mail:xuehu987@163.com

Abstract

In this article, we comparably analyzed domestic and foreign tent flame retardant standards, and the difference between domestic and foreign tent flame retardant standards reflected the gap and problems between Chinese textile flame retardant standard system with foreign standard system, and we also put forward countermeasures and advices for the improvement and perfection of Chinese textile flame retardant standard system.

Keywords: Tent, Flame retardant standard system, Problems

1. Introduction

As a sort of outdoor equipment, tent is more and more popular by tourists. Especially after 5.12 Sichun Earthquake, it more displays the importance of tent. The large-sized earthquake make numbers of house break down in the disaster areas, but it needs long time to rebuild the homes, so tents become into the temporary habitations for people hit by the natural calamity, and the demand quantity is large. At that time, not only the quantity but also the quality should be ensured for tents. But the flame retardant performance of tent is the most easily ignored by production enterprises and consumers, and the ancient "baked wheaten cake joins camp" has indicated the importance of flame retardant performance of tent, especially for makeshift shelter, if we don't consider its flame retardant performance, the tragic of one disaster after another may happen. Based on humanity and harmonious society, to better protect human life and property, in this article, we comparably analyzed domestic and foreign tent flame retardant standards, and the difference between domestic and foreign tent flame retardant standards reflected the gap and problems between Chinese textile flame retardant standard system with foreign standard system, and we also put forward countermeasures and advices for the improvement and perfection of Chinese textile flame retardant standard system.

2. Introduction of domestic and foreign tent flame retardant standards

2.1 Introduction of Chinese tent flame retardant standard

The national standards involving the performance of tent flame retardant include three items.

(1) MZ/T 011-2001 12m^2 Tent for Disaster Relief (Cui, 2001). The standard definitely regulates the style specification, technical requirement, experiment method, testing rule, symbol, packaging, transpiration and storage of 12m^2 tent for disaster relief, and regulates that the standard is the same with the protection and testing for the disaster relief tent which is mainly made by waterproof and flame-resistant chemical fiber tarpaulins (seen in "1 range" of the standard). For the performance of flame retardant, the standard only regulates the damaged length ≤150mm, and the time after flame and the smouldering duration ≤15s (seen in "3.8.1 Table 4" of the standard), and adopts vertical burning testing method to test (seen in "4.4.4 the test of material flame retardant performance keeps to GB/T 5455"). Except that, there are not any relative regulations about flame retardant performance in the standard.

(2) BB/T 0037-2006 Flame-resistant and Water-proof Fabrics and Tarpaulins Coated with PVC on Both Sides (Wang, 1997). This standard regulated the product type, specification, technical requirement, experiment method, testing rule, symbol, packaging, transpiration and storage of flame-resistant and water-proof fabric and tarpaulins coated with PVC on both sides. This standard is fit for the cloths and tarpaulins coated with PVC on both sides which take vinylon fiber, nylon fiber, polyester fiber and glass fiber as the foundation (seen in "1 range" of the standard). For the flame resistant performance, the standard only regulates that the flame burning time ≤10.0s and the oxygen index ≥27.0%, (seen in "4.3 Table 4" of the standard), and adopts the limiting oxygen index method to measure (seen in "5.7 the measurement of oxygen index" of the standard).

(3) GA 91-1995 General Technical Conditions for Flame Retardant Tarpaulins (Ma, 1995). This standard regulates the technical requirements and testing method of chemical fiber flame retardant tarpaulins coated with rubber or plastic on

both sides. The standard is the same with tarpaulins coated with natural rubber and synthetic rubber or PPVC on both sides which take vinylon fiber or other chemical fiber canvas which physical and mechanical performance is above vinylon as the foundation (seen in "1 main contents and applied range" in the standard). For the flame retardant performance of tarpaulins, this standard regulates that the oxygen index ≥26.0%, and the afterflame time and the aftergrow time≤5.0s, and the damaged length ≤80mm, (seen in "3.2 Table 1"), and the standard respectively adopts limiting oxygen index method and vertical burning method to test (seen in "4.2 the measurement of flame retardant performance"). Except for that, the standard also regulates the performance of accelerated weathering and leaching (breaking strength and water-proof performance) (seen in 3.2 continued Table 1).

2.2 Introduction of foreign tent flame retardant standard

There are many foreign flame retardant standards about tent, and we mainly briefly expatiate on the tent flame retardant standards of US and Canada in this article.

(1) US tent flame retardant standard CPAI-84 (Michael, 1995) "A Specification of Flame-resistant Materials Used in Camping Tentage". This standard regulates the flame retardant of the fabrics and other materials which are easily influenced in camping tent, and the performance standard and the appraisal rules of supplier, and describes the label program that users look out their harmful behaviors for the flame retardant treatment (seen in "1.1 range of standard"). For the concrete contents, this standard respectively regulates the flame retardant performance and testing method for the flooring material and the wall and top material of tent, and regulates that "no specimen from a sample unit of flooring material shall be damaged within 25mm of the edge of the hole in the flattening frame; no specimen from a sample unit of wall and top material shall have an afterflame time (length of time a specimen continues to flame after removal of the test flame source) of more than 4 seconds; the average after-flame time for all specimens in a sample unit shall not exceed 2 seconds; portions or residues that break or drip from the test specimens shall not continue to flame after they reach the floor of the test cabinet; they should self-extinguish before (or as) they contact the floor of test cabinet; the maximum damaged length for an individual specimen is 255mm" (seen in "3 performance requirement", "5 flammability test method, flooring material" and "6 flammability test method, wall and top material"), and the standard also regulates that the accelerated weathering and leaching procedure of flooring material and wall and top material (see in "4 conditioning"), and elaborates on the sampling of sample unit (seen in "2.3 sample unit"), the certification materials and label procedure, and regulates the label of camping tent should permanently accrete with the product and include the certification that proves the materials has achieved the flame retardant requirements, the manufacturer's ID certification, and the warning label of "Warning: keep all flame and heat sources away from this tent fabric. This tent meets the flammability requirements of CPAI-84" (seen in "7 certification and labeling"). Except that, the standard also explains the future work in the appendix (seen in "appendix B future work on CPAI-84").

(2) Canadian tent flame retardant standard (Canada, 2001) is included in "Hazardous Products Act-Test Method for the Flame resistance of Tents", and this regulation is basically same with US tent flame retardant stand CPAI-84 for the tent flame retardant performance index requirement and testing method except for accelerated weathering test, and adopts burning tablet method to implement the test (seen in "5 procedure"). Except for that, the standard also regulates the health and safety problem (seen in "6 health and safety") and the precision and bias (seen in "9 precision and bias") of test in the testing process, and it also detailedly regulates the label procedure (seen in "appendix Ⅰ") as US CPAI-84. At the same time, the appendix also explains some measures adopted to prevent the fire when camping (seen in "schedule Ⅰ the following precautions should be taken when camping").

3. Comparably analyzing domestic and foreign tent flame retardant standards

From the introduction of foreign and domestic tent flame retardant standards, we can see that except that the technical indexes with same parameters of Chinese tent flame retardant standard are little lower than foreign standard and part standards possess different testing indexes, there are following differences.

(1) As viewed from the standard layer, most foreign standards are compelling rules of law or standard forms, but Chinese standards are national standards and industrial standards. Difference standards layers decide that the contents of Chinese standards are narrow than foreign standards and lack in humanity. Chinese standards only regulate the performance index and testing method of flame retardant, which generalizes the whole content by part and lacks in people-oriented flame retardant performance to comprehensively evaluate the tent. However, except for performance index and testing method, the tent flame retardant standards of US and Canada all regulate the label which warns users, and US standard also regulates the material certification and manufacturers' ID certification to meet the standard, which all consider consumers' feelings and let consumers could favorably purchase the tent fulfilling the requirement of flame retardant standard. Canadian standard also regulates relative measures to prevent the fire when camping, which starts from the safety for consumers and users, fully embodies the humanity and the people-oriented standard constituted strategy.

(2) As viewed from applied range of standard, Chinese tent flame retardant standard mainly aims at the production

standard which doesn't directly aim at consumers, but foreign standards are trading standards which directly aim at consumers, and the applied range of Chinese tent standard is narrower than foreign standards. Foreign trading standards have strong applicability, and they take the market as the orientation, serve for the market and consumers, could effectively adapt the development of market economy, enhance the market competition because of easy operation, and have certain encourage function for the technical advancement for enterprises in the implementation.

Up to now, China has no one standard which is completely aims at the tent flame retardant performance which only is involved in the standard of 12m^2 Tent for Disaster Relief, and other BB/T 0037-2006 Flame-resistant and Water-proof Fabrics and Tarpaulins Coated with PVC on Both Sides and GA 91-1995 General Technical Conditions for Flame Retardant Tarpaulins regulate the flame retardant standard by the regulations to different raw materials, i.e. the production standard, and most of them are recommended industrial standards. For the tent flame retardant standard, China is almost blank, which could not follow the tendency of harmonious society and humanism development, so the establishment of national tent flame retardant standard is imperative under the situation.

(3) As viewed from contents, foreign standards respectively regulate the flooring material and wall and top material of the tent flame retardant performance, and also regulate the flame retardant performance when materials should meet the standard requirement after accelerated weathering and leaching procedure. Chinese standard doesn't distinguish the flame retardant performances of flooring material and wall and top material. Because the structure of tent decides materials of different parts should have different flame retardant performances, and if we only regulate the flame retardant performance index for the whole tent, the flame retardant performance of the tent could be comprehensively and exactly evaluated. In addition, Chinese standard doesn't consider the change of flame retardant performance induced in practical using environment because of illumination and rain, and the influence of actual use on the flame retardant performance from users' views.

4. Problems existing in Chinese textile flame retardant standard system

The standard of tent flame retardant is a typical example in the flame retardant standard of Chinese textile, and we could see that many problems still exist in the study of the flame retardant performance standard system in Chinese textiles.

(1) For the application range of standard, the applicability of textile flame retardant standard is feeble, and both blank and redundancy exist. For example, for the redundant standards, the tent standard regulates the tent flame retardant performance index for different raw materials, and different standards make regulations for same type of product at the same time, which has certain repetition and brings certain disagreements. With the development of society, science and economy, new products continually come forth, and if the flame retardant standard has weak applicability, it must lag in the development of new products, and corresponding standard will certainly influence the development of new products. The tent flame retardant performance standard is a bright example, and with the continual enhancement of human consumption level and safety consciousness, the standard of tent flame retardant performance should be the order of the day early.

(2) For the requirement of standard performance, Chinese textile flame retardant standard is not exact and comprehensive enough for some regulations. Because Chinese textile flame retardant standard mainly aims at the production standard which doesn't directly sell to consumers, and foreign standards aim at the trading standards which directly sell to consumers, so Chinese standards have not complete, concrete and strong applicability like foreign standards and lack in humanity in some performance requirements. For example, foreign standards explain the product label and glossary, and the warning label describes the standard from human safety. For the glossary, only part Chinese standards come down to the explanation of glossary, which will induce the illegibility of concept and influence the directional function of enterprise on consumers. In addition, for the tent flame retardant standard, Chinese standard doesn't consider the flame retardant performance form the structure and using environment of the tent, which induce the index evaluation is not exact enough.

(3) The flame retardant standard of Chinese textile lacks characters of system, programming and currency. The Chinese textile flame retardant standards are established when the deficiency is found, and as time passes, the standards will be in confusion, which will make manufacturers don't know which sort of standard would be used to test the quality of the product, and make against the production of enterprise and the export of products.

5. Countermeasures and advices

(1) Establishing general flame retardant standard or technical regulation of law. To simplify and compensate the blank of Chinese flame retardant standard and further increase the applicability of Chinese flame retardant standard, we should establish general flame retardant standard or technical regulation of law, and with the development of standard application, we should continually compensate the contents of the standard, but not establish new standard. For example, we can use foreign the mode of law for reference, adopt the citation of certain method standard which should be the up to data method standard for the part of testing method, and regulate the applicability of product when considering the compatibility to adapt new method standard, promote the development of new products, adapt the occurrence of new

products, and make Chinese technical standard more restrictive and compelling, and accordingly enhance domestic flame retardant technology and product performance and improve the export of product.

(2) Transform from production standard to trading standard, and transform from the standard establishment decided by national behavior to civilian behavior. The flame retardant standard of Chinese textile should follow the development tendency of global integration, and transform from production standard to trading standard (Yu, 2006), and the product standard should not be constituted by the product variety but by the final purpose of the product, and the cover range should be increased when the purpose is divided, so the performance requirement will be more comprehensive, strict and practical. For example, we can add the requirements of label, glossary and security direction, and constitute the trading standard as viewed from users. At the same time, new products will meet the standard in time.

(3) Further enhancing and improving the performance index of Chinese textile flame retardant standard. In the standard, proper and reasonable performance index will better improve the continual advancement of flame retardant technology, and in the process, we should consider the structure and using environment influencing the flame retardant performance of textile, and comprehensively and exactly test the flame retardant performance of the products.

6. Conclusions

With the development of the integration of global economy, green trade barrier will occur continually, and the security of textile has been one of bottleneck to restrict the export of Chinese textiles, and it is more and more concerned by insiders. Advanced standards would drive the innovation of technology, and the patent of technology, the standard of patent and the monopolization of standard have been a sort of tendency, and who holds the standard and technology and who will hold the market. With continually mature technology of flame retardant, the flame retardant standard of textiles should form a set of systematic and perfect standard system. At the same time, people-oriented and humanism concept would more and more go deep into human hearts, and the work of standardization should start from that to continually improve and perfect Chinese textile flame retardant standard system and reduce the gap with foreign countries and accordingly promote the export of Chinese textiles.

References

Canada. (2001). Hazardous Products Act-Test Method for the Flame resistance of Tents. *Health Canada*.

Cui, Xiumin et al. (2001). *12m^2 Tent for Disaster Relief*. Beijing: Standards Press of China.

Ma, Xiaoning et al. (1995). *General Technical Conditions for GA 91-1995 Flame Resistant Tarpaulins*. Beijing: Standards Press of China.

Michael J. Ravnitzky. (1995). CPAI-84 A Specification for Flame-resistant Materials Used in Camping Tentage. *St. Paul: Industrial Fabrics Association International*.

Wang, Xingdong et al. (1997). *BB/T 0037-2006 Flame-resistant and Water-proof Fabrics and Tarpaulins Coated with PVC on Both Sides*. Beijing: Standards Press of China.

Yutao. (2006). *Study on the Transformation of Textiles from Production Standard to Trading Standard*. Tianjin: Tianjin Polytechnic University.

Modern Applied Science

www.ccsenet.org/journal.html

Vol. 3, No. 3

March 2009

Physiological Responses of Tomato Seedlings (*Lycopersicon Esculentum)* to Salt Stress

Yan Li (Corresponding author)

Biology Department

Dezhou University

Dezhou 253023, China

E-mail: lylxy0524@126.com

Abstract

Tomato seedling was treated under different concentration of NaCl ranged from 0 to 300 mM. Effects of salt stress on the content of growth and osmotic adjustment substance, the superoxide dismutase (SOD), peroxidase (POD), catalase (CAT), and ascorbate peroxidase (APX) activities and generation rate of $O_2^{\cdot-}$ of tomato seedling were studied. The result showed that the content of fresh weight (FW), dry weight(DW), K^+, K^+/ Na^+ and soluble sugar(SS) decreased with the increasing of NaCl concentration. Conversely, the contention of Na^+, Proline and malondialdehyde (MDA), SOD, POD, CAT and APX activities and generation rate of $O_2^{\cdot-}$ increased. Growth of seedling shoots was suppressed by salt treatment. Osmotic adjustment substance play a critical role in the growth of tomato seedling under the condition of salt stress, and meanwhile the continual increasing bioactivity of antioxidant enzymes could scavenge reactive oxygen species (ROS) resulted from salt stress to exert the existence of tomato seedling.

Keywords: Tomato, Growth, Osmotic adjustment substance, Salt stress

1. Introduction

Salt stress is one of the mainly environmental factors interfering with the growth, development and biomass production of plants. Today, 20% of the world's cultivated land and nearly half of all irrigated lands are affected by salinity (Tanji, 1990, PP. 1-7). High concentrations of salts causes ion imbalance and hyperosmotic stress in plants. 300 million mu cultivated land in China is affected by salinity, which occupies 25% of arable land. With the quick development of industry, the leap of population, the acceleration of town construction, the sharp reduction of arable land area and unreasonable agricultural measures lead to secondary salinization of a large amount of arable land (Tester, 2003, PP. 503-507, Zhao, 1999). Destruction of arable land ascribed to saliniization seriously affected the civilization of remote antiquity and modern times at all times (Blumwald, 2004). Salinity has been one of the cardinal factors affecting the development of social economy (Shono, 2001, PP. 193-199). Tomato belongs to fruit vegetable of horticulture crops, and its flesh is applied not only as salad and ingredients of food, but also fresh food. It is one of the important routine fruits and vegetables. Study on the physiological responses of tomato seedlings to salt stress could give novel insight into the planting and modifying of tomato cultivars.

2. Materials and methods

2.1 Plant material and growth conditions

Tomato seeds (Zhongsu 5) were purchased from China Academy of Agriculture Science. Seeds of tomato were sterilized in 0.1% $HgCl_2$ for 10 min, and then rinsed with water. Plump kernels were selected for planting. Selected seeds were then germinated on moistened plastic basins containing thin sand. The seeds germinated after 3 days. The obtained seedlings were transferred to continuously aerated Hoagland solution in a greenhouse in which day and night temperature, everyday light, light intensity and relative humidity is 30-20℃, 15 hours, 700-900umol/m^2.s and 70-80%, respectively. Seedlings were subsequently transferred, at the stage of 4-5 fully expanded leaves (20 days later), in buckets filled with neat thin sand. Each basin four seedlings irrigated with aerated Hoagland solution. After planted for one month, concordant seedlings were selected for treatment. Tomato seedlings were treated with NaCl at the concentration ranged from 0 until 300 mM with the increasing rate of 50 mM every 12 hours, and subsequently irrigated with water every day. Irrigation quantity is 2 times of water capacity of thin sand, and relative physiological indices were investigated after a week.

2.2 Methods

2.2.1 Measure of FW and DW

The thin sand of roots was gently removed by tap water, quickly rinsed with distilled water to flush the dust in the surface. Then the roots were washed carefully and their surface water was completely dried by absorbent paper. FW was measured and then fresh seedlings were transferred to 110 ℃ oven in order to deactivation of enzymes and subsequently dried to constant weight at 80 ℃. DW was measured. Plant water content and degree of succulence were calculated as follows:

Plant water content=(FW-DW) /FW×100%

Degree of succulence=FW/DW

2.2.2 Content measure of osmotic adjustment substance

Dried plant samples were ashed in Muffle furnace at 550℃ after grinded and ash was extracted with HNO_3 with constant volume. Na^+ and K^+ in the seedling tissues was measured by Atomic Absorption Spectrophotometer (AAS) (Hitachi, Z-8000, Japan)(Zhang, 1990, PP. 259-260). Proline was measured as described by Chou etc.(Zhang, 1994, PP. 62-65, Chou, 1995, PP. 96-97, Zhu, 1990, PP. 249-252). MDA and SS content was measured as described by Zhang(Zhang, 2003, PP. 274-277, Zhao, 1994, PP. 207-210).Leaves of tomato seedling were rinsed distilled water to flush the dust in the surface , washed carefully and then their surface water was completely dried by absorbent paper. Samples prepared for treatment were immediately frozen in liquid nitrogen, stored at -80℃ for 15 min and subsequently lyophilized. Osmotic potential of obtained cell sap was measured by freezing point osmometer (Osmomat 030).

2.2.3 Measure of antioxidant enzyme activities

The enzyme activities of SOD, CAT and POD were assayed as described by Li(2000, PP. 167-169), Li(2000, PP. 165-167) and Zhang(2003, PP. 154-155), respectively; APX activity was assayed as described by Nakano and Asada(1981, PP. 867-880); generation rate of $O_2^{\cdot-}$ was measured as described by Wang(1990, PP. 55-57).

3. Results

3.1 Effects of salt stress on the growth

In the treatments of different saline contention, the growth of tomatoes varied obviously and suppressed by salt stress, which was associated with salt content. In the treatment of 300 mM NaCl, leaves of tomato suffered greatly damage with all yellow leaves and growth was almost arrested. With the increasing of NaCl, FW and DW of tomato seedlings reduced gradually, while water content and degree of succulence increased obviously. Results showed that the growth of tomato seedlings was suppressed by salt treatment, but survived due to the water content and degree of succulence. Osmotic adjustment substance might play a critical role in the growth of tomato seedling under the condition of salt stress.

3.2 Effects of salt stress on the content of osmotic adjustment substance

Na^+ ions both in leaves and roots increased gradually with the increasing of salt concentration, and the increasing degree of Na^+ ions was higher in leaves than that in roots. Conversely, K^+ ions both in leaves and roots decreased gradually with the increasing of salt concentration, and the decreasing degree of K^+ ions was higher in roots than that in leaves. K^+/ Na^+ decreased gradually in leaves and roots, and the decreasing degree was obviously higher in roots than that in leaves. All the results showed that Na^+ and K^+ ions was correlated with the physiological responses of tomato seedlings to salt stress as one of cardinal factors attributed to salt stress.

Proline content increased gradually by increasing NaCl concentration, and was 12.36 and 22.29 times of the control at the treatment of 100 and 300 mM NaCl, respectively, with great significance.

SS content decreased by increasing the NaCl concentration. SS content of leaves decreased by 17.38% compared to the control at the treatment of 100mM NaCl. At the treatment ranged from 200 to 300 mM NaCl, SS content decreased by 65.85%-74.7% compared to the control. At the treatment of 100-200 mM NaCl, SS levels were progressively decreased.

MDA content increased by increasing the NaCl concentration. MDA content of leaves increased by 4.6% compared to the control at the treatment of 100mM NaCl. At the treatment ranged from 200 to 300 mM NaCl, MDA content increased by 10.38%-23% compared to the control. When NaCl concentration was above 100mM, MDA content was obviously higher than the control.

Osmotic potential increased with the increasing of NaCl concentration. Osmotic potential of leaves increased by 43.55% compared to the control at the treatment of 100mM NaCl. At the treatment ranged from 200 to 300 mM NaCl, MDA content increased by 91.94%-116.13% compared to the control. At all treatments, osmotic potential was obviously higher than the control, which indicated that with the enhancement of salt stress tomato accumulated large amount of osmotic adjustment substances in order to preserve adequate water necessary for existence.

3.3 Effects of salt stress on antioxidant enzyme activities

SOD activity increased by 9.9% at the treatment of 100 mM NaCl compared to the control, while at the treatment of 200-600 mM NaCl, SOD activity decreased obviously. With the increasing of NaCl concentration, POD activity decreased gradually at the concentration of 100-500 mM and reduced by 2.338-40.92 times than the control. At the concentration of 600 mM, POD activity increased and was 9.72 times of that at the concentration of 500 mM. CAT activity increased gradually which was 2.5 times of the control at the concentration of 100 mM, and then decreased gradually.

The generation rate of $O^{\cdot}{}_2^-$ in leaves increased with the increasing of NaCl concentration and raised by 28.6%, 85.7% and 142.86%, respectively, compared to the control.

4. Discussions

Whether halophyte or non-halophyte, during the period of adapting to saline, in order to avoid water loss, the most efficacious measure is osmotic adjustment (Xu, 1996, PP. 249–257). With the accumulation of Na^+ in vacuoles, cells kept the osmotic equilibrium between cytoplasm and vacuole through osmotic adjustment. This adjustment relied on synthesizing or accumulating some solutes, namely inorganic salts and organic solutes, which did not affect the biochemistry reactions in cells.

The content of fresh weight (FW), dry weight (DW), K^+, K^+/ Na^+ and soluble sugar (SS) decreased with the increasing of NaCl. Conversely, the contention of Na^+, Proline and malondialdehyde (MDA) and osmotic potential increased. Growth of seedling shoots was suppressed by salt treatment. Osmotic adjustment substance plays a critical role in the growth protection of tomato seedling under the condition of salt stress.

Zhu (2001, PP. 66-71) noted that high concentrations of salts cause ion imbalance and hyperosmotic stress in plants. As a consequence of these primary effects, secondary stresses such as oxidative damage often occur. Generation and scavengeing of free radials coexisted in plants, and was normally in a balance state. Once plants was suffered salt stress, this balance system would be broken, free radicals would accumulate, membrane permeability discrepancy lost, which lead to the enhancement of membrane pore and permeability and metabolic disorder, and thus plants were suffered injury(Zhao, 1993, PP. 519-525). Enzymatic protection system existed in plants to scavenge free radicals. SOD, POD, CAT and APX is mainly components of this system in which SOD could disproportionate $O^{\cdot}{}_2^-$ into O_2 and H_2O_2.

High concentration H_2O_2 in tissues was mainly scavenged by CAT which led to a low level of H_2O_2, while low concentration H_2O_2 was mainly scavenged by POD during the period of oxidation of relative substances. When SOD, POD, CAT and APX were consistent and in harmony with one another, free radicals from ROS in plants could be kept at a low level which exerted the plant grow and metabolize naturally (Jiang, 1999, PP. 229 - 234).

Investigation showed that the content of FW, DW decreased with the increasing of NaCl. Conversely, the activities of SOD, POD, CAT and APX and generation rate of $O_2^{\cdot-}$ increased. Growth of seedling shoots was suppressed by NaCl treatment. Continual increasing bioactivity of antioxidant enzymes could scavenge reactive oxygen species (ROS) resulted from salt stress to make the existence of tomato seedlings.

References

Blumwald, E., Grover, A., & Allen, G. (2004). Breeding for abiotic stress resistance: challenges and opportunities. *Proceedings of the 4th international crop science congress,* 26 sep-1 oct 2004, Brisbane, Australia.

Chou, Q. (1995). Plant physiological experiment guidebook. China agriculture press, 96-9.

Li, H.S. (2000). Principles and techniques of plant physiology and biochemistry experiment. Beijing: High education press, 165-167.

Li, H.S. (2000). Principles and techniques of plant physiology and biochemistry experiment. Beijing: High education press, 167-169.

Nakano, Y., Asada, K. (1981). Hydrogen peroxide is scavenged by ascorbate-specific peroxidase in spinach chloroplasts. *Plant and Cell Physiology*, 22: 867-880.

Jiang, M.Y. (1999). Generation of OH and oxidation injury of plants under the condition of water stress. Acta Botanica Sinica, 41 (3) : 229 - 234.

Tanji, K.K. (1990). *Nature and extent of agricultural salinity*. In: Tanji KK ,Agricultural Salinity Assessment and Management. New York: American Society of Civil Engineers pp 1-7.

Shono, M., Wada, M., & Hara, Y., et al.(2001). Molecular cloning of Na^+-ATPase cDNA from a marine alga, *Heterosigma akashiwo*. *Biochim Biophys Acta,* 1511:193-199.

Tester, M ., Davenport , R. (2003). Na^+ tolerance and Na^+ transport in higher plants. *Ann Bot*, 91(5): 503-507.

Wang, A.G., Luo, G.H. (1990). Quantity correlation of superoxide radicals and hydroxylamine reactions. *Plant*

physiology communications, 26 (6): 55-57.

Xu, D., Duan, X., & Wang, B., et al. (1996). Expression of a late embryogenesis abundant protein gene, HVA1, from barley conferred tolerance to water deficit and salt stress in transgenic rice. *Plant Physiology*, 110: 249–257.

Zhang, D.Z. (1994). Determination method of free proline in wheat leaves. *Plant physiology communications*, 30(4): 62-65.

Zhang, Z.L. (1990). *Plant physiological experiment guidebook*. Beijing: High education press, 259-260.

Zhang, Z.L. (2003). *Plant physiological experiment guidebook (third editon)*. Beijing: High education press, 154-155.

Zhang, Z.L. (2003). *Plant physiological experiment guidebook (third editon)*. Beijing: High education press, 274-277.

Zhao, K.F., Chou, Q., & Li, D.Q. (1993). Effects of salt and water stress on the membrane lipid peroxidation of halophyte and non-halophyte. Acta Botanica Sinica, 35 (7): 519-525.

Zhao, K.F., Li, C.F. (1999). *China halophytic plants*. Beijing: Science press.

Zhao, S.J., Xu, C.C., & Chou, Q., et al. (1994). Determination modification of MDA in plant tissues. *Plant physiology communications*, 30(3): 207-210.

Zhu, G.L. (1990). Plant physiological experiment, Beijing University press, 249-252.

Zhu, J.K. (2001). Plant salt tolerance. *Trends Plant Sci*, 6: 66-71.

Table1. Effects of salt stress on the grows of tomato

	0	100	200	300
FW	17.5	15.8	14	12.2
DW	5.5	4.7	3.2	2.3
Water content	68.57%	70.25%	77.14%	81.15%
Degree of succulence	3.18	3.36	4.38	5.3

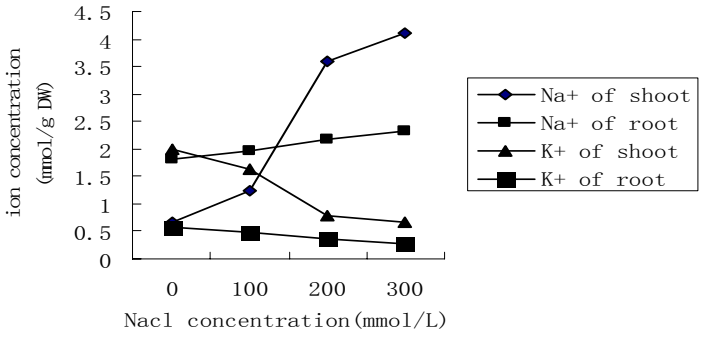

Figure 1. Effect sof salt stress on the Na+ and K+ contents of shoot and root of tomato

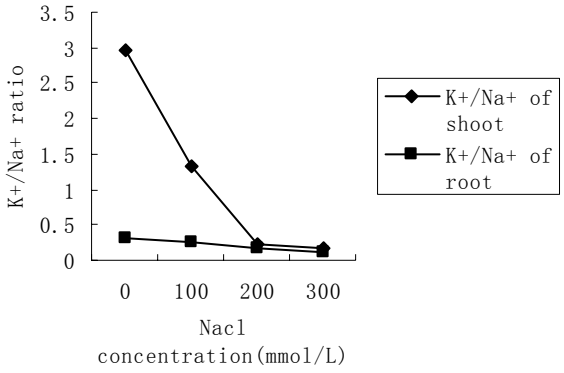

Figure 2. Effects of salt stress on the K^+/ Na^+ of shoot and root of tomato

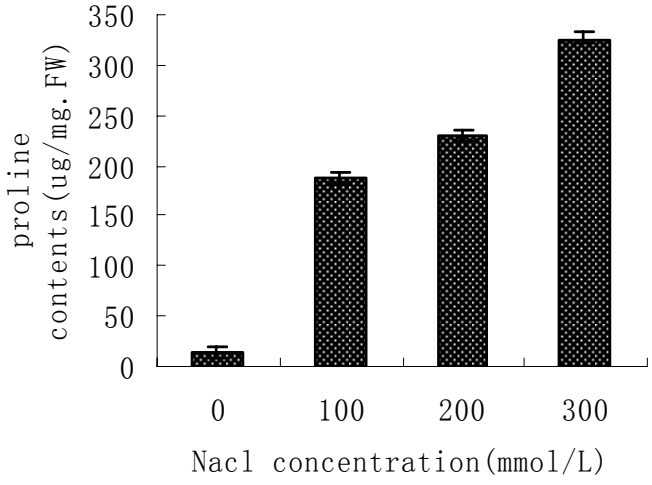

Figure 3. Effects of salt stress on the proline content of tomato

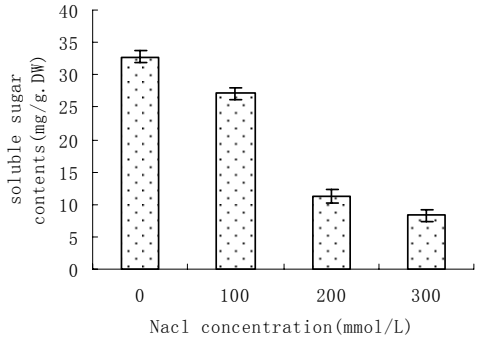

Figure 4. Effects of salt stress on SS contents of tomato

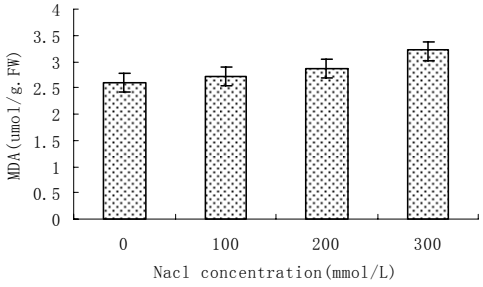

Figure 5. Effects of salt stress on MDA content of tomato

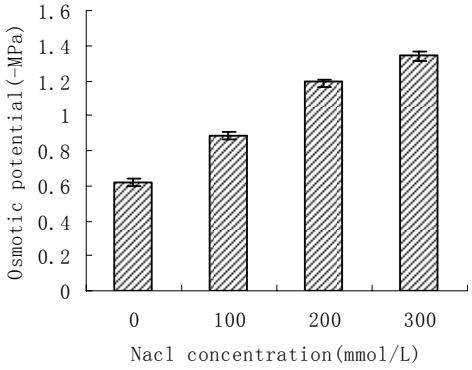

Figure 6. Effects of salt stress on osmotic potential of tomato leaves

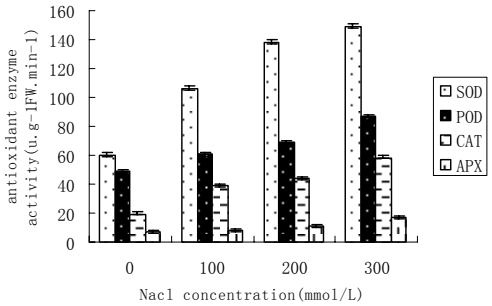

Figure 7. Effects of salt stress on antioxidant enzyme activities of tomato

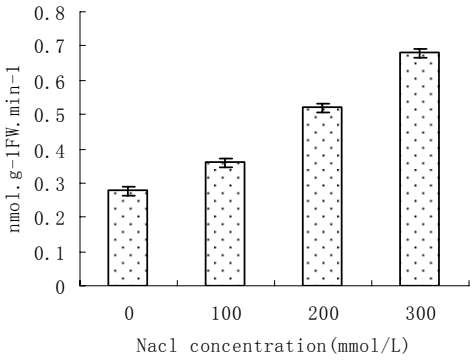

Figure 8. Effects of salt stress on the $O_2^{\cdot-}$ content of tomato

A journal archived in Library and Archives Canada
A journal indexed in CANADIANA (The National Bibliography)
A journal indexed in AMICUS
A journal indexed in Zentralblatt MATH
A journal included in DOAJ (Directory of Open-Access Journal)
A journal included in Google Scholar
A journal included in LOCKSS
A journal included in PKP Open Archives Harvester
A journal listed in Journalseek
A journal listed in Ulrich's
A peer-reviewed journal in applied science research

Modern Applied Science

Monthly
Publisher Canadian Center of Science and Education
Address 4915 Bathurst St. Unit # 209-309, Toronto, ON. M2R 1X9
Telephone 1-416-208-4027
Fax 1-416-208-4028
E-mail mas@ccsenet.org
Website www.ccsenet.org
Printer William Printing Inc.
Price CAD.$ 20.00

ISSN 1913-1844